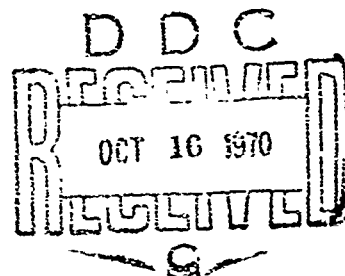AD712750

ON THE ORIGIN OF SHOCKWAVES FROM
CONDENSED EXPLOSIONS IN AIR

By
L. Rudlin

NOL

19 JUNE 1970

UNITED STATES NAVAL ORDNANCE LABORATORY, WHITE OAK, MARYLAND

NOLTR 69-74

131.

ON THE ORIGIN OF SHOCKWAVES
FROM CONDENSED EXPLOSIONS IN AIR

Part 3: Airshock Radiation from Small Explosions
at Sea-Level Conditions

Prepared by:
L. Rudlin

ABSTRACT: Photographic and spectral observations have been made of
the earliest stages of HE explosions. Strong (in the neighborhood
of Mach number = 20), non-luminous airshocks have been photographed
as close in as 1/2-charge radius from the explosive surface. The
present results support earlier observations on the existence of a
transmitted airshock created by the detonation shockwave.

The spectra obtained show no evidence of the expected shocked-air
species. Identification of the spectral features suggests that the
intense early light of an explosion is created within the fireball
by a wide range of chemical species requiring from about 2 to 20 ev
for excitation.

i

Part 3:   Airshock Radiation from Small Explosions at Sea-Level
          Conditions

This is the third report of a series (see RUDLIN 1962, 1963 in
References, Section 6) exploring the origin of shockwaves from
condensed explosions in air. As in the earlier two reports, so here,
the origin of shockwaves remains elusive. Time-honored concepts are
questioned and even challenged: highly-shocked air is not observed
to be luminous. New ideas are advanced in a tentative fashion:
perhaps the luminosity observed in explosions and hitherto identified
as shocked air, is not hydrodynamic in origin but due to the inter-
action of explosion particles with the air.

During the course of this investigation, standard techniques have
been used as well as novel, new ones. Pressure-time measurements
have been attempted along with ionization probe efforts. High-speed
photography has been extended to include spectrographic techniques.
Old theories have been reviewed, analyzed, and, in some instances,
abandoned in favor of new concepts better fitting the interpretation
of the experimental data. But the interpretations, analysis, theory,
indeed the procedures and instrumentation employed in these investi-
gations are themselves subject to question and disagreement. Indeed,
in-house discussions on the validity of the techniques and interpre-
tations have been lively and informative but non-conclusive. Perhaps
this is as it should be for exploratory studies -- honest and critical
discussion and presentation of ideas without necessarily reaching
absolute conclusions. It is so with this study and this report.

The origin of shockwaves has not been proved but in the process of
the search, much new information on shock behavior has been uncovered.
The rich spectral characteristics of explosions are reported. Novel
and ingenious methods for detecting shocks are described; many of
these techniques should have significance in future explosions work.
Old ideas have been questioned and new ones, perhaps as shaky as the
old, are advanced. This leads, at least, to an uncovering of long
standing problem areas, and hopefully to revitalizing efforts to
solve the problems. So, although many questions and arguments can
be and are raised with respect to this report, it is published essen-
tially as written by the author, as a significant and stimulating
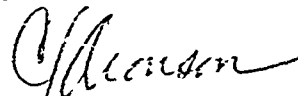contribution to knowledge of the origin of explosions.

ii

The experimental work for this program was conducted at the Denver Research Institute (DRI), Denver, Colorado, under various contracts with this Laboratory.

The disclosure of commercial instrumentation and materials in this report is solely for identification and does not constitute either endorsement or criticism of these products.

GEORGE G. BALL
Captain, USN
Commander

C. J. ARONSON
By direction

CONTENTS

TABLE

ILLUSTRATIONS

ILLUSTRATIONS (cont'd)

ON THE ORIGIN OF SHOCKWAVES
FROM CONDENSED EXPLOSIONS IN AIR

Part 3:   Airshock Radiation from Small Explosions
at Sea-Level Conditions

1.   INTRODUCTION

1.1 Background. Several years have now gone by since the appear-
ance of Part 2 of this series of reports on the early stages of an
explosion. During this time a number of experiments have been con-
ducted, aimed at clarifying how a shockwave is created by an
explosion. The need for these experiments arose out of the contra-
dictory results of Parts 1 and 2. In Part 1 (RUDLIN, 1962)[*], we
claimed that the earliest hydrodynamic disturbance created outside a
spherical condensed charge was the transmitted airshock -- resulting
from the passage of the detonation shock across the explosive boundary
into air. This mechanism is in distinct contrast to the situation
where the explosion products act like a spherical shock tube to create
an airshock.

With the transmitted-shock mechanism in mind, we thereupon planned
a series of 8-lb explosions of TNT charges. These were made of dif-
ferent densities so as to change the details of the transmitted
airshocks -- thereby changing the airshock pressures even out to large
distances and simultaneously establishing the significance of the
transmitted-shock mechanism. We could not, however, detect any
differences in the airshock pressure-distance curves from these
explosions (RUDLIN, 1963). We concluded Part 2 on these negative
results with the hope that further experiments and theoretical
treatments would be performed to clarify the early-time explosion
phenomena.

Theoretical calculations of TNT and pentolite explosions have
now been published (LUTZKY). We report on the experiments that have
been performed in this report.

1.2 Scope of this Report. The most vital assumption of Part 1
was that the luminous front moving out into air at earliest times
from an explosion is the airshock, exciting air to radiate during its
propagation. All measurements and interpretations were based on this

---

[*] References are given in alphabetical order in Section 6.

1

assumption -- almost universally accepted as axiomatic (see, for example, ZEL'DOVICH and RAIZER). During the course of our experiments we began to have reasons to question the validity of this assumption.

Initially, our experiments were primarily devoted to obtaining pressure measurements simultaneously with μ-second photography of an explosion so that we could correlate photographs (like those of Part 1) with p-t records (like those of Part 2) at earliest times. We ran into many difficulties with the pressure measurements (c.f., Appendix C) some of which we thought could be avoided by use of spectral measurements. We speculated, for example, that we could distinguish a "strong" shock from a "weak" shock by finding atomic lines in the spectra of the "strong" shock as contrasted with molecular bands to be expected from the "weak" shock. We were never able to detect in our spectral measurements those species expected from shock-excited air; i.e., we have not found any radiation attributable to the airshock (c.f., Appendix A).

There are several possible sources of light in an air explosion at the earliest times -- (A) the airshock, (B) the explosion products, (C) interactions between the products and the air. (A) Excitation processes by the airshock could produce light at or near the shockfront and even throughout the shockwave for those processes that require larger excitation times. (A description of this sort of a radiation model is given in Appendix D from the work of Adushkin.) (B) The explosion products themselves could produce chemiluminescent reactions during the expansion of the original explosive material, which reactions do not require the presence of any outside gas. (We have not found any suitable references in the literature for such a model of explosion luminosity, but this model certainly is possible.) (C) Particles produced by the explosion could interact with the outside gas producing luminosity which depends on the nature of the gas. (Evidence for this model on 13-gm explosions of pentolite spheres was obtained by REED. In these explosions, we should note that the airshocks appeared after the luminosity measurements were over.) It is possible that on a given explosion that light could be produced by any one, or more probably some combination, of the above mechanisms during the earliest stages of explosion. The most generally accepted model today, however, is (A) -- airshock-produced luminosity. Such airshock radiation has been found to be compatible with present theoretical estimates of the equilibrium radiation obtainable from shock-excited air species.[*]

When we failed to detect the presence of shocked-air radiation in our spectra of explosions, we, then, attempted to detect the existence of non-radiating airshocks from HE explosions at the earliest times after explosion.[**] We have used pressure sensors, ionization sensors, Doppler microwaves, and high-speed photography in our experiments to detect the early airshock.

[*] Personal communication of 22 Dec 1965 from Dr. M. P. Sherman, General Electric Space Sciences Laboratory, on high-temperature air radiation.
[**] We take zero time to be that of the first appearance of light from the explosion.

In the text of this report we present photographic evidence of strong, non-radiating airshocks. In Appendix A we repo t our spectrographic measurements and make comparisons with theoretical predictions for shocked equilibrium air. In Appendix C we report our experiences in attempting to detect the airshock with simple pressure and ionization techniques. Although these pressure and ionization records are not satisfactory, we have deduced from them a new model to fit our empirical observations which we propose for the release of energy from an explosion (Fig. C-8).

2. EXPERIMENTAL DETAILS

2.1 General. All charges were fired in the open at the East Range of the Denver Research Institute, under the direction of John Wisotski. Over one hundred explosions were observed by five photographic spectrographs and by several electronic detectors. Wavelength capability ran from about 2500 to 9000 Å. Time resolution capability ranged from none to a few μ-seconds on both photographic and electronic spectrographs. Simultaneously, μ-second photography observed the overall explosions. Most experiments were performed with 8-lb spheres of pentolite. But explorations were made over a charge-weight range from about 0.5 to 100 lbs and included several explosive materials and charge shapes. A tabulation of charge material, weight, and shape is given in Table 1.

Some views of the experimental set-ups are shown in Figures 1-5. Set-ups varied slightly from shot to shot to meet requirements. The following description fits most cases:

(1) Charges were fired at ~12 ft above the ground in front of a scotchlite screen, illuminated by an Air Force Flash-lamp (D-6)* to bring out shockwaves. The D-6 was located at the Instrumentation Station, typically 60 feet away. Charges were usually held in position by a cardboard tube support; no nets or ropes were allowed on the charge. All explosions, even with liquid explosives, were initiated by an Engineer's Special (Hercules) Detonator, usually positioned into the top of the charge and pointed toward the ground. Power for the detonator was obtained from a 5000v circuit across 1 μfarad (~1 ohm resistance). Reproducibility of detonation time, except for charges cooled to -50°F, was found to lie within 1 t 3 μsec. Detonator ringing was usually a feature on oscilloscope records, lasting for about 5-10 μsec.

(2) The Beckman-Whitley cameras were housed within one of the instrumentation shelters (c.f., Figure 1), about 60 feet away from the charge. Oscilloscopes and other electronic equipment were housed within the other shelter. Both shelters were made by cutting a refinery "drum" in half. The Beckman-Whitley cameras looked at the explosion by means of a front-surfaced mirror located ~4 feet outside of the shelter. A controllable shutter, depositing lead-vapor onto glass, was placed in the path of light to the camera to cut off light at the desired time. Despite the high attenuation of the lead-vapor shutter, some explosions were so intense that explosion light burned through the shutter, overwriting the desired frames of the earliest stages of the explosion. The other cameras, Dynafax, Fastax, etc. were used out in the open, looking directly at the explosion. Similarly, the spectro-scopes, both photographic and electronic, were used in the open. Sometimes lenses were used to increase the light

* Built by Raytheon for aerial night photography at medium and low altitudes (Manual AN 10-30AJ-1).

irradiance (always with the AVCO); sometimes not. Sometimes the spectroscopes were focused directly on the charge surface, thereby collecting light from all sources capable of radiating light; sometimes they were focused ahead of the charge.

(3) Close-in detection of the airshock (within about 10 charge radii (a_0)) was attempted with throw-away gages. These throw-away gages were made of micarta, roughly, 0.003 x 7 x 2 inches into which 1/8 x 0.004-inch quartz[*] discs were inserted. In the early versions, the leading edge of the micarta was rounded concavely to fit onto the surface of the charge and leads were painted on with conducting paint. Later, the leading edge was pointed and hardwire leads were soldered to the discs, the entire unit being coated with a silicone resin lacquer (G. C. Electronics Co.). The quartz discs were used with gold-chrome and silver-chrome coatings (Valpey Corporation). At larger distances than $10a_0$, tourmaline gages from Tulsa Laboratory were used. These same gages were used earlier to obtain the data of Part 2.

(4) Attempts to monitor ionization were made by using lead discs in a condenser-discharge circuit. These discs were about 3/4 inch diameter and about 1/16 inch thick. Prior to the explosion, a 0.002 µfd condenser was charged to its full voltage by a 90v source. So long as the resistivity across the explosive remained sufficiently high, the oscilloscope trace stayed at a neutral position. When, however, the detonation wave within the explosive, created enough conductivity from the center of the explosive (where the copper case of the detonator ended) to the edge of the charge, the condenser discharged, recharging upon removal of a sufficiently conducting path. Ionization was also monitored on a small number of explosions with 3-cm Doppler microwave instrumentation.[**]

2.2 Cameras. The Beckman-Whitley Model 192 camera, producing about 80 frames at µ-second rates, was used on each shot from #1 to #107. For later shots Model 189a, with 25 frames, was used. Camera speeds were varied over a range from about 250,000 to 1.2×10^6 fps, the former figure being most often used as appropriate for our requirements.

Most of the explosions had some additional camera coverage from one to all of the following:

a. Dynafax: nominal 25,000 fps; 75mm f/3.5 lens with 1-µsec step.

---

[*] A quartz disc, loaded hydrostatically on both circular sides, is known to produce no electrical signal. In our use in the throw-away gages, times to equilibrium for the quartz crystalline structure appear to have been long enough to produce a signal suitable, at least, to indicate the existence of a pressure pulse.

[**] The author is indebted to Mr. Donald L. Jones, then at the Boulder Laboratories of the National Bureau of Standards, for making these microwave measurements.

b. Fastax: nominal 5000 fps; 50mm f/8 lens

c. Eastman High Speed: nominal 2500 fps; 63mm f/2 lens.

2.3 Spectrographs (Photographic).

a. Cenco: Grating, Catalog No. 87102. Inverse dispersion ~16 Å/mm. No time resolution.

b. Jarrell-Ash: Grating, Model No. 78-000. Inverse dispersion ~11 Å/mm. No time resolution.

c. Hilger: Prism, Medium Quartz E498. Inverse dispersion ~5 Å/mm at 2200 Å, ~38 Å/mm at 4000 Å, and 200 Å/mm at 7500 Å. No time resolution. Field of view at charge (60 feet away) when used without a lens: 36 x 30 inches.

d. Cine Spectrographs: The streak instrument moved 70mm film at 25mm/millisec; the frame instrument discontinuously produced 5 spectra/millisec. The basic instrument has been described by STEWART and HARRINGTON. Inverse dispersion by prisms varied on both from about 40 Å/mm at 2700 Å to about 400 Å/mm at 6000 Å. Millisecond time markers were automatically provided on both instruments. A novel feature of the frame spectrograph is the availability of light attenuators so that five different images of the spectrum can be recorded simultaneously, at transmission values of 100, 30, 10, 3, and 1 percent. Both instruments are built sturdily for use in the open. Our two spectrographs were of Canadian design and manufacture* and differ in minor details from the descriptions by STEWART and HARRINGTON. Lenses were seldom used on these instruments, which we estimate have effective f/numbers of about f/6. In such use, without a lens, the field of view of either is about 20 x 20 feet at 60 feet away.

e. AVCO Streak Spectrograph: This instrument was developed by the Denver Research Institute especially for use on these explosions. Matched Eastman Aero-Ektar f/2.5 lenses are used for condenser and collimator lenses, so as to present a 1:1 image ratio to the 60° dense-flint-glass prism. The slit system used is the Hilger & Watts F 1386 symmetrical slit. A Bausch & Lomb f/4.5 10-inch lens is used to focus the slit onto the rotating mirror of the AVCO camera (Model MC300-1). This mirror streaks the spectrum onto two pieces of 70mm film. As used, these films were often of different spectral response to obtain more comprehensive coverage per shot. We estimate the effective f/number to be about f/6.

Writing speeds up to ~3.8mm/µsec can be obtained. Most often we found that a speed ~1.5mm/µsec was appropriate for these explosions. No timing markers were available.

---

* We are indebted to Dr. P. A. Tate, DREO, Ottawa for making these spectrographs available to us.

In use, the AVCO has always been focused with a fused-quartz lens on the charge or slightly ahead for a tangent view of the luminosity. At the charge, usually 60 feet away, the AVCO could see a rectangle that was varied slightly with requirements: in height, from 1 to 4 in. and in width, from 0.04 to 1.0 in. When used to look directly at the charge, this view was focused at the center of the charge. Inverse dispersion of the AVCO: between Hg lines 4047 and 4358 Å, ~80 Å/mm; between Hg lines 5460 and 5780 Å, ~237 Å/mm.

2.4 Spectrographs (Electronic).

a. Py-I: The Pyrometric Instrument (Py-I) was developed at DRI for obtaining thermometric data on blackbody radiators and designed to meet those particular needs (KOTTENSTETTE). We have, however, found it to be a useful instrument for explosions. In this instrument photodiodes (of the size used to read IBM-card holes) were placed on the back face of a prism; each sees only those wavelengths of the light that are dispersed to it. Each photodiode integrates over its own particular wavelength interval as a function of time, the output being sent to an oscilloscope with μ-second resolution. We estimate that the response time of any photodiode was about 3 to 5 μsec as used with an Electron Tube Corporation Model K480 4-beam oscilloscope.

Five "bands" -- that is, wavelength intervals -- could be used. Unavailability of oscilloscope channels usually limited our use to only 3 bands. Two different Py-I versions were used for these experiments. We list the band passes for both (10% transmission points):

	Shots 40-84		Shots 84-117	
	Range	Peak	Range	Peak
Band 0	5160-5840 Å	5330 Å	4350-5300 Å	4550 Å
Band 1	5500-6350	5910	4850-5900	5350
Band 2	6000-7150	6500	5400-7000	6400
Band 3	6650-8200	7310	6350-9500	7200
Band 4	7500-9660	8480	8100-11,250	9500

Fore-optics were used to see an area 2-3 in. in height by 1/4-3/4-in. in width at the charge. This accepted light passed to a mirror and, finally, to a prism before reaching the photodiodes.

b. Other photoelectronics: Although the rugged and reliable Py-I was the workhorse for photoelectronic measurements, upon occasion, other detectors were used. These include Solar Cells, 1P28, 931, and SD-100. In all cases these were used without fore-optics and, therefore, viewed the entire presented area of the explosion. These signals were fed to oscilloscopes with μ-second resolution.

2.5 <u>Oscilloscopes</u>. Two 4-beam oscilloscopes (Electron Tube Corporation, Model K-480) were available, giving a total of 8 available channels for recording. Sample records from Shot 55 are shown in Figure C-2.

2.6 <u>Films</u>. A variety of films was used. On the cameras, color films were almost universally used -- primarily Eastman High-Speed ER and EF Ektachrome.

On the spectroscopes, 35mm and 70mm films were used: Eastman Tri-X, Shellburst, High-Speed Infrared, 2475, and 2485.

2.7 <u>Calibration</u>. No intensity calibrations were made since our interests were qualitative. Wavelength calibration was placed on most spectral films by use of a mercury lamp, prior to each shot. The readily identified CN, Ca, Ca^+, and NaD wavelengths, nearly always found on each explosion, could also be used for wavelength identifications.

2.8 <u>Charges</u>.

    a. Various explosive materials were used:

        TNT (cast and pressed)
        pentolite (cast)
        PETN (loose powder and pressed)
        RDX (loose powder)
        NM + TNM (nitromethane and tetranitromethane, liquids)
        RDX + TNM (solid below critical temperature)

    b. Charges were usually spherical but cones and rectangular blocks were also fired (see Table 1). Most cast charges were made at the Naval Ordnance Laboratory and shipped to Denver for firing. Some, however, were cast at DRI. All explosive materials came from the same lot of material to avoid variations from lot to lot of the "same explosive".

    c. Only one type of detonator was used for all explosions -- Engineer's Special (Hercules). Only one failure to explode was encountered during the 117 events.
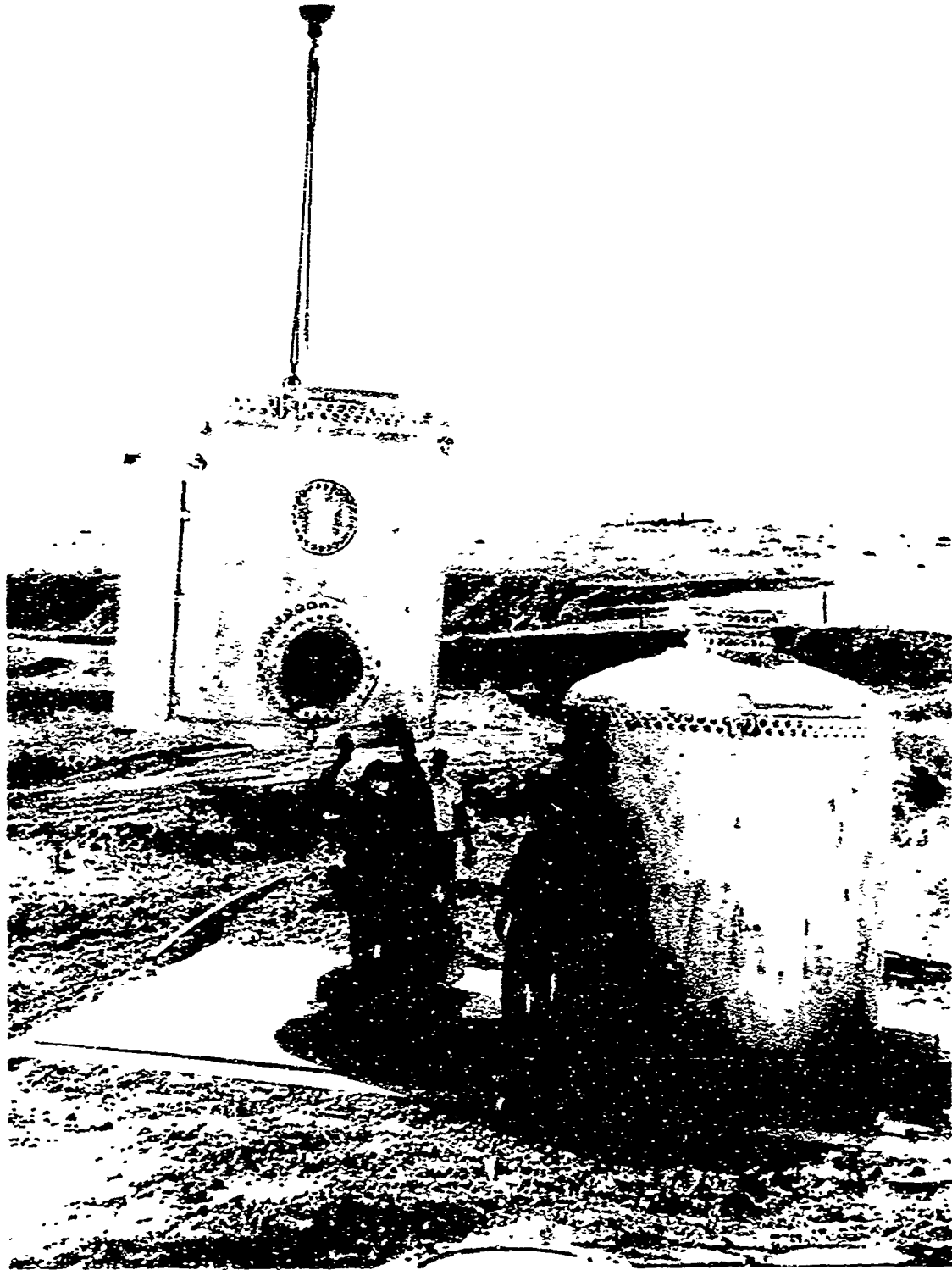
FIG. 1 INSTALLATION OF INSTRUMENTATION SHELTER OVER BECKMAN-
WHITLEY CAMERA AT DRI RANGE.

FIG. 2 SET-UP FOR 9-LB PENTOLITE SHOT 74. ON TOP OF THE CONE IS A 0.5-LB HEMISPHERE PENTOLITE BOOSTER. ARROW-LIKE OBJECTS SUPPORT TINY PIEZOELECTRIC GAGES. BACKBOARD IS SCOTCHLITE SCREEN.

FIG. 3 SET-UP FOR 8-LB PENTOLITE SHOT 98. THE DETONATOR LEAD CAN BE SEEN AT THE TOP OF THE CHARGE, WHICH IS SUPPORTED ON A CARDBOARD TUBE. BRIGHT OBJECT ATTACHED TO THE RIGHT-HAND SIDE OF OF CHARGE IS A LUCITE TUBE. BACKBOARD IS SCOTCHLITE SCREEN.
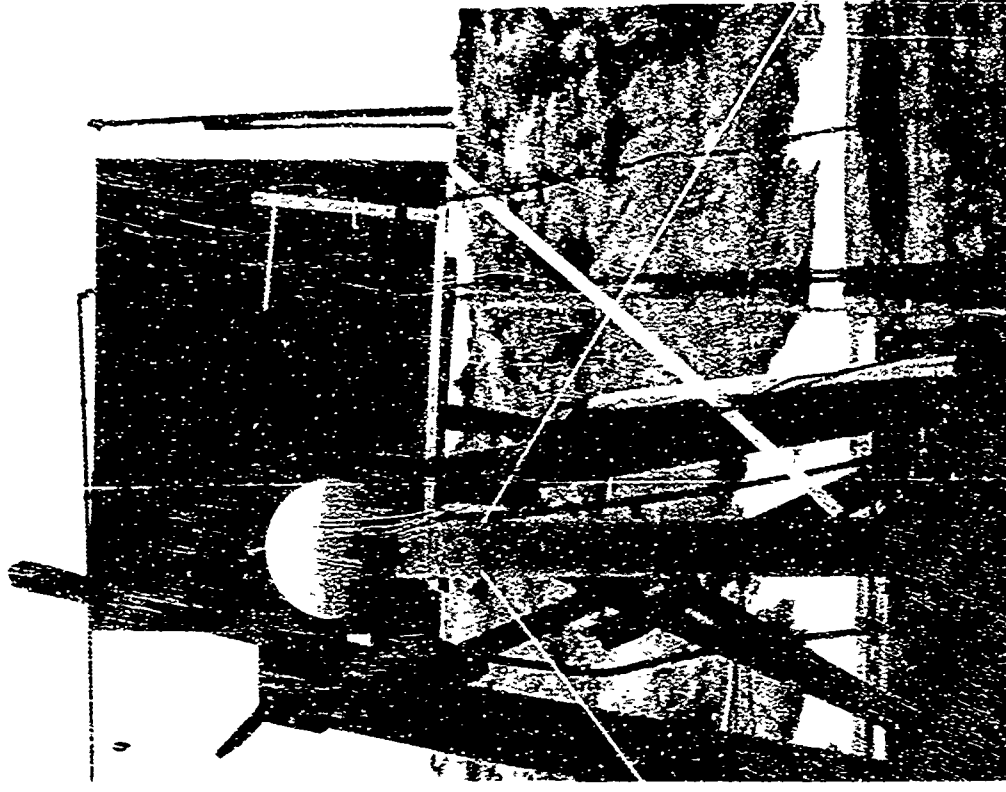
SHOT 73 (32-LB TNT)
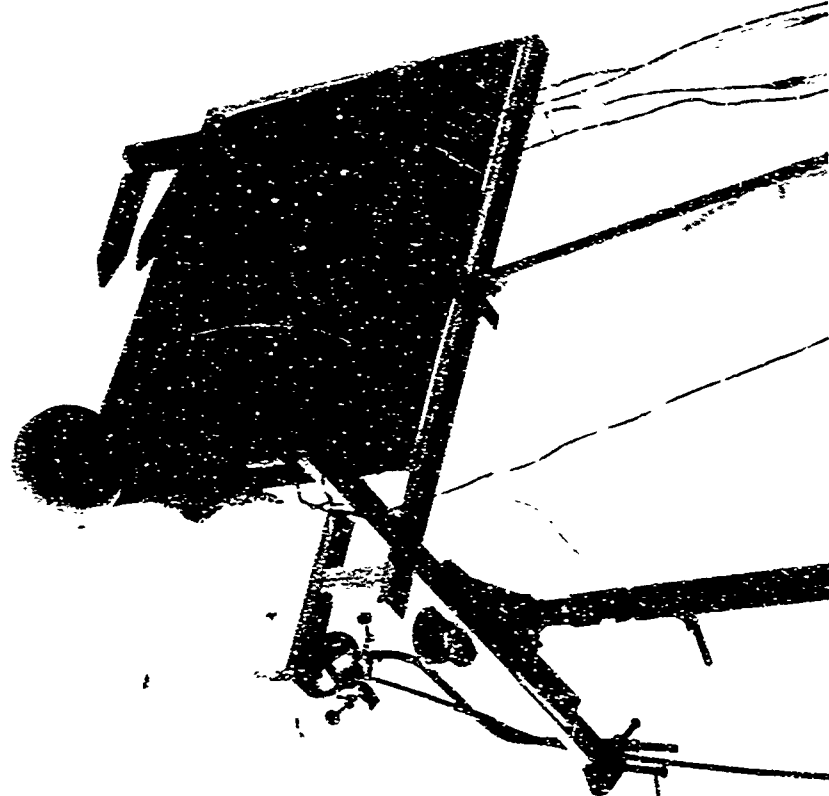
SHOT 52 (8-LB PENTOLITE)

FIG. 4   Typical set-up pictures. Throw-away quartz discs are mounted in the micarta holders, seen above pointing at the charge, 1/4 inch from each point. The hard-wire leads to the discs can be seen weaving in and out of the micarta. Behind charge of Shot 52 is argon lamp, excited by explosive to give backlighting for charge. In background of Shot 73 is a scotchlite screen, on which are fiducial markers and shot number.
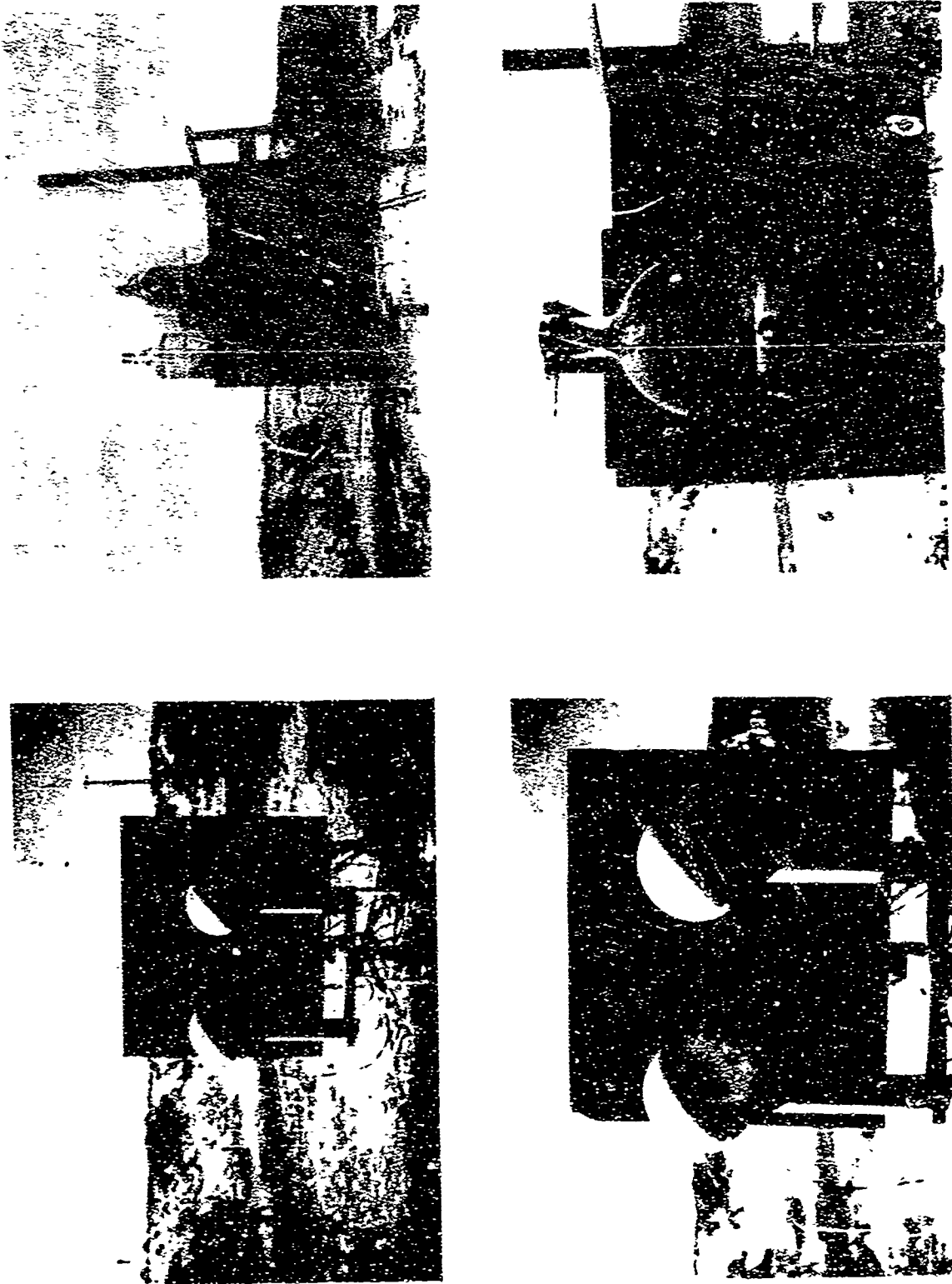
FIG. 5 SET-UP VIEWS OF TWO 8-LB PENTOLITE CHARGES USED FOR SHOT 88 AND MIXING OF TNM WITH NM (DONE REMOTELY) FOR SHOT 84. DISCS ON BOTTOM OF PENTOLITE CHARGES ARE IONIZATION GAGES. ARROW-LIKE OBJECTS IN SHOT 84 SUPPORT TINY PIEZOELECTRIC GAGES. BACKBOARDS ARE SCOTCHLITE SCREENS.
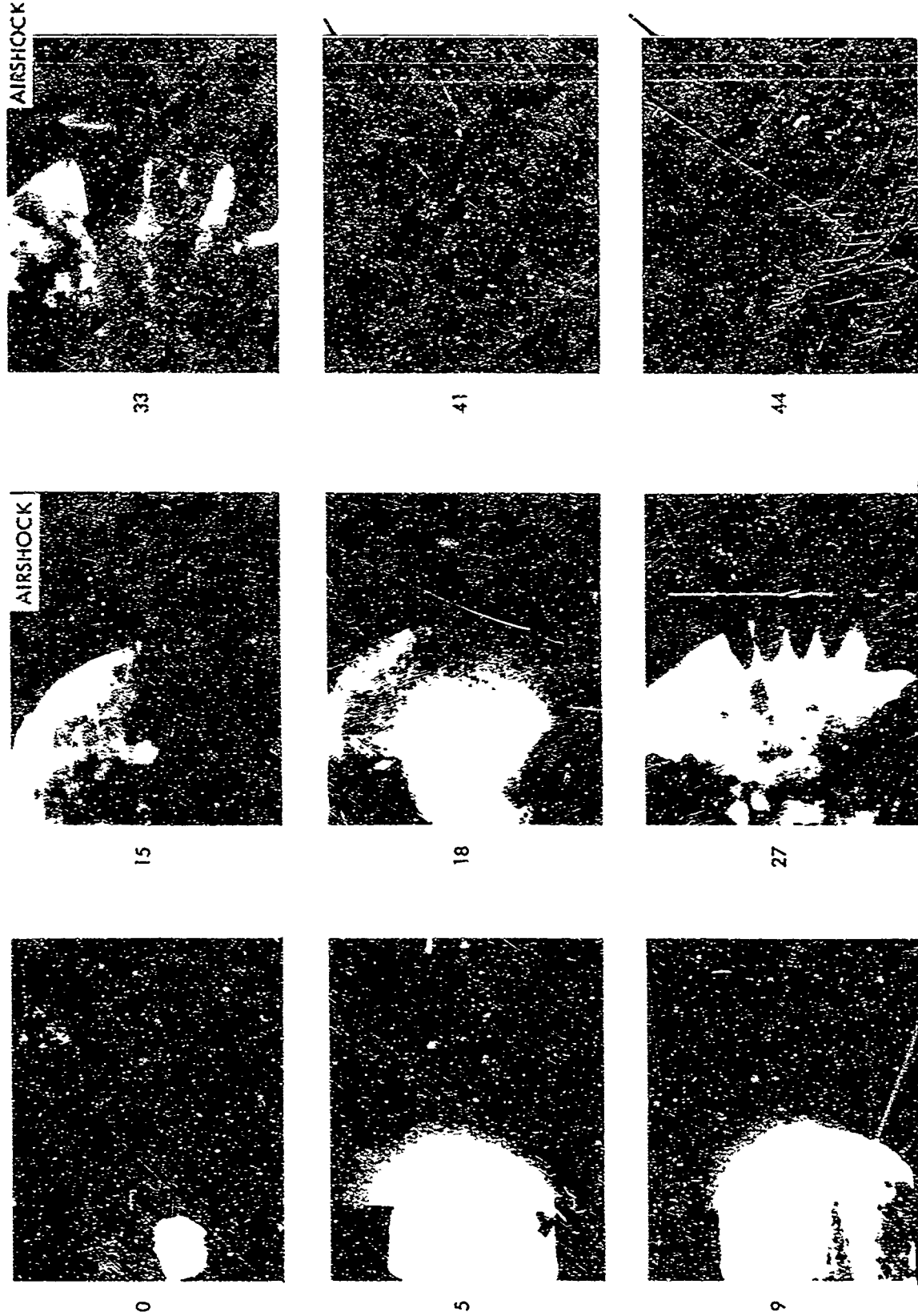
FRAME

TIME BETWEEN FRAMES ~ 4 μ SEC

FIG. 6   2.6-1.B RDX EXPLOSION (SHOT 55)

FIG. 70 RADIUS-TIME GROWTH

PENTOLITE 8-LB SPHERES

1 — SHOT 45
2 — SHOT 43
3 — SHOT 49
4 — SHOT 50
} SLOW CAMERA

5 — SHOT 77
6 — SHOT 78
7 — SHOT 82
8 — SHOT 83
} FAST CAMERA

○ ION-GAGE ARRIVAL
□ P-π GAGE ARRIVAL

CURVE: WUNDY PENTOLITE

DISTANCE (R/a_o)

TIME $\left(\frac{t + r}{r}\right)$
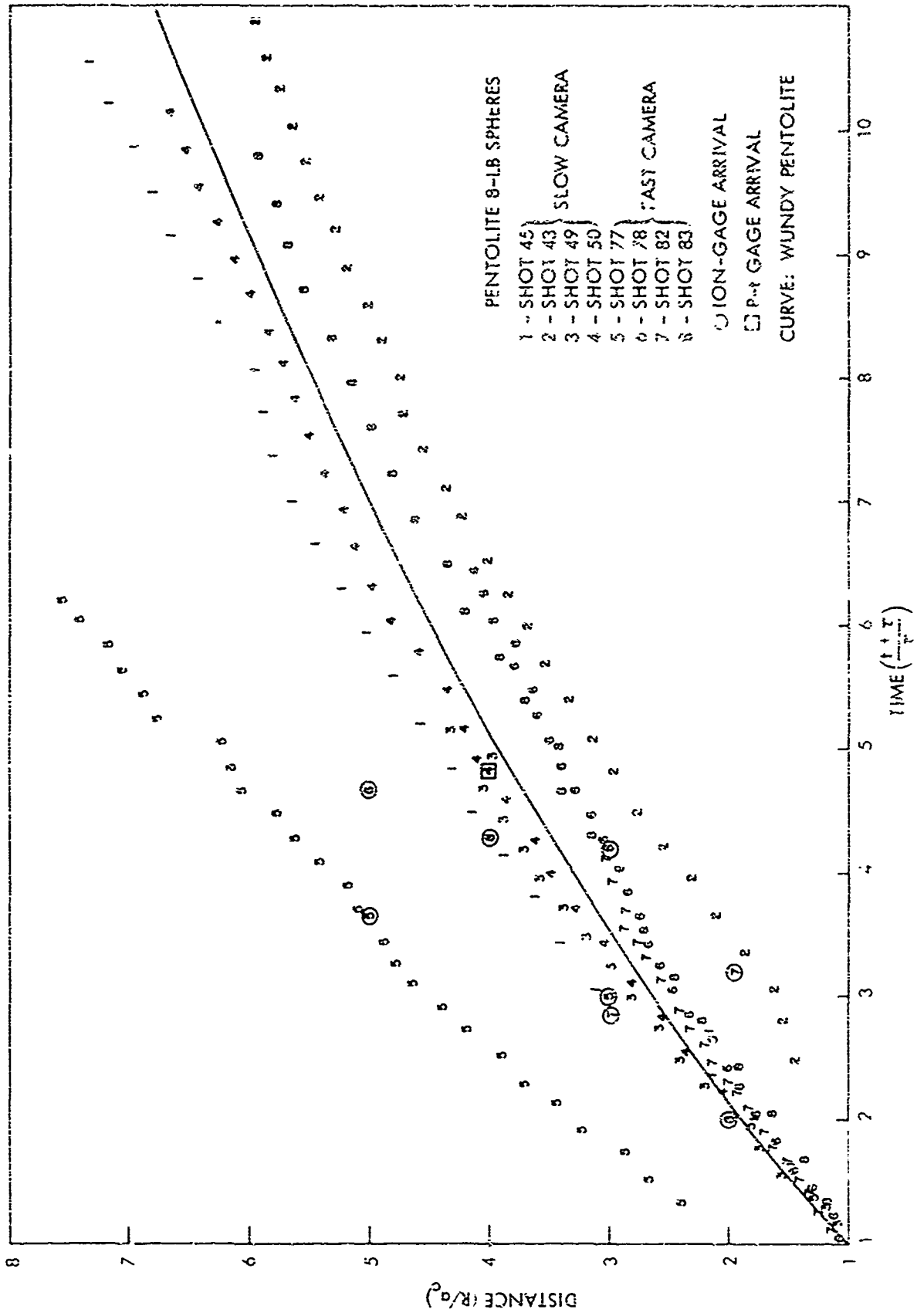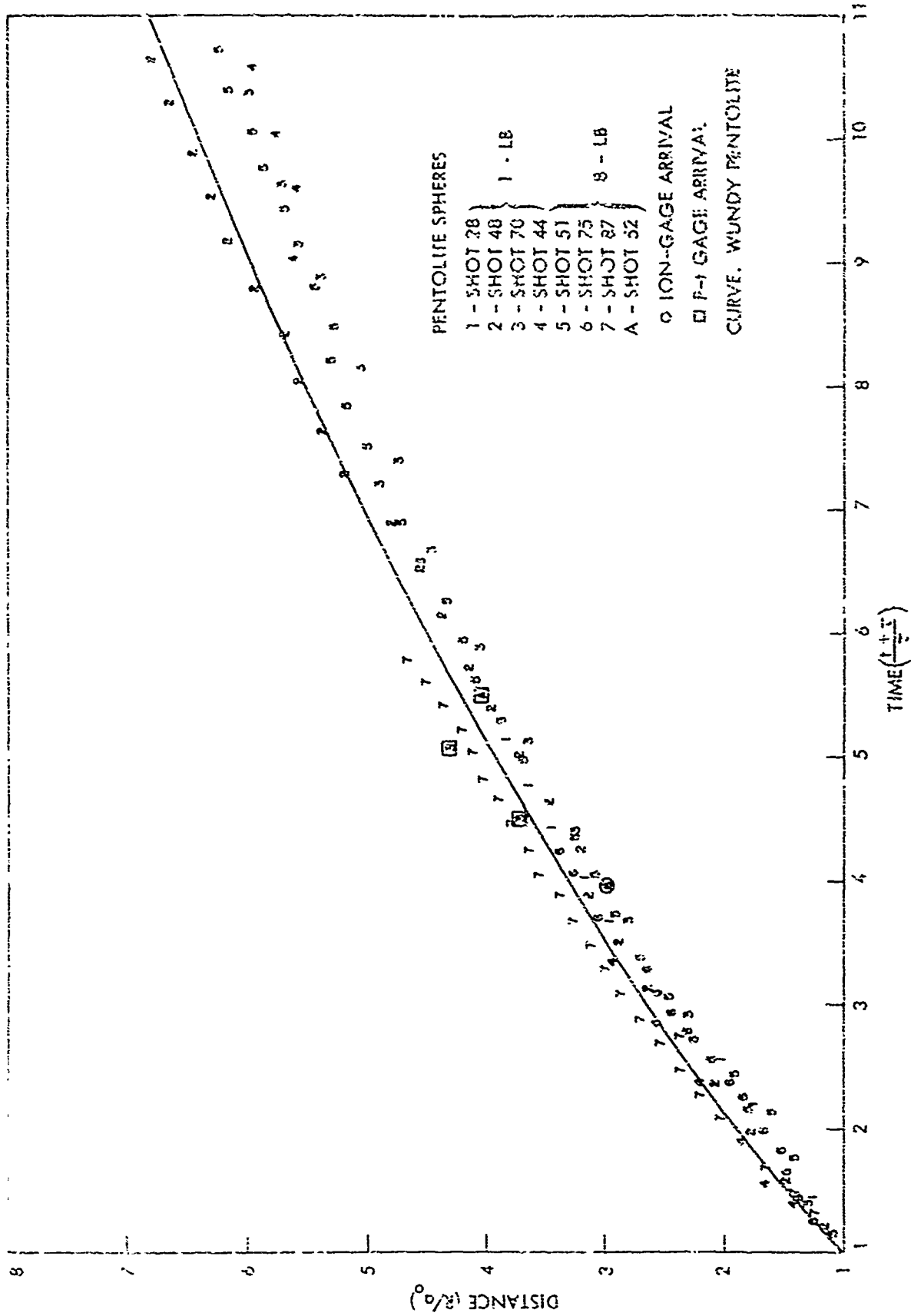
FIG. 7b   RADIUS-TIME GROWTH
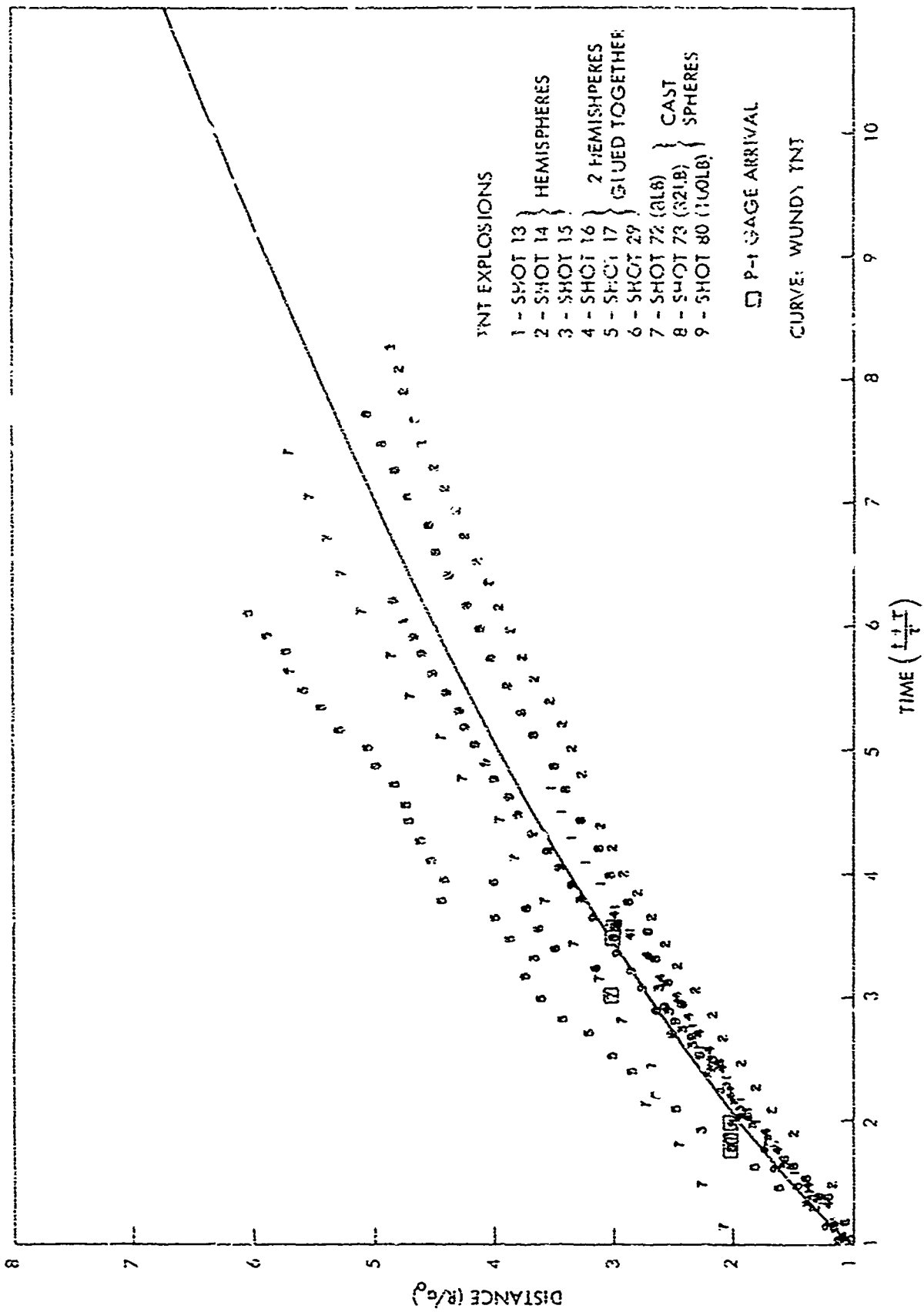
FIG. 7c RADIUS-TIME GROWTH

FIG. 7d RADIUS-TIME GROWTH

SPHERICAL EXPLOSIONS

1 – SHOT 56
2 – SHOT 58 } NM +TNM
3 – SHOT 84
4 – SHOT 67 } RDX + TNM
5 – SHOT 27 } PETN
6 – SHOT 21 }
7 – SHOT 8} COMP B
A – SHOT 76} PETN

O ION-GAGE ARRIVAL
□ P-t GAGE ARRIVAL

CURVE: WUNDY PENTOLITE

FIG. 7e   RADIUS–TIME GROWTH

PENTOLITE EXPLOSIONS

● FAST CAMERA, 8 LB (SHOTS 77, 78, 82, 83)
○ SLOW CAMERA, 8 LB (SHOTS 43, 45, 49, 50)
□ UNUSUAL, 8 LB (SHOTS 44, 51, 75, 87)
△ 1 - LB (SHOTS 28, 48, 70)
CURVE: WUNDY PENTOLITE
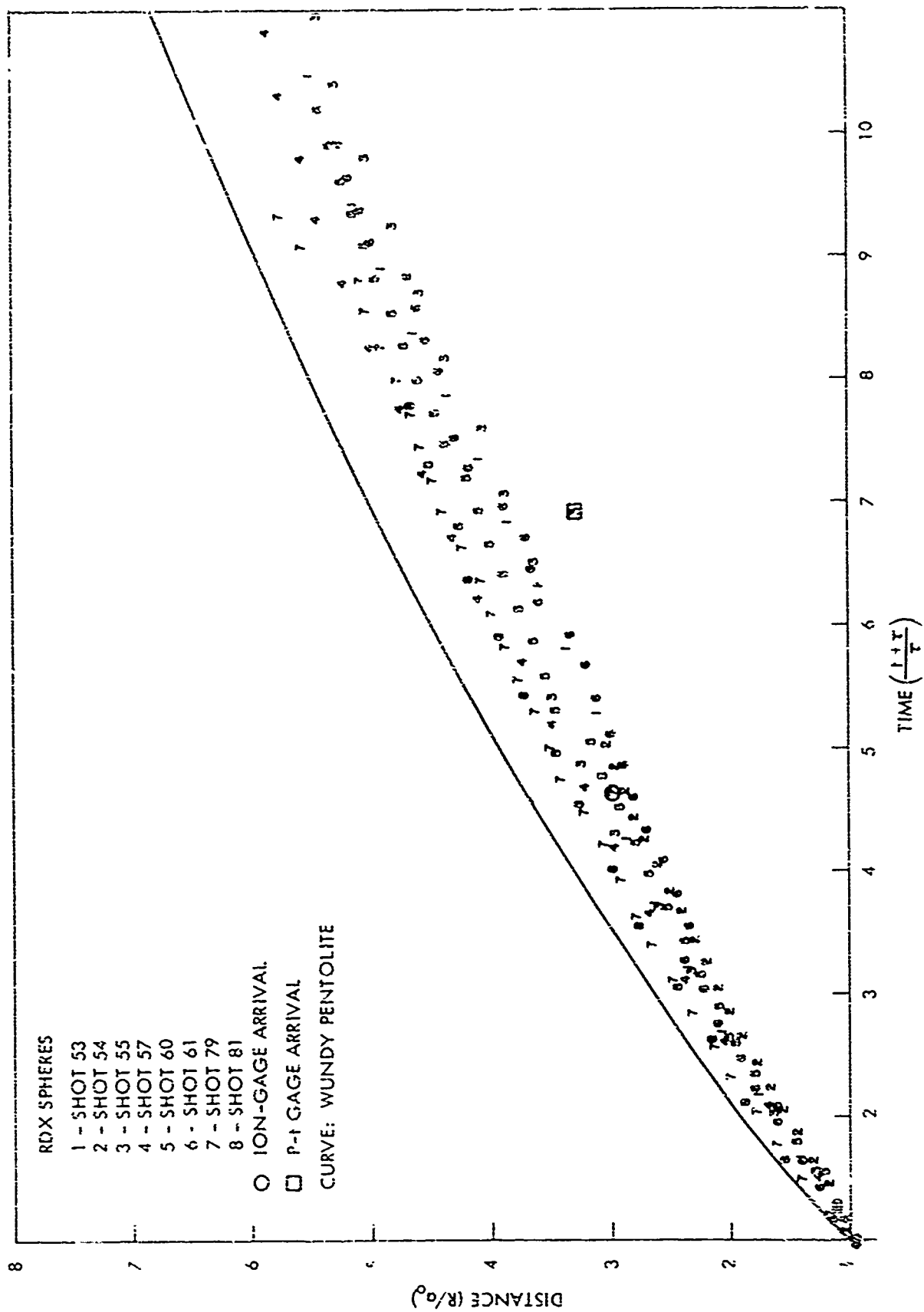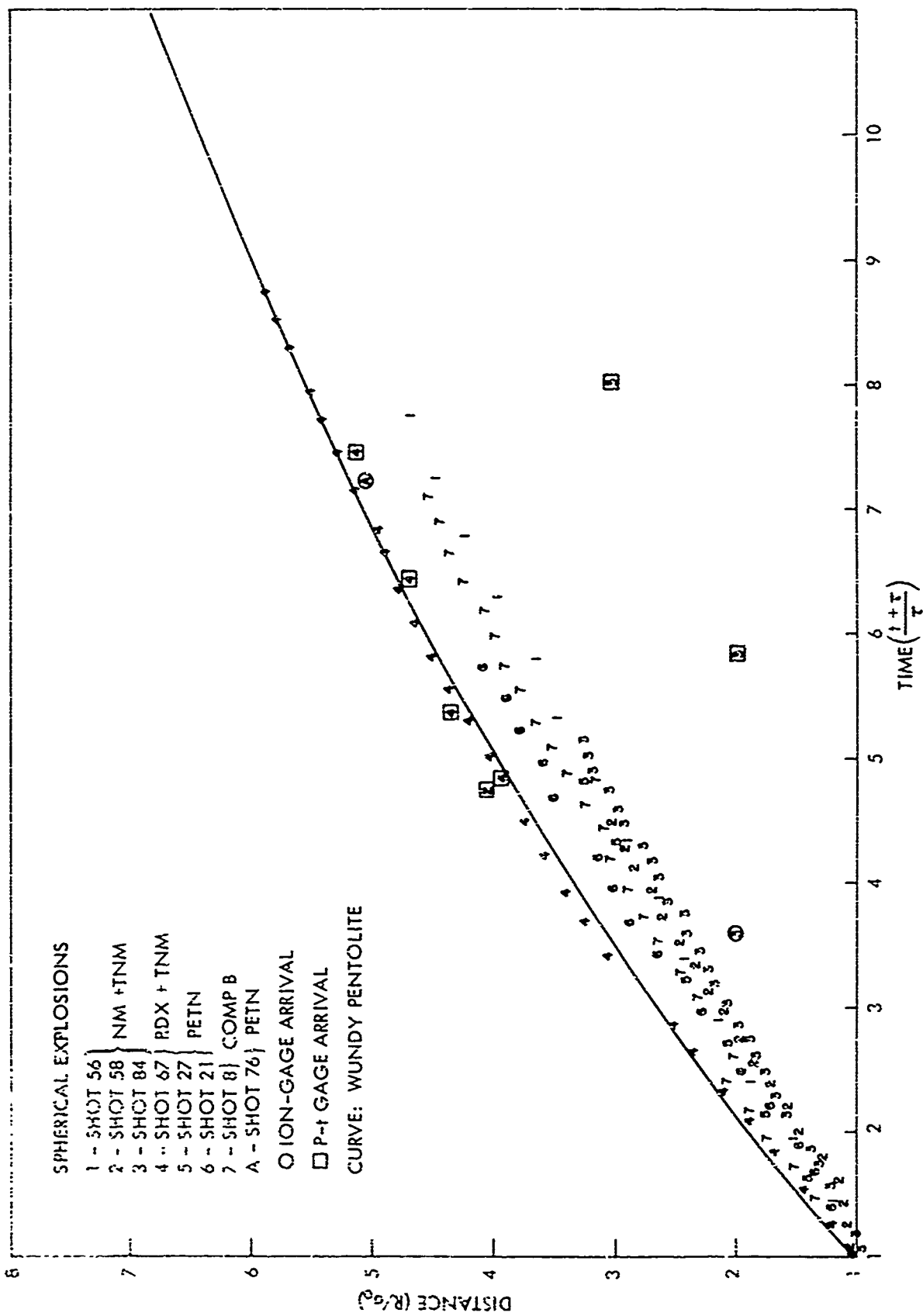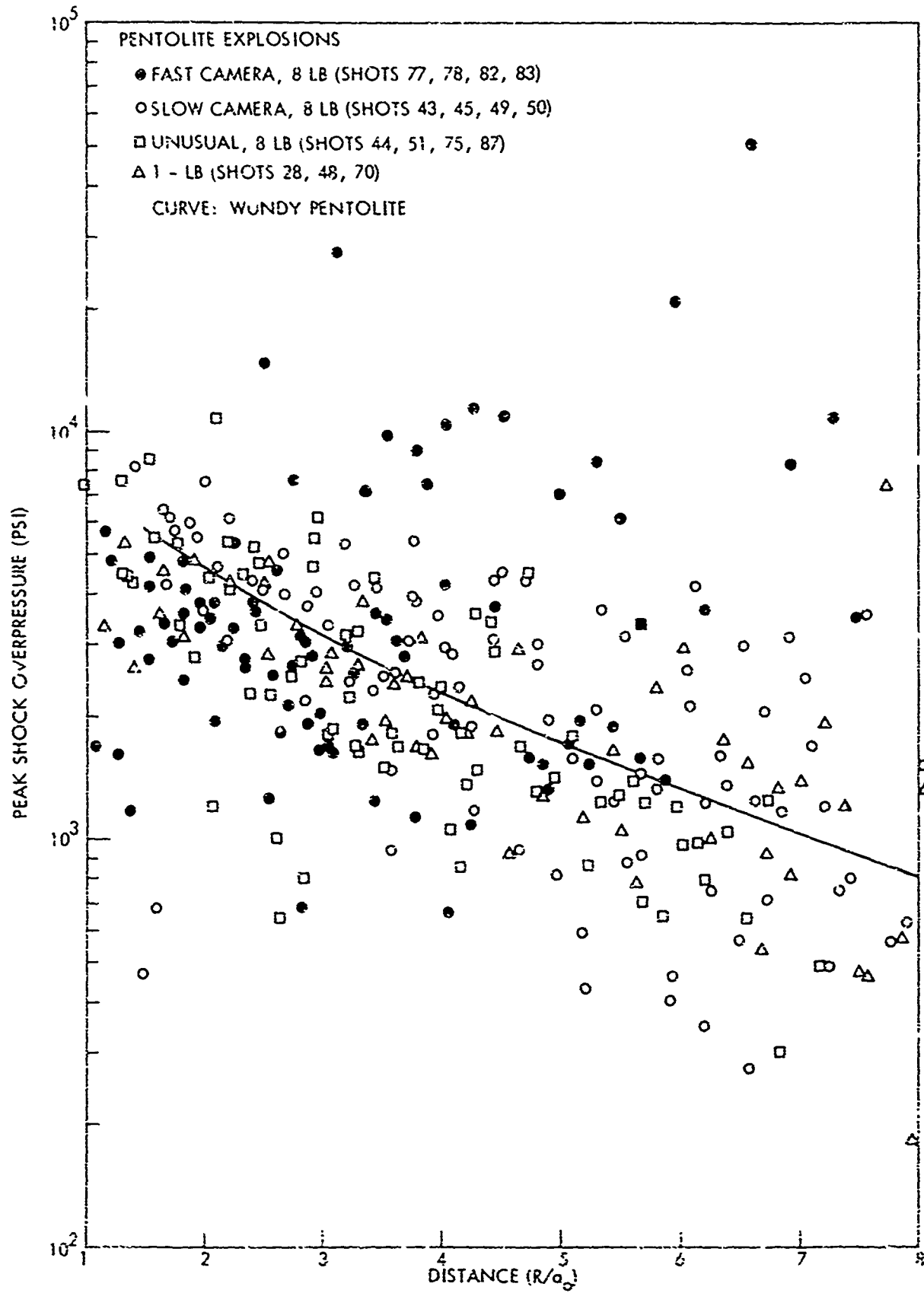
FIG. 8a SHOCK PRESSURE VS. DISTANCE

3. RESULTS

3.1 Typical Early Explosion History. A μ-second Beckman-Whitley
color film was taken of each explosion using a scotchlite background.
Black-and-white reproductions of selected frames from a sample film
(Shot 55) are given in Figure 6. In Frame 0 the charge has not yet
been completely detonated. The loose-powder charge was made by hand-
packing RDX powder into a 5-inch diameter lucite sphere. Just before
firing the upper lucite hemisphere was removed, so that we see initially
in the films two different surface -- the lower hemisphere, lucite;
the upper hemisphere, RDX -- which have different radiating properties.
The four pointed objects to the right are micarta holders for pressure
sensors (Appendix C). The grid pattern which appears in the back-
ground was superimposed onto this particular film prior to the explo-
sion. The light grey backgrounds are scotchlite screens used to aid
in visualizing shockwaves.

By Frame 15 the fireball has passed over the quartz discs located
close to the points on the holders. The dark front about the bright
fireball is the airshock, which we can recognize more easily in
later frames when the airshock has left the fireball. The bright
spot in the center of the fireball is light, created at the scotchlite
screen by the explosion products being suddenly heated up by the
collision with the screen. The opacity of the RDX fireball is much
less than that of TNT fireball and the "reflected" light created at
the screen easily burns through the RDX fireball.

By Frame 27, the airshock has left the fireball sufficiently
behind to be easily recognizable. At this stage, the airshock has not
yet achieved the smooth front that appears later and the front still
carries some irregularities from the expansion of the explosion
products. We can see in this frame that the micarta holders have
remained intact even within the fireball.

In the subsequent frames, the airshock can be seen moving farther
away from the fireball. We note in Frame 41 that radiation is
excited at the support for the micarta holders by the airshock. The
yellow color of this light on the original color film suggests that
this light is from the sodium-D lines.

Airshocks can first clearly be seen on our μ-second films only
when the fireball has expanded to 3 or 4 a_o (a_o = 1 charge radius).
These then appear as non-luminous, black fronts propagating away
from the brightly luminous fireball. The time taken for the shock
or, better, the luminous front to reach 3-4 a_o is of the order of
tens of μ-seconds, say 30-50 μsec. By such times most of the light
in the blue and in the visible has disappeared on our spectral records.
(c.f., Appendix A). To find spectra from the airshock itself we
needed to locate the airshock at much closer-in distances than 3-4 a_o.
and to separate, if we could, the airshock radiation from the
intense fireball radiation.

Many of our experiments were planned toward that end. We need
not describe them; they failed to reveal a luminous close-in shock.
One such experiment, for example, was tried twice (#87 and #88).
The intent was to increase the temperatures and pressures at the
front of the airshock by colliding it with another airshock. (We
did not want to reflect one shock off a target -- that would only
serve to increase impurity radiation.) The result of these airshock-
airshock collision experiments was to create more intense, longer
lasting wavelengths from fireball species.

3.2 Radius-Time and Derived Pressures. Measurements were made
of the luminous-front growth (and thence of the airshock, if it
could be detected) on our μ-second films. These were made on a
Telereadex machine for direct processing by an IBM-7090 computer.
The results are given in Figures 7a through 7e. We make the
following comments:

      a. Not all films could be read -- r-t data or fiducial
markers were missing, edge of image too indistinct, etc.
The films are not all equally suitable for r-t data, since
the frame rate varies over a wide range. On many films we
were willing to obtain less sharp images (the exposure time
per frame increases with longer interframe time) in order
to record for longer times. Typically, the non-luminous
shock cannot be separated from the bright fireball until
about 5 or 6 a_0. In Figure 7a, we purposely separated our
films into two groups: slow (interframe time $\sim$4 μsec or
more) and fast (interframe time $\sim$2 μsec or less).

      b. We measure distance from the center of the charge in
units of the radius of the charge, a_0: R/a_0. We measure
time from the arrival of the detonation wave at the surface
of the charge. We first see light, therefore, on the
explosion at $R/a_0 = 1$ and $(t + \tau)/\tau = 1$, where τ is the time
taken by the detonation wave to travel from the center
of the charge. Because the detonation wave is not symmetrical
and does not break out all over the charge at the same time,
measurements were made along several rays emanating from
the center of the charge and corrections were made to a
common value of time for $R/a_0 = 1$ and $(t + \tau)/\tau = 1$ along
each ray.

      c. Plotted in each Figure is a solid line from our WUNDY
hydrocode[*] for the theoretical curve, either for pentolite
or TNT.

      d. We see that the experimental scatter is large. Partly,
this large scatter is caused by our not using the highest

---

[*] These calculations are similar to those discussed by LUTZKY. They
are, however, not identical. These later results are believed to be
more accurate than the earlier results obtained by LUTZKY because
of a number of computational improvements. The author is indebted to
Mr. Delbert L. Lehto for carrying out these new WUNDY runs.

camera speeds available; but mostly, we think, the scatter
is inherent in the explosions themselves. The unusual
behavior of pentolite Shot 77 and TNT Shot 17, lying far
above the other explosions is mystifying; we have not been
able to find an explanation.

e. For explosives other than TNT or pentolite we have used
the pentolite theoretical curve as a basis for comparison,
in lieu of explicit calculations for these explosives. The
scatter in these data seems less than that for TNT or
pentolite, RDX data being rather reasonably together.

f. Scattered throughout the plots of Figure 7, we have
included arrival times for p-t and ion sensors (see
Appendix C) when such data were available. In some cases
agreement is fair to good; in others, poor.

With the r-t data from these explosions we should have been
able to process, by one of our computer programs (such as discussed
in LEHTO and BELLIVEAU, or in Part 2, or in RUDLIN 1967), the data
to obtain shockfront pressures. We could not do so.

The difficulties lay not so much in the scatter of the data which
is troublesome, but more fundamentally in the nature of the procedure.
This procedure involved fitting an arbitrary function to the r-t
data which was then differenciated to give shock velocity, these
velocities then being transformed to pressures via the Rankine-Hugoniot
relations. We found that the fundamental problem was that these
arbitrary functions (such as polynomials, log functions, etc.) could
not be forced to fit the close-in explosion data with any physical
significance. This was in distinct contrast to past situations
where far-out explosion data have been fitted with ease.

A new data-handling procedure, therefore, had to be developed,
which did not depend on arbitrary functions. We used the slope
between successive frames of a given film to give a velocity value
from which a pressure could be computed from a real-air equation of
state.

The results from this computer program for the close-in shock
pressures are given in Figures 8a through 8d. The scatter in these
computed pressures is so large that we have not drawn any "average
curve" through them. Instead, we have superimposed the theoretical
curves of pentolite and TNT as a basis for comparison. About all
that we can conclude is that the theoretical curves make fair
"average curves" for pentolite and TNT. The scatter in these
pressure results is real -- that is, we have not forced it in by
the computational procedure -- and we can do no better because the
camera data themselves have large scatter.

3.3 Close-in Airshock Observations. Airshocks have been
routinely observed leaving the luminous fireball front at distances
of 5 to 6 a_0. With especially good observation conditions we have
detected the airshock at 3 to 4 a_0.

11

On three occasions we were able to photograph airshocks at
distances < 3 a_0. They are especially intriguing because they show
essentially non-luminous shockwaves at high enough pressures and
temperatures that we should expect luminous shockwaves.

We proceed to discuss these three significant experiments in
some detail.

     a. Experiment (1) Laser Photography (#89-100): We planned
to filter out fireball light as much as possible and use a
laser beam to locate the airshock by refracted light off
a scotchlite screen. A set of shots (#96, 97, 98) is
shown in Figure 9a and b.

Pentolite spheres were detonated by placing detonators at
the top of the charge, accounting for the protuberances
visible at the top of charge. Black diagonal stripes were
painted on the usual scotchlite material to help in detecting
the airshock at an early time. A 20-kilowatt ruby laser
was used to probe for the airshock. The laser beam had
broadened to an ellipsoidal shape at the screen, of width
about 4 a_0. The laser pulse used was rather odd, consisting
of 100-nanosec pulses every 2 μsec for a total pulse duration
of ~0.5 millisec. This pulse behavior accounts for the odd
appearance of the frames shown in Figure 9. Unless a frame
on the Beckman-Whitley camera and a laser pulse happened
to fall together, no light would have been observable on
the scotchlite screen.

In column c, Frame 3 (Figure 9a and c), is the earliest time
that we have detected the airshock in a straight-forward
pentolite explosion. A bright ring or halo of light sur-
rounded the fireball in Frames 1 and 2 and we see only a
slight indication of the dark shockfront in Frame 2. In
Frame 3 the shock first clearly appeared -- a dark ring
ahead of the bright halo seen in Frame 2. The shock con-
tinued staying ahead of the luminous fireball throughout
the film. Because of the laser and the filtering, we have
reduced the time for first observation of the airshock to
about 4 μsec and the distance to about 0.4 a_0 from the
original charge surface.

We summarize these laser experiments: with suitable
photographic conditions the airshock can be detected at
less than half a charge radius from the surface of a pen-
tolite charge, at a time, roughly, of 4 μsec. The airshock
appeared in front of the fireball luminosity, staying ahead
from then on. By 30 μsec, or ~3 a_0, the airshock began to
separate from the fireball. During this time, 4 to 30 μsec,
the shock speed averaged about 0.5 cm/μsec, or an average
Mach number of M = 17.

b. Experiment (2) Convergent Shocks (#108 and 109): With
the help of the laser light source we have found the air-
shock at less than $1/2 a_0$. But where is the airshock before
that? The fireball lightfront moves so closely to the
airshock during these earliest stages of an explosion that
it makes observation of the airshock difficult, perhaps
impossible.

What we needed to do was to separate the shock from the
fireball. We hoped to accomplish this by converging a
section of a spherical explosion. As we converged, the
shock could move off from the fireball -- since the shock
has no fundamental limitations, whereas the chemical
reactions creating the light of the fireball would likely
be rate limited. We planned to create this convergence
by ramming a spherical charge into the large end of a
conical cavity.

The set-up used is shown in Figure 10. The cone was cast
in a 14-in long block of ice, converging from about a
5.8-in diameter hole at the large end to about a 0.5-in
diameter hole at the small end. A mirror was placed at a
slight distance from the small end. The explosion was
illuminated by the D-6 flash lamp.

In the first frame of Figure 10 the 8-lb pentolite sphere
had just gone off. In Frame 4 the charge had expanded and
a luminous front within the cone can be seen. In Frame 11
this luminous front was just about ready to leave the
block of ice. In Frame 15 the luminous material had already
moved out and away from the ice. On the top of the block
a dark shock can be seen a centimeter or two ahead of the
original fireball. This non-luminous shock continued
pulling ahead in later frames. In the next frame shown,
Frame 18, this shock had excited some luminosity of its
own, which can be seen at the foot of the shock and rising
into the original fireball. Probably, most of this light
is from the Na-D lines. In the same Frame 18, a non-luminous
shock had formed about the ejected luminous material. A
second puff of material had now been ejected from the hole
in the block. Finally, in the last frame shown, we see
that the non-luminous shock about the ejecta had moved
several centimeters away from the material. (On the
original color film, the first puff was still radiating
in brilliant white but the second puff had cooled to a much
lower intensity than the first puff.) We also note that the
shock atop the block of ice had fallen behind its luminous
front, which had now steepened and climbed up behind the
shockfront.

We had not expected the phenomena observed. We had expected
to see, first, a converged airshock, followed by the material
which forms the fireball. The pictures of Figure 10 do not

13

show this converged airshock. Ins'··.d the shock seems to
have been formed by the ejected puff of material.

But we have observed two non-luminous airshocks in this
experiment -- the ejecta shock and the shock atop the ice --
which are fairly strong shocks. The ejecta shock moves
out at ~ 0.4 cm/μsec (M = 13); the ice-block shock,
approximately half this speed. If equilibrium conditions
could have existed, the ejecta-shock speed would have
corresponded to a temperature of about 5500°K and a pressure
of 3000 psi.

c. Experiment 3 (#117): An airshock has also been observed
closer in than 3-4 a_o on a hemispherical explosion of
(NM + TNM). This observation was accidential: The experiment
was designed primarily for other purposes.

Selected frames at an interframe time of about 2 usec are
shown in Figure 11. The two liquids, nitromet.ane and
tetranitromethane, were mixed remotely into a lucite
hemisphere. The liquid surface was left open. The mixture
was fired with the usual Engineer's Special detonator.

The brilliantly luminous mound moved off the top of the
surface while the entire configuration expanded. By
Frame 7, a dark front can be seen on the original color film,
moving off to the right, a fraction of a centimeter ahead
of the luminous mound. This non-luminous shock is not
readily observable in the reproductions of Figure 11. It
extends from the top of the original liquid surface to the
bottom of the bright cap of light on top of the mound. In
frames after the first appearance, the dark front can be
seen advancing slightly away from the expanding right
vertical side of the mound.

The shock first appeared at about 14 μsec, when the mound
had expanded about 0.8 a_o and the lucite bottom had expanded
about 1.6 a_o. The speed of the shock, over the first few
frames after first appearance, is roughly 0.6 cm/μsec (or
about M = 20). If the normal Rankine-Hugionot relations had
held for this shock, then the temperature would have been
10,000°K and the pressure about 8000 psi.

4.   CONCLUSIONS

4.1 _Airshocks: Non-Luminous_. We have attempted to understand
the earliest behavior of explosions in air through use of photographic
observations and other instrumentation discussed in the Appendices.
In particular, we have looked for details on when and how the airshock
is formed by an explosion. We usually have not been able to observe
an airshock until the explosion had expanded to 5 or 6 charge radii (a_0).
At about this distance we can readily see a dark, non-luminous front
(through use of a scotchlite background) the growth of which we can
tie to the expected airshock from an explosion. Under exceptional
observation conditions we can find the non-luminous shockfront as
close in as 3 to 4 a_0.

Prior to 3 or 4 a_0 the airshock cannot be distinguished in normal
scotchlite photography from the luminous front (the fireball) produced
by the explosion processes. With the aid of a laser light-source and
selective filtering, we have been able to detect the airshock within
1/2 a_0 of the charge surface. Not until about 3 a_0 did we detect
separation of the airshock from the fireball in these laser photographs.
As in the normal-scotchlite photography, we distinguish the airshock
in the laser photographs as a non-luminous dark front observable ahead
of the brightly luminous fireball and have, therefore, labeled the
airshock a "non-luminous" shock.[*] Since the airshock was traveling
at speeds greater than $M = 17$ from 1/2 a_0 to 3 a_0, we might have
expected luminosity to have been produced at the shockfront.

But in these spherical-explosion experiments, confirmed by the
convergent-cone photographs (Fig. 10) and by the liquid-explosive
photographs (Fig. 11), we have observed strong airshocks without
(significant) luminosity.[**]

Perhaps, the dark front we have observed is not really a shockfront.
All we can really claim in a scotchlite experiment, when a dark front
is observed, is that a change in the refractive index of air was
present. In neutral air, a change in refractive index can only be
produced by a change in density. So, we can claim that a density
perturbation, perhaps a discontinuity, moving at speeds like 0.5 cm/μsec

---

[*] We cannot determine the radiance of the airshock with respect to
the irradiance of the laser beam or of the D-6. In the scotchlite
technique the shock is observed by refraction of an external, directed
beam of light. If the self-luminosity of the shock were equal, or
greater, than that of the beam, it is unlikely that the shock would
be detectable. The observation of a dark front, on the other hand,
suggests that the self-luminosity of the shock is less, or even much
less than that of the beam at the shock. If the self-luminosity of
the airshock were intense enough, then we should have observed shocked-
air radiation in the spectral measurements.

[**] Similarly, non-luminous shockwaves have been noted in electromagnetic
shock tubes. MUNTENBRUCH has given a review of Western observations
with T-tubes, conical theta and Z-pinch tubes. No comparable review
of the extensive Russian work has yet been made.

were observed in our experiments. For our money, such a fast moving density variation is a shock.

We make no attempt to explain why the airshocks in these explosions are non-luminous, although several explanations might be proposed.

We would like to emphasize that the airshocks and the luminous fronts in these explosions are not one and the same. In our experiments the airshock and the luminosity front could be considered to travel together until about 3 a_0; by 5 or 6 a_0, the airshock has separated significantly from the fireball. For other explosives or other experimental conditions, say high-altitude conditions, these numbers may be very different. The point is: we cannot be certain of the airshock motion by looking at motion of the luminous front in HE explosions.

4.2 Radius-Time Growth and Derived Pressures: The radius-time data from our films of a fairly large number of explosions display an unexpectedly large amount of scatter. Although we did not try to optimize these data, sacrificing time-resolution for longer viewing times, we do not believe that we can attribute much of this scatter to the measurements. Rather, we think that explosion luminosity is by its very nature irreproducible. This point of view is not inconsistent with the presence of "impurities" suggested by the spectral analyses of Appendix A.

Airshock pressures, derived from application of the Rankine-Hugoniot equation to the scattered radius-time data, are widely scattered. But there does seem to be rough agreement of the theoretical pressures with an "average" curve through the data for TNT and pentolite explosions.

4.3 Explosion Spectra: Most of the information recorded on spectral instrumentation comes from the earliest μ-seconds of explosion, when the explosion radiance is at its greatest values. If shocked-air radiance is to be observed on these explosions, it should be detectable on spectra of the earliest times of explosion. Further, since we could not detect the airshock closer-in than about 1/2 a_0 with photography, we were especially determined to find some evidence of the airshock at closer-in positions than 1/2 a_0 with the spectral observations.

But we have found no evidence in any of our spectra of species that we would have expected to have been produced by an airshock (Appendix A).

(The spectral results, therefore, do not aid us at all in understanding the airshock phenomena. We include our spectral results in this report, primarily, for possible use where intense luminosity might be of interest, such as laser pumping, or for possible purposes of explosion detection.)

16

5. CONCLUDING REMARKS

We began th' close-in experiments described in this report to clarify the deta.ls of airshock formation that were first examined in Part 1. Those results suggested the existence of an airshock, formed at the surface of the explosive at zero time, resulting from the transmission of the detonation shockwave from inside the explosive into the outside air.

We arrived at the existence of such a transmitted shockwave from observations of the motion of the luminous front created by the explosion. We thought that this luminous front was the airshock. We were wrong. The present results indicate that the luminous front is not produced by shock-excited air species. However, since the air-shock and the luminous front travel indistinguishably together in normal photographic films until about 3 or 4 a_0, our conclusions on the existence of a transmitted airshock obtained from those luminous-front data of Part 1 turn out to be correct. In fact, our detection of the existence of an airshock as close as 1/2 a_0 serve to confirm that picture of a transmitted airshock.

The question may well be raised: but where is the airshock from the charge surface to 1/2 a_0? Our observations her' cannot tell us. Much more sophisticated techniques will be necessary to detect the airshock in the intense luminosity of this stage of explosion. But we offer the following argument to suggest that the airshock must be present from 0 to 1/2 a_0, despite our failure to detect it. We have observed that it takes a fair amount of time to form an airshock in an explosion. Specifically, for example, the time needed for the ejecta material to form an airshock in the convergent-cone experiment (Fig. 10) was about 12 to 15 µsec. But in the laser experiments we detected the airshock at about 4 µsec (time from charge surface to 1/2 a_0). We would argue that this is too short a time for the shock to have been formed outside of the explosive and that the shock must have existed at zero time. That is to say, the detected airshock must have been the transmitted airshock.

Along with these photographic observations of the airshock, we have attempted to use sensors to pinpoint the location of the shock-wave. Our experiences are described in Appendix C. We have used these records to put together a new model for the main release of explosion energy after the formation of the transmitted airshock in Figure C-8.

6. REFERENCES

ADUSHKIN 1961: Adushkin, V. V. and Korotkov, A. I., "Shock Wave Parameters in an Airblast Near an Explosive Charge," Zh. prikl, Mekh. tekh. Fiz. No. 5, 119, 1961.

ADUSHKIN 1963: Adushkin, V. V., "Forming of Shock Wave and Scattering of Products of Explosion in Air," Zh. prikl. Mekh. tekh. Fiz. No. 5, 164, 1963.

ALLEN, R. A., "Air Radiation Graphs," NASA CR-566, August 1966.

BAUER, E., J. Quant. Spectrosc. Radiat. Transfer 9, 499, 1969.

BREENE, R. G. and NARDONE, M. C., cited by John J. Martin in Atmospheric Reentry (Chapter 5), Prentice-Hall, Englewood Cliffs, N. J., 1966.

BRONSHTEN, VA. A. and Liubarsky, K. A., "The Radiation from Meteors and Bolides," in Meteornaia Materiia V. Atmosfere Zemli (edited by V. V. Fedynshil), Nauka, Moscow, 1966.

CHAMBERLAIN, J. W., Physics of the Aurora and Airglow, Academic Press, New York, 1969.

GAYDON, A. G., "Spectra of Flames" in Advances in Spectroscopy, Vol II, Interscience, New York, 1961.

GRUN, A. E., Zeit. fur Naturfor. 9a, 1017, 1954.

HARRINGTON, F. D., "High-Speed Time-Resolved Spectroscopic Instruments," Paper F-4, Pro. 5th Int. Cong. High Speed Photo. Washington, 19 October 1960 and "Time-Resolution Spectroscopy" in Developments in Applied Spectroscopy Vol 2, Plenum Press, New York, 1963.

HEATH, D. F., "New Data on the Emission Spectrum of Air," Los Alamos Scientific Laboratory Report LA 2335, January 1960.

HUDDLESTON, J., Phys Rev XVII, 327, 1921.

KOTTENSTETTE, J. P., Inst. Soc. Am. Trans. 4, 27, 1965.

LUTZKY, M. "Theoretical versus Experimental Results for Airblast from One-Pound Spherical TNT and Pentolite Charges at Sea Level Conditions," Naval Ordnance Laboratory Report NOLTR 65-57, July 1965.

McCORMAC. B. M., Aurora and Airglow, Reinhold, New York, 1967.

MUNTENBRUCH, H., Phys. Fluids Suppl. 1, I-11, 1969.

NARDONE, M. C., Breene, R. G. · Radiance of Species in
High Temperature Air," General ... e Co. Report R 63SD3, June
1963.

NOXON, J. F., Active Nitrogen at High Pressure. Thesis, Harvard
University, May 1957.

REED, K. W. and Rudlin, L., "Optical Spectra Produced by 13-gm
Pentolite Spheres in Several Gases at Atmospheric Pressure,"
Naval Ordnance Laboratory Report NOLTR 69-37, 12 February 1969.

RUDLIN (1961): Rudlin, L., "An Approximate Solution of the Flow
within the Reaction Zone behind a Spherical Detonation Wave in
TNT," U. S. Naval Ordnance Laboratory NAVWEPS Report 7364,
April 1961.

RUDLIN (1962), L., "On the Origin of Shockwaves from Spherical
Condensed Explosions in Air, Part 1: Results of Photographic
Observations of Pentolite Hemispheres at Ambient Conditions,"
Naval Ordnance Laboratory Report NOLTR 62-192, November 1962.

RUDLIN (1963), L., "On the Origin of Shockwaves from Condensed
Explosions in Air, Part 2: Measurements of Airshock Pressures
from 8-lb TNT Spheres of Various Densities at Ambient Pressures,"
Naval Ordnance Laboratory Report NOLTR 63-13, January 1963.

RUDLIN (1967), L., "The Early Optical Spectrum and Airshock from
a 500-Ton TNT Explosion," Naval Ordnance Laboratory Report
NOLTR 67-94, October 1967.

STEWART, H. S. and Lovell, D. J., J. Op. Soc. Am. 44, 799, 1954.

SWINGS, P., Rosen, B. and Houzioux, L., Ann. d'Ap. 20, 76, 1957.

WILLETT, J. E. and Lehto, D. L., "Normal Shock (Rankine-Hugoniot)
Relations for Various Altitudes from Sea Level to 300,000 Feet,"
Naval Ordnance Laboratory Report NAVORD 6075, April 1958.

WRAY, K. L., J. Quant. Spectrosc. Radiat. Transfer 9, 255, 1969.

VANYUKOV, M. P. et al, Optics and Spectroscopy 10, 294, 1961.

ZEL'DOVICH and RAIZER, Yu. P., Physics of Shock Waves and High-
Temperature Hydrodynamic Phenomena, Academic Press, New York, 1967.

TABLE I – SUMMARY OF EXPLOSIONS

SHOT	EXPLOSIVE	WEIGHT (LB)	SHAPE
1	TNT	8.0	SPHERE
2	TNT	8.0	SPHERE
3	TNT	8.0	SPHERE
4	PENTOLITE	2.5	HEMISPHERE
5	PENTOLITE	1.0	SPHERE
6	PENTOLITE	2.5	HEMISPHERE
7	PENTOLITE	5.0	SPHERE
8	COMP. B	5.0	SPHERE
9 a	PENTOLITE	8.0	SPHERE
10	PENTOLITE	2.5	HEMISPHERE
11	TNT	2.0	HEMISPHERE
12	TNT	2.0	HEMISPHERE
13	TNT	2.0	HEMISPHERE
14	TNT	2.0	HEMISPHERE
15	TNT	2.0	HEMISPHERE
16 b	TNT	8.0	2 HEMISPHERES
17 b	TNT	8.0	2 HEMISPHERES
18 b	TNT	9.0	HEMISPHERE
19 c	PENTOLITE	8.0	SPHERE
20 c			
21	PETN	0.5	SPHERE
22	PENTOLITE	8.0	SPHERE
23 c			
24	PETN	0.5	SPHERE
25	PETN	0.5	SPHERE
26	PETN	0.5	SPHERE
27	PETN	1.0	SPHERE
28	PENTOLITE	8.0	2 HEMISPHERES
29 b	TNT	8.0	2 HEMISPHERES
30 d	TNT	16.0	2 HEMISPHERES

SHOT	EXPLOSIVE	WEIGHT (LB)	SHAPE
31	PENTOLITE	1.0	SPHERE
32	PENTOLITE	1.0	SPHERE
33	PENTOLITE	1.0	SPHERE
34	PENTOLITE	8.0	SPHERE
35	PENTOLITE	8.0	SPHERE
36	PENTOLITE	8.0	SPHERE
37	PENTOLITE	8.0	SPHERE
38	TNT	8.0	SPHERE
39	PENTOLITE	8.0	SPHERE
40 a	PENTOLITE	8.0	SPHERE
41 a	PENTOLITE	8.0	SPHERE
42	PENTOLITE	8.0	SPHERE
43	PENTOLITE	8.0	SPHERE
44	PENTOLITE	8.0	SPHERE
45	PENTOLITE	8.0	SPHERE
46	PENTOLITE	8.0	SPHERE
47	PENTOLITE	1.0	SPHERE
48	PENTOLITE	1.0	SPHERE
49	PENTOLITE	8.0	SPHERE
50	PENTOLITE	8.0	SPHERE
51 f	PENTOLITE	8.0	SPHERE
52 f	PENTOLITE	8.0	SPHERE
53	RDX	2.6	SPHERE
54	RDX	2.7	SPHERE
55	RDX	2.6	SPHERE
56 g	TNM + NM	2.7	SPHERE
57 f	RDX	2.9	SPHERE
58 g	TNM + NM	2.5	SPHERE
59 h			
60	RDX	2.8	SPHERE

a – fired in argon
b – TNT from United Kingdom
c – detonator test
d – sphere made of { UK TNT hemisphere / US TNT hemisphere
e – fired in freon

f – charge cooled to $\sim -50°F$
g – liquid contained in lucite sphere
h – dud
i – fired in water
j – mixed with 20% AlO_3

TABLE 1 - (CONTINUED)

SHOT	EXPLOSIVE	WEIGHT (LB)	SHAPE
61	RDX	2.8	SPHERE
62	RDX	2.6	SPHERE
63	RDX	2.7	SPHERE
64	RDX	2.7	SPHERE
65	PENTOLITE	8.0	SPHERE
66	TNT	8.0	SPHERE
67	RDX·TNM	4.1	SPHERE
68	RDX	2.6	SPHERE
69	PENTOLITE	8.0	SPHERE
70	PENTOLITE	1.0	SPHERE
71	RDX·TNM	3.9	SPHERE
72	TNT	8.0	SPHERE
73	TNT	30.0	SPHERE
74	PENTOLITE	9.3	CONE
75	PENTOLITE	8.0	SPHERE
76	PETN	2.0	SPHERE
77	PENTOLITE	8.0	SPHERE
78	PENTOLITE	8.0	SPHERE
79	RDX	2.6	SPHERE
80	TNT	99.0	SPHERE
81	RDX	2.6	SPHERE
82	PENTOLITE	8.0	SPHERE
83	PENTOLITE	8.0	SPHERE
84	TNM·NM	15.0	SPHERE
85	TNT	32.0	BLOCK
86	PENTOLITE	9.0	CONE
87	PENTOLITE	8.0	2 SPHERES
88	PENTOLITE	8.0	2 SPHERES
89	PENTOLITE	8.0	SPHERE

SHOT	EXPLOSIVE	WEIGHT (LB)	SHAPE
90	PENTOLITE	8.0	SPHERE
91	RDX	2.7	SPHERE
92	RDX	2.7	SPHERE
93	RDX	2.7	SPHERE
94	RDX	3.0	SPHERE
95	RDX	3.0	SPHERE
96	RDX	3.0	SPHERE
97	PENTOLITE	8.0	SPHERE
98	PENTOLITE	8.0	SPHERE
99	PENTOLITE	8.0	SPHERE
100	PENTOLITE	c	SPHERE
101	PENTOLITE	8.0	SPHERE
102	PENTOLITE	8.0	SPHERE
103	PENTOLITE	8.0	SPHERE
104	PENTOLITE	8.0	SPHERE
105	PENTOLITE	8.0	SPHERE
106	PENTOLITE	8.0	SPHERE
107	PENTOLITE	8.0	SPHERE
108	PENTOLITE	8.0	SPHERE
109	PENTOLITE	8.0	SPHERE
110	PENTOLITE	8.0	SPHERE
111	PENTOLITE	8.0	SPHERE
112	PENTOLITE	8.0	SPHERE
113	PENTOLITE	8.0	SPHERE
114	PENTOLITE	8.0	SPHERE
115	PENTOLITE	8.0	SPHERE
116	RDX/PENT.	8.0	2 HEMISPHERES
117	TNM·NM	1.8	HEMISPHERE

k - mixed with 20% graphite
l - liquid contained in glass sphere
m - fired in air at 117 mm po
n - fired in air at 40 mm po
o - fired into cone in ice

p - fired into cone in ice, filled with O_2
q - fired in oxygen
r - fired in nitrogen
s - liquid contained in open-top lucite hemisphere
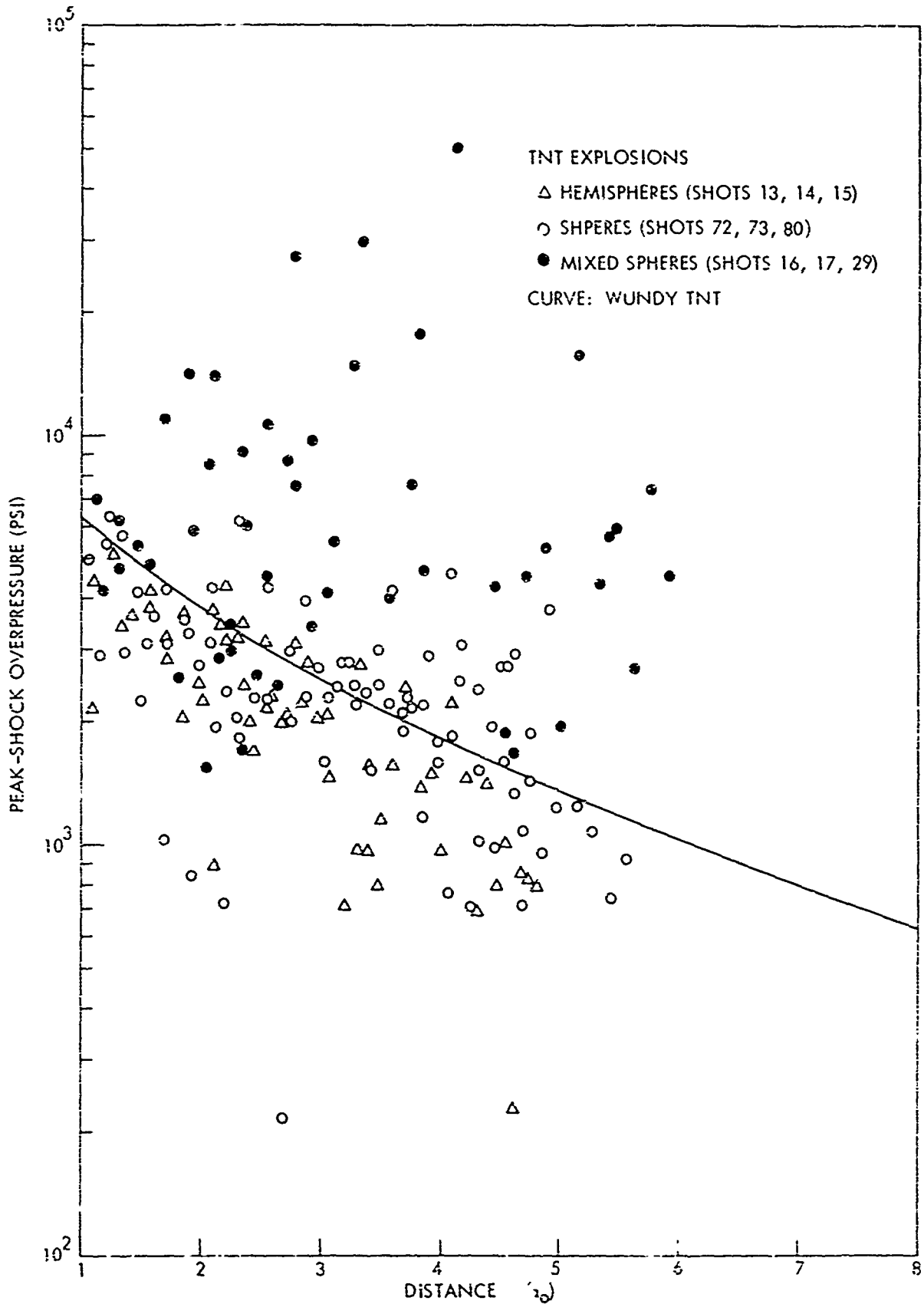
FIG. 8b SHOCK PRESSURE VS. DISTANCE
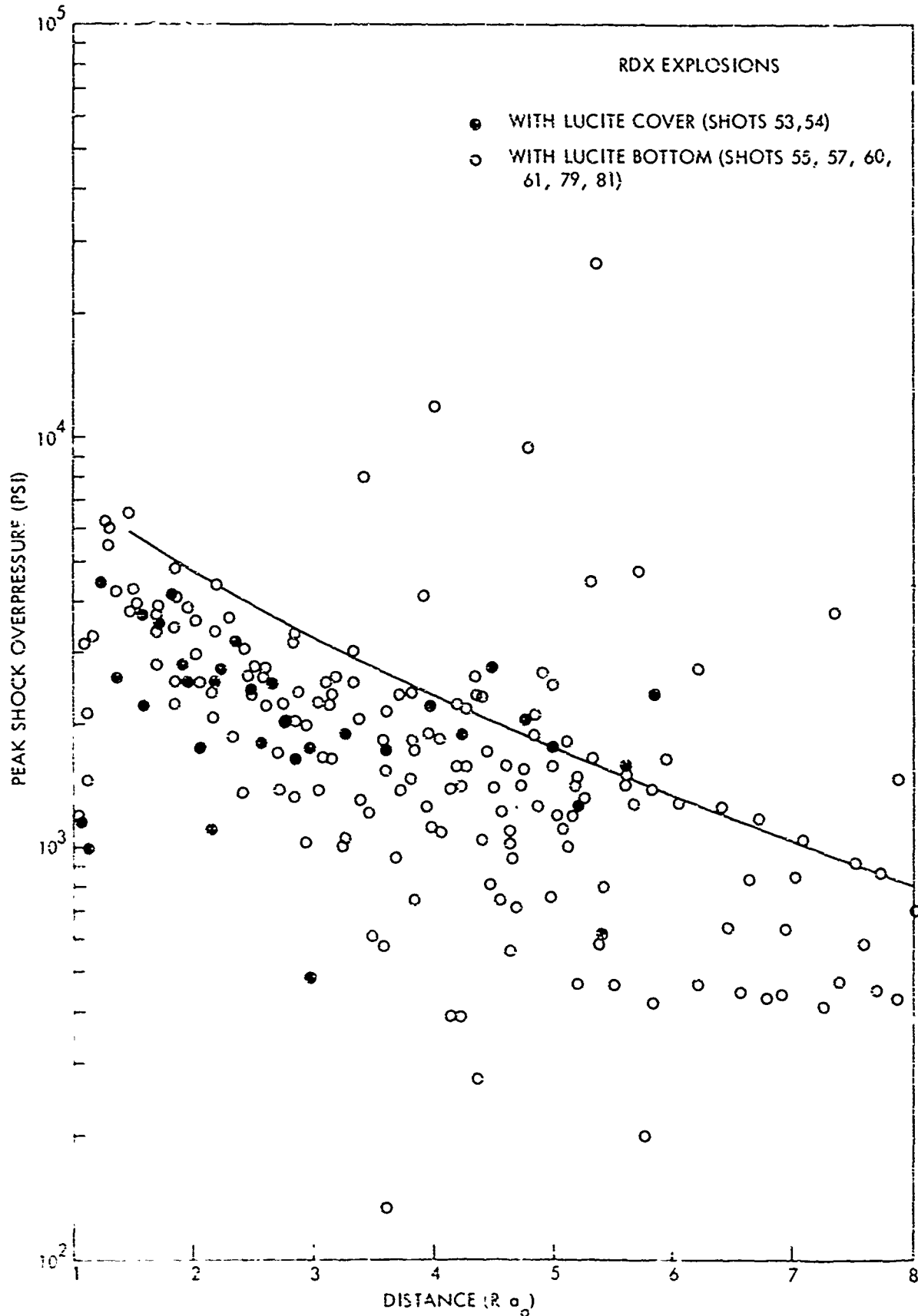
FIG. 8c SHOCK PRESSURE VS. DISTANCE
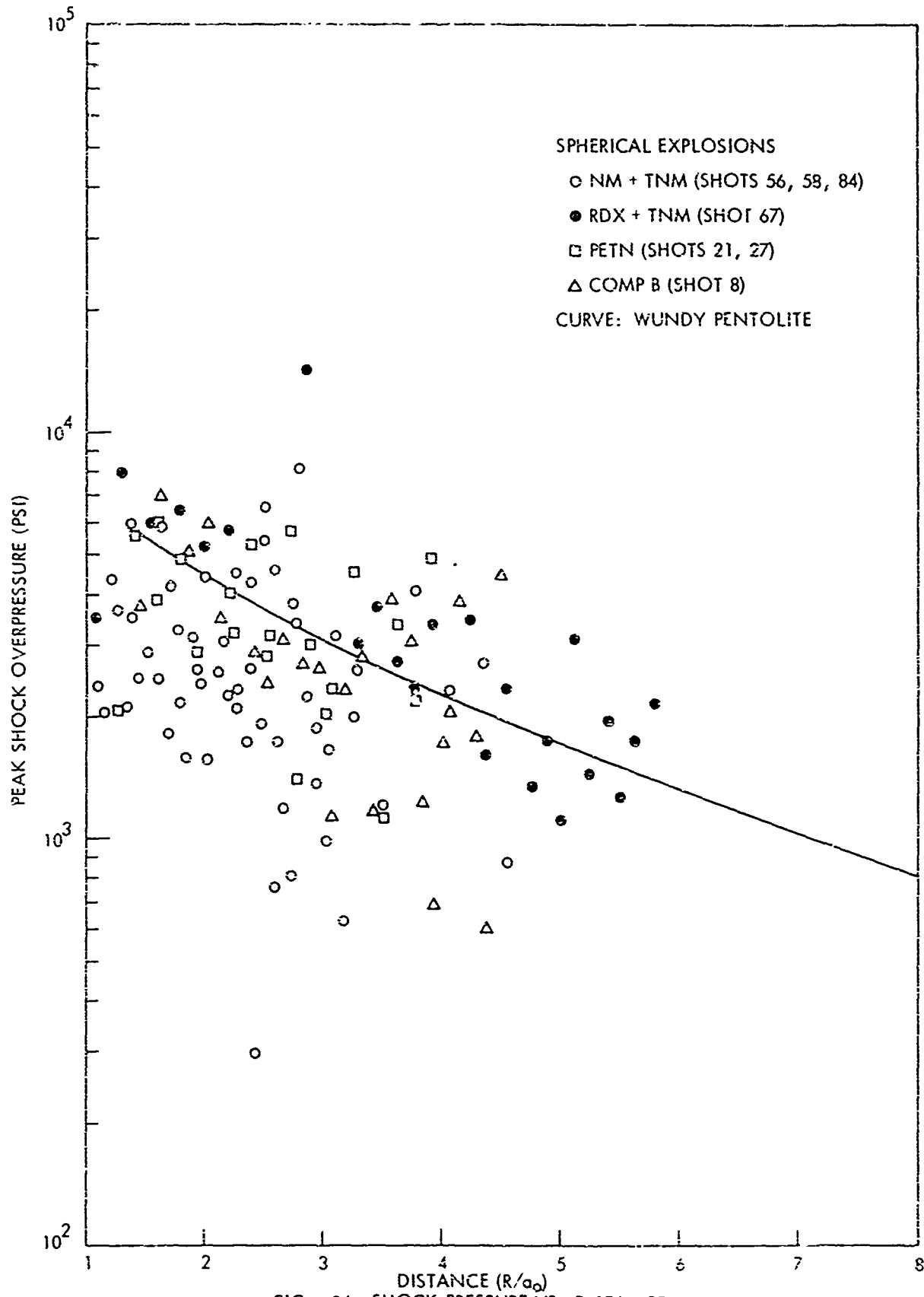
FIG. 8d   SHOCK PRESSURE VS. DISTANCE

FRAME
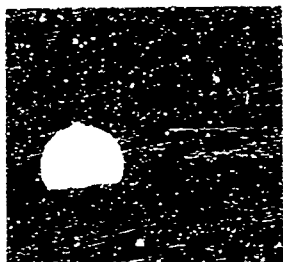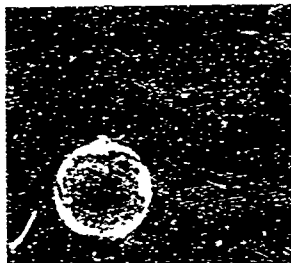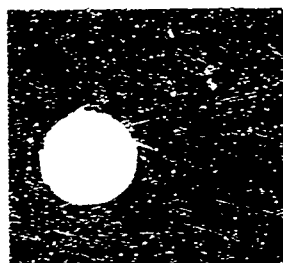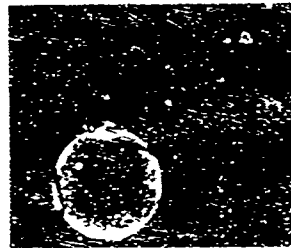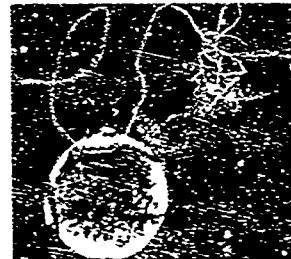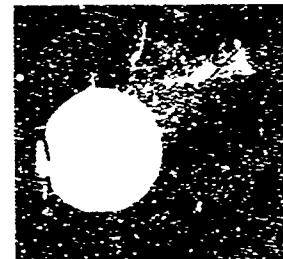
A. 6100-7100 Å   B. 6700-7100 Å   C. 6800-7100 Å

FIG. 9a LASER PHOTOGRAPHY OF 8-LB PENTOLITE SPHERE
INTERFRAME TIME~2 μSEC.
LASER ~ 6943Å

FRAME

6
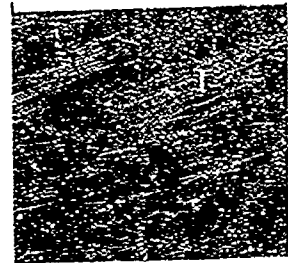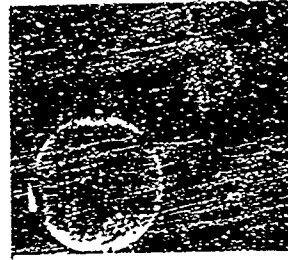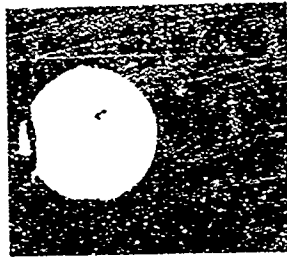
7
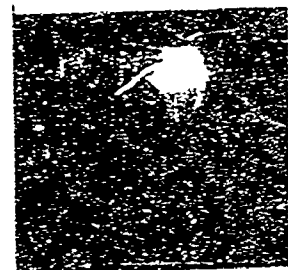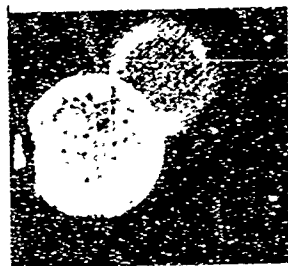
8
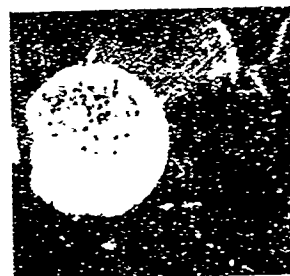
9
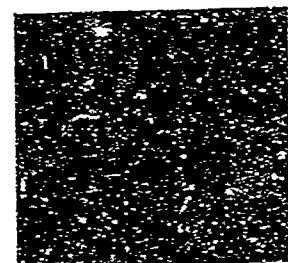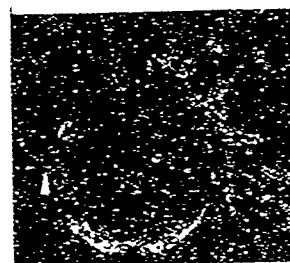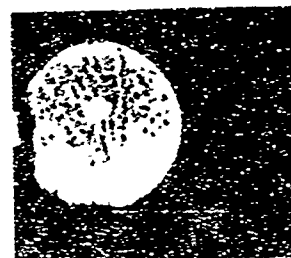
A. 6100-7100 Å   B. 6700-7100 Å   C. 6800-7100 Å

FIG. 9b LASER PHOTOGRAPHY OF 8 LB PENTOLITE SPHERES

INTERFRAME TIME ~ 2 μSEC.
LASER ~ 6943Å

FRAME 3

FRAME 4

AIRSHOCK

AIRSHOCK
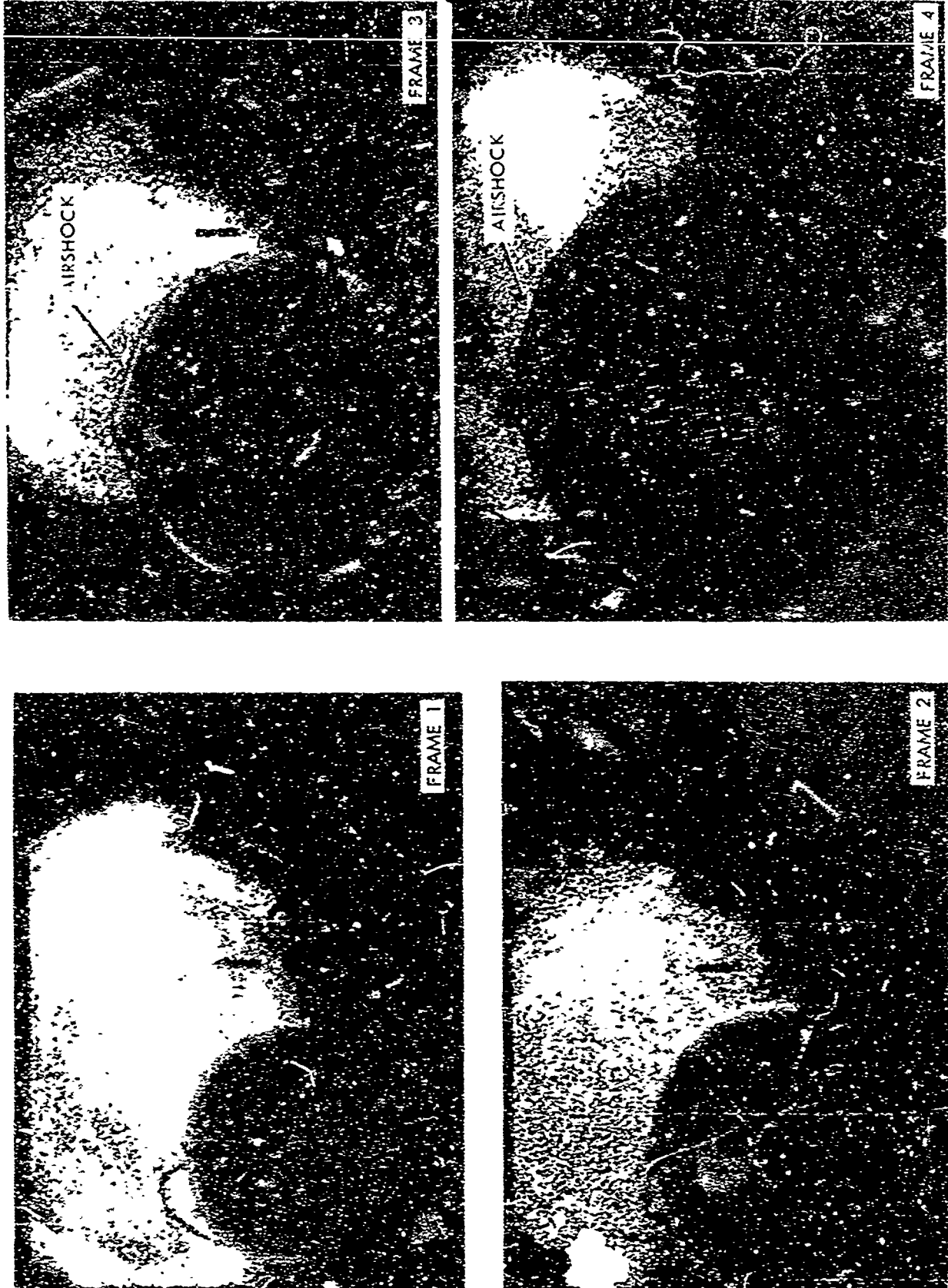
FRAME 1

FRAME 2

FIG. 9c EARLIEST APPEARANCE OF AIRSHOCK IN PENTOLITE EXPLOSION (FRAME 3)
(ENLARGEMENT OF SELECTED FRAMES IN COLUMN C OF FIG. 21a)

FRAME
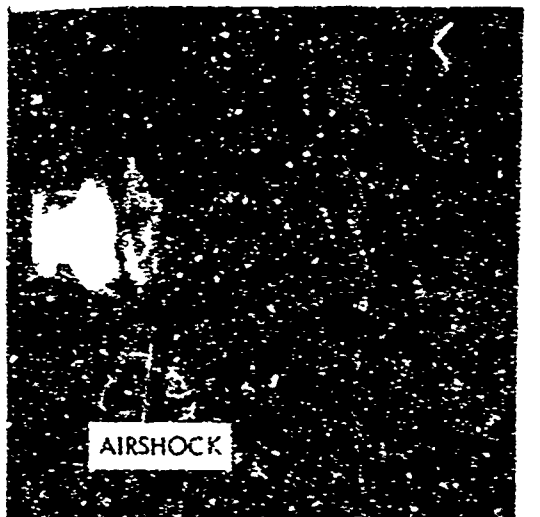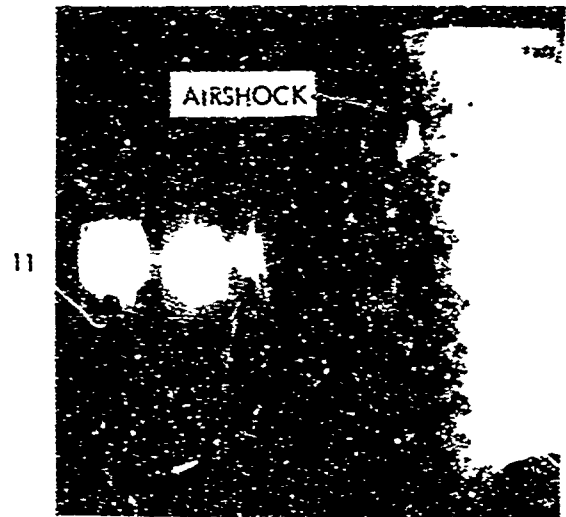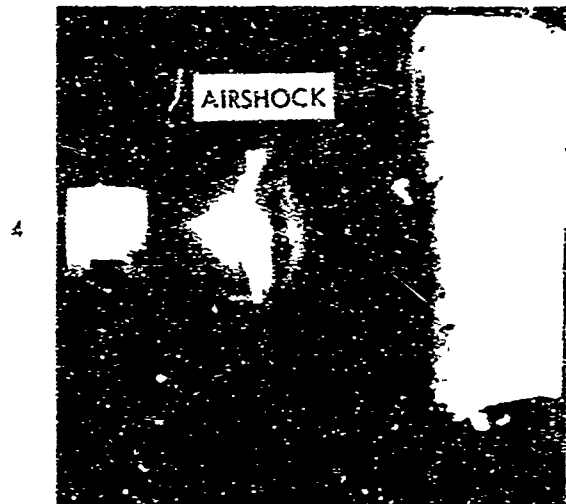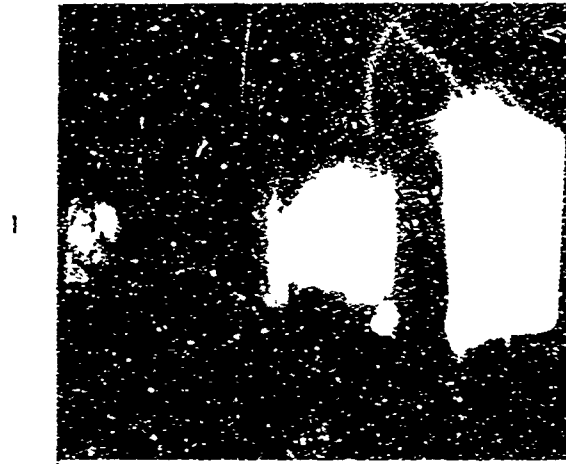
INTERFRAME TIME ~ 4 μSECONDS

FIG. 10 CONVERGING-SHOCK EXPERIMENT PRODUCING NON-LUMINOUS AIRSHOCKS (SHOT 108)

FRAME
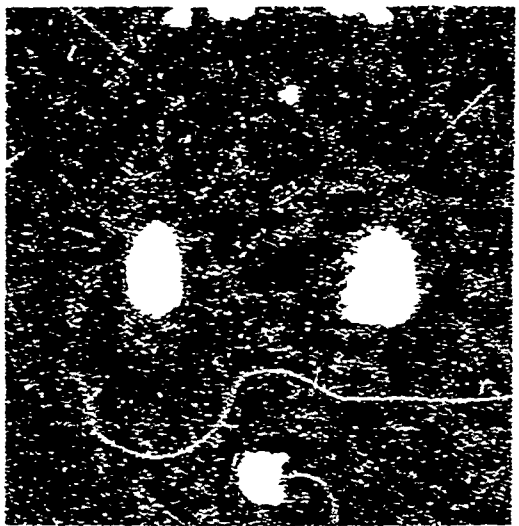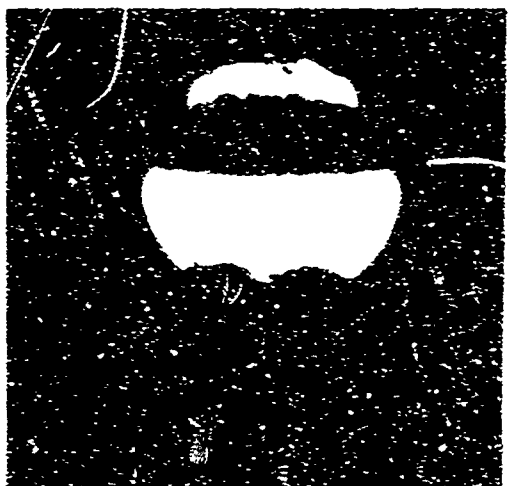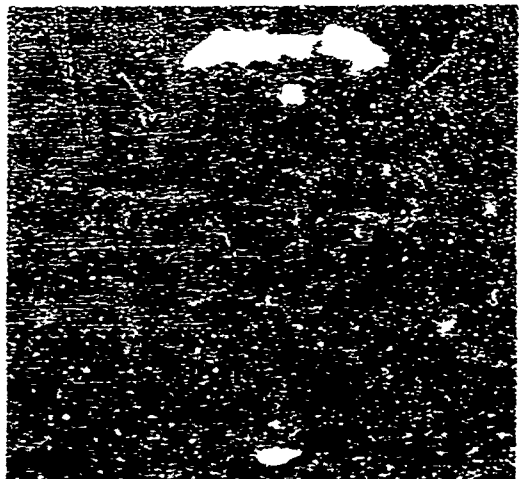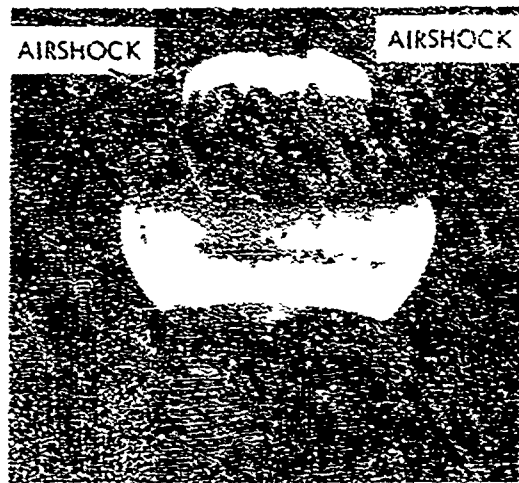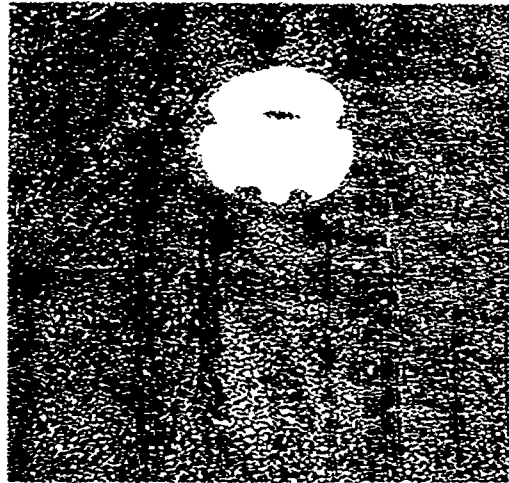
AIRSHOCK · AIRSHOCK

INTERFRAME TIME ~ 2 μ SECONDS

FIG. 11 NON-LUMINOUS AIRSHOCK IN LIQUID EXPLOSION (SHOT 117)

APPENDIX A: SPECTRA OF EXPLOSIONS

A-1: Photographic Spectra

A-1.1: General. The appearance of a spectrum of an explosion will depend on a large number of variables, only a few of which can be easily controlled. At the charge, the spectrum will depend on the radiating species released or created by the explosion and the density, f-number, lifetime and geometrical distribution of these species over both an area and an optical depth. The spectrum also will depend on the shape of the charge and the hydrodynamic time (proportional to the cube root of charge weight); both serve to determine how long the radiating species will remain in the field of view of the spectrograph and how fast the radiators might change in time. At the spectrograph, the spectrum will depend on all the familiar variables -- dispersion, effective f/-number, slit size, type of lenses, etc. In addition, we have found that the explosion spectrum -- which appears to be a collection of hundreds of lines and bands, intensely radiant for only a few µseconds -- varies decisively with some undetermined aspects of the film. That is to say, recognition of these lines and bands on a given piece of film depends on a number of interrelated factors between film and spectrograph, above and beyond the grain size, resolving power, or the acutance of the film. For example, Shellburst film and High Speed Infrared film are ranked about the same in the three characteristics above, Shellburst having a higher acutance class and a slightly lower speed rating. For recognizing spectral features, however, we have found the infrared film more desirable.

By "spectral feature", we mean a line or band for which we can measure a wavelength. Therefore, a spectral feature must be distinguishable from its background, first of all, but also have a sufficiently sharp density gradient, if we are to find a place on the feature to measure from. In our spectral records we may often not find features because (1) the feature is too dim to permit a satisfactory measurement or (2) the feature is not sufficiently recognizable from its bright background to permit such a measurement. Both happen, often on the same record. In the deep blue, features are usually too dim; in the deep red, the background is usually too

bright. Parts of explosion spectra often do look like continua, so that spectral features might be expected to be absent. Often, however, these "continua" can be cleaned up, perhaps by increasing dispersion or decreasing exposure.

We cannot claim that no explosion continua exist. There are a number of processes that produce continua that might be anticipated in an explosion. Often, apparent continua do appear, resulting from overlapping or overexposure, or perhaps even scattering in the spectral film. The creation of an apparent continuum can be seen in the AVCO spectrum of Shot 78 of Figure A-1. In this experiment a piece of glass was placed a small distance from the surface of the charge. When the radiating species reached the glass, the light intensity was dramatically increased (probably through an increase in temperature when the explosion particles were brought to rest at the glass). So intense was the light that it burned past the film spectral cut-off (on the right).

We have given in Figures A-1 through A-6 a random sampling of explosion spectra as seen from different explosives, as seen by different spectrographs, and as seen by different films. The figures are mostly self-explanatory and we make only some brief comments.

   a. The appearance of most explosions on the AVCO streak spectra are rather similar. The total duration of much of the light lasts only a few μ-seconds (the light evident on these records before marked zero time is rewrite on the continuously recording records). Intensity increases from the blue, cut-off just below CN 3883 Å in all AVCO records, to the red, where the film response cuts off the record. Only a few bright, strong spectral features stand out, and these same radiators on nearly all records: Ca 3934, 3968 Å, CN 4216 Å band, Ca 4227 Å and the Na-D lines 5890, 5896 Å. The four lines running the height of the film with equal intensity are Hg calibration lines that were burned in prior to the explosion. (We should note shot 75 in Figure A-2, which is unlike all other spectra shown. The charge was cast with aluminum added to the pentolite mix. We see that the intensity

distribution is much like the other pentolite shots, but
some lines and bands are recognizably different. CN is
not detectable: nor are the $Ca^{\ddagger}$ lines. Ca 4227 Å still
remains. The new bright radiators are Al 3944 and 3952 Å
and the AlO bands.) Intensitites do vary from explosive to
explosive but these prints can be misleading. In Section A-2
we shall look at photoelectric measurements which are more
reliable for intensity. The qualitative comparison in
Figure A-4 for 3, 32, and 100 lb TNT spheres is correct,
since the films were exposed and processed under similar
conditions and the charges were cast from the same powder at
identical conditions. We can see in this set of prints
rather easily how the increased hydrodynamic times of the
explosions lead to different-looking spectra, even though
the radiating species must be identical in these three
explosions.

b. In Figure A-5 are typical millisecond spectra from
the streak Cine Spectrograph. The rectangular-looking
portion of the spectrum to the blue is not real. The
height results from the slit-height used on the instrument.
When the explosion light first reaches an intensity
sufficient to record, all light is integrated over a time
approximately equal to that time to cross the height of
the slit. This slit time for all records in Figure A-5
is ~100 μsec, except for #50 which is 200 μsec. Any light,
sufficient to record, that appeared at any time during the
first 100 (or 200) usec would appear in the rectangular
portion. Only if it persisted beyond 100 (or 200) usec
would it be streaked beyond the rectangle. We see that
only wavelengths above, say, 5200 Å persisted longer than
the slit time. Most of the explosion spectra shown lasted
only about 1 millisec -- that is, had intensity sufficient
to record for about 1 millisec.

Exposure conditions were about identical for all the shots
in Figure A-5. Spectral coverage ranged from about 3300 Å
in the blue to film cut-off in the red. The intense explosion

NOLTR 69-74

light has overexposed many of the films. The typical dip
in all films, which occurs at about 5000 Å or so, can be
seen to be filled in by the intense light. The exception
might be #88, which had an especially deep dip in film
sensitivity. But even here we can see light scattered into
the dip.

Finally, we note that the millisecond spectrum for #84 in
Figure A-5 is very different from the μ-second spectrum of
#84 in Figure A-3. Since the two instruments have rather
comparable light-gathering capabilities, we assume that the
(TNM + NM) explosion developed its light intensity several
μ-seconds later than did the other materials.

In Figure A-5 the sharp black lines on #72 are scratches, not
absorption lines. In #76, an absorption line can be seen
at the Na-doublet, which goes from emission to absorption
with time.

c. Sample spectra from the Hilger, with no time resolution,
are given in Figure A-6. The superior capability of the
Hilger to resolve lines and bands in the blue, which do not
appear at all or appear to be continua on the time-resolving
instruments, suggests a dynamic-exposure problem in obtaining
explosion spectra. In the time-resolving instruments light
is swept by a particular grain on the film. In the Hilger
the light dwells on a particular grain for as long a time
as the intensity is sufficient to record. The Hilger, thus,
records hundreds of lines in the blue, which are readily
measured on the originals but not in the reproductions in
Figure A-6. This desirable recording ability in the blue,
however, leads to overexposure in the red. Lines and bands
seldom can be recognized above, say, 5000 Å.

A-1.2: Identification of Spectral Features

A-1.2.1. Construction of Table A-1. In Table A-1 we have
compiled wavelengths for the spectral features that we have found on
our explosions, without regard for the explosive material. In
compiling the wavelengths, we took only those values that occurred on

A-4

several shots. A far longer list would have been obtained had we
listed all wavelengths that have been measured. The reason for
our caution lies in the difficulties in identifying, and measuring,
a feature on these spectral records. There are, probably, hundreds
of lines and bands produced by an explosion -- we list over 400 in
Table A-1. In many records these features blend into an unmeasurable
"continuum." On a given explosion different types of film respond
differently to the explosion light. Thus, High-Speed Infrared film
might give easily recognized lines, whereas these same features would
be unrecognizable on Tri-X or Shellburst film. Explosion light,
furthermore, is not especially reproducible. Presumably identical
charges can produce different looking spectra. The overall average
picture is nearly the same, but recognition of the features (lines
or bands) will be variable. On a given explosion and a given film,
the intensity varies over a wide range. Spectral features can
hardly be found in the ultraviolet range because the intensity level
is so low. Spectral features are even harder to find in the near-
infrared range because the intensities are so high that lines and
bands merge into one another.

Lifetimes also cause difficulties. Most of the features below
5000 Å last only a few μ-seconds. Those above 5000 Å last for milli-
seconds. On a μ-second-resolution record many of these short life-
time features just do not show up as individual lines but rather
as a "continuum." In fact, we have never been able to resolve the
CN 3883 Å sequence structure (and below) on our AVCO records. The
structure is clear on our millisecond line spectra and clearest on
our time-independent spectra. The long lifetime radiators, especially
at 6000 Å and above, give trouble in the other direction. This part
of the spectrum is always badly overexposed on any spectrum obtained
from any spectrograph slower than the AVCO. (And on most AVCO records
the deep red is slightly over-exposed because of the tremendous
intensity produced by the explosion species in the deep red.)

Because of these difficulties with explosion spectra, we have
read records unconventionally. A given spectral film was enlarged
to about 4X and printed onto various papers, exposures were varied
on a given paper, and dodging used for various parts of the spectrum.

Upon occasion 10 to 12 manipulated prints were made of one film;
more typically 4 to 6 prints were made. Spectral features were,
then, recognized and marked on the prints with a needle, several
different prints of a film always being necessary to find all the
features. The needle holes were subsequently read with a Bausch
and Lomb Measuring Magnifier (Catalog No. 81-34-35), with 0.1mm
markings. Wavelengths could usually be obtained by fitting a
Hartman curve to three recognizable wavelengths produced by the
explosion, such as Ca 3934, Ca 4227, and Na 5893, or to mercury wave-
lengths usually placed on the spectral film prior to the explosion.
Clearly, this procecure for reading the spectral features is inac-
curate compared to the conventional procedures. But we justify it
on the basis that we were able to find hundreds of features that
otherwise would have gone undetected. With a given type of explosive
and type of film the spectra from a given spectrograph could be
read with a reproducibility of a few Angstroms. If the explosive,
or the film, or the spectrograph were changed, the uncertainty
increased -- but that increase is not so much caused by the reading
procedure as it is by the problems of recognizing a feature.

Wavelengths found from prints of our explosion records are
listed in the first four columns of Table A-1, under the appropriate
spectrograph heading. Since the recognition problems differ for
each instrument, the following comments should be noted.

AVCO: u-second resolution. Only species that were formed
during the first few u-seconds can be observed. Spectral
features can be recognized only above 3893 Å. Below, only
a blurred continuum appears. Response into the red goes
out as far as the available films go, say 9000 Å, but the
dispersion becomes poor above, say 6000 Å, making both
recognition and wavelength measurements of features difficult.
The AVCO column represents a summary c 27 explosions of TNT,
pentolite, RDS, (NM + TNM), and (RDX - NM). Films included
Tri-X, Shellburst, 2475, and High-Speed Infrared.

Cine: millisecond resolution. Both streak and frame
spectra available. The slit height used determined that
light on the streak instrument was integrated in time over

the first 100 μsec or so. On the frame instrument the
first spectrum could appear at any time during the first
200 μsec. Spectral features can be recognized down to
3000 Å upon occasion; more typically, down to 3500 Å. In
the red end, response was limited by the films to about
9000 Å; but the dispersion, similar to that of the AVCO,
makes recognition increasingly difficult above 6000 Å. The
Cine column represents 16 explosions of TNT, pentolite,
PETN, and (NM + TNM). Films included Tri-X, Shellburst,
and High Speed Infrared.

Grating: no time resolution; opened before a shot and
closed afterwards. Grating spectrographs have been wholly
unsatisfactory for explosion spectra. Despite a number
of attempts only two readable grating records were obtained--
one Cenco and one Jarrell-Ash -- and compiled in Table A-1.
The wavelength range on both runs from about 3900 to 5900 Å
for readable features. For both spectra 8-lb pentolite
spheres were fired. The films were both 2475.

Hilger: no time resolution; opened and closed manually.
Because of its superior response under explosion conditions,
the Hilger records can be read down to about 2500 Å. In
the red end the Hilger offers poor recognition. Overexposure
is greater on the stationary film than on the moving films
of the AVCO and the Cine instruments. Because of its
superior dispersion, however, some details can be recognized
out to the film cutoff. The Hilger column represents
8 explosions, including pentolite, RDX, and (TNX + NM). Films
included Shellburst, 2475, and High Speed Infrared.

Because of these instrument variations and the variations in the
explosion material, entries in the first four columns of Table A-1
are not directly comparable. Upon occasion all four columns list
the same wavelength, such as 3968 Å or 4227 Å, radiated by Ca and
Ca. Such agreements are caused by strong radiators, easily recognizable
on any film; there are not many such radiators identifiable in
explosion spectra.

Because of the recognition problems, we find it difficult to estimate the accuracy of the wavelengths listed in Table A-1. Based on reproducibility of the wavelength values from one explosion film to another off the same spectrograph and from one spectrograph to another on the same explosion, we would estimate that wavelength accuracy runs about $\pm$ 1 to 3 Å below 4000 Å, increasing to about $\pm$ 5 Å below 5500 Å, and thereon increasing continuously to perhaps $\pm$ 30 Å in the infrared. These estimates were used in assigning identifications in the table.

A-1.2.2: <u>What Species Shall We Look For?</u> Now that we have compiled our list of wavelengths produced by an explosion, we begin the search to identify what radiators might be producing the light.

If we assume, along with much of explosion literature, that the early explosion luminosity is produced by air species, excited by the shockwave, then we can go to theoretical predictions for the radiation from hot air. Such predictions vary, of course, with the temperature of the air. From hydrocode computations of pentolite explosions (such as those by LUTZKY) we find that the shock temperature might be 6-8000°K during the first few μ-seconds of shock motion. Since shock temperatures are notoriously dependent on zone sizes used in the hydrocode, we might be suspicious and prefer to estimate from experimental data. From RUDLIN (1962) we estimate that the luminosity front moves from an explosion at somewhere between 1 and 0.5 cm/μsec, at least for the first few μ-seconds. From the tables of WILLETT we find that the corresponding shock temperatures, <u>if this luminous front is a shock</u>, would be somewhere between 7500 and 16,000°K. Putting both estimates together, we, then, look at theoretical predictions for sea-level air, shocked to a temperature somewhere between 6-16,000°K.

A number of theoretical predictions for hot air at equilibrium have been made. Amongst the best known are those by various AVCO people (such as ALLEN) and by BREENE et al. Those by BREENE are most convenient for looking at variations with wavelength. There are important differences among the predictions but all agree in the following discussion. There has been very little work done on non-equilibrium predictions.

Radiation from air in thermal equilibrium occurs in two very different regimes. Below about 8-10,000°K radiation should come from molecular transitions, such as those from N_2 or from products formed such as NO. Above, say, 12,000°K such molecules can no longer exist and the radiation should come from excited atoms, molecular ions and from electron transitions, both free-free and free-bound. In other words, at the low end of our temperature estimate, air radiation should be strongly dependent on the chemical species present and we would, therefore, expect to see many spectral features on our records from the banded structure radiated by molecules. On the other hand, at the high end of our temperature estimate electron transitions should predominate leading to a strong continuum on our records, with some band structure from ionized molecular species, such as N_2^+ especially since this is a strong radiator, and atomic species such as N, since there is so much of it in air.

Examination of our spectral records quickly suggests that high-temperature air is not present. First, continua do not appear to be present (when resolution is high enough); second, atomic lines of N and O are not clearly present (permitted lines, that is -- some forbidden lines may be present): and third, N_2^+ cannot be unequivocally identified.

Therefore, we go to the low-temperature predictions. From BREENE we find, for 6,000°K equilibrium air, that the strong radiators should be -- roughly in order of diminishing intensity:

$$NO\ (\beta)$$
$$O^-\ (free\text{-}bound)$$
$$O_2\ (Schumann\text{-}Runge)$$
$$NO\ (\gamma)$$
$$N_2\ (1^+)$$
$$N_2^+\ (1^-)$$
$$N_2\ (2^+)$$
$$NO\ (Infrared)$$
$$O\ (free\text{-}free).$$

A-9

We also find that the predicted intensity, integrated over the radiators above, decreases from the blue to the red. This variation with wavelength is not at all what we see on explosion spectra, where intensity increases from the blue to the red.

This difference between predictions and our spectra makes us suspicious that the explosion luminosity does not come from hot air. We become more suspicious if we look at spectra as a function of time. If the early luminosity is created by the airshock, then this luminosity must go out at some time when the airshock no longer is sufficiently strong to excite air species. Subsequently, the luminosity would then have to come from the explosion products left behind the airshock. Thus, there must necessarily be a distinct break, or change in the spectrum, when the shocked air ceases radiating and the "fireball" light comes through. We have seen no evidence of such a break in any explosion spectrum or photographic film.

We are not quite yet ready to throw away the airshock concept at this point -- perhaps (1) the theoretical variation with wavelength is wrong[*] (after all, equilibrium calculations hardly describe the complex non-equilibrium processes behind an explosion shock); or (2) the break is so smooth as to be undetectable.

At any event, we lay aside, for the moment, the airshock as the source for explosion light and speculate on other possibilites. There are many physical phenomena in which light is created by the release of energy. We review briefly some of the spectral features of these,

> Flames: GAYDON (1961) has given an excellent summary of flame spectra -- which we might suppose would be somewhat similar to explosion spectra. (Energy released and temperatures reached in explosions are, however, much larger than those in flames.) In flames, spectral details do vary somewhat with the burning materials and with the richness

---

[*] A critical discussion of some of the assumptions and the complexities in making these predictions for air has been given by BAUER.

in a given flame. A rich mix can produce a continuum which approaches closely the blackbody continuum.[*]

Pre-mixed hydrocarbons show an outer cone with strong OH bands, some continuum in the blue, and some CO_2 bands. The inner cone produces most of the flame light in the visible from C_2 (Swan) and CH, along with some OH and CHO bands. In hotter flames, (near stoichometric with oxygen) additional bands of C_2 and CH appear, perhaps with CO (4th positive) bands. In flames with combined nitrogen CN (violet) is very strong but weak in flames with molecular nitrogen.

In other types of flames other bands can appear. For example: flames of $CO + O_2$ show the (Schumann-Runge) bands super-imposed on a strong continuum; flames with NO show strong CN bands, some NO (γ) bands, and NH at 3360 Å; and, finally flames of H_2 with NO (or NH_3 with O_2) show the NH_2, CH, and NH bands.

In a detonated gas, such as a hydrocarbon plus O_2, there appears mostly continuum and not the usual C_2 and CH bands. Gaydon makes the pertinent comment that most people (including spectroscopists) are familiar with discharge-tube spectra and have come to regard those spectra as normal. But in discharges excitation is by relatively fast electrons, accelerated in the external electric field and is quite different from that which occurs under equilibrium conditions by thermal means. We can readily verify Gaydon's comment by trying to find our explosion spectra in the usual spectral tables compiled for the usual sources, such as the arc, spark, or discharge tube, in which strong external electric fields are present; there is no correlation.

Natural Phenomena: Very rich and complex spectra can be produced by 13-gm charges which do not produce a shockwave

[*] G. J. Peters (NOL Internal Memorandum of 7 February 1966 on "Optical Spectra from Burning TNT") has found that TNT, lit with a match, produces a continuum, similar to that of a 800°K blackbody, and the sodium doublet at 5890 and 5896 Å.

(REED) -- at least, shockwaves are not produced until late
time. REED's conclusion was that light was created in
those experiments by collisions of particles released, or
created, by the explosion with the ambient gas -- solid-gas
collisions. We might ask, then, what are the spectra of
single-particle phenomena like meteors, comets, or even
man-made reentry bodies?

BRONSHTEN has given an excellent summary of meteor spectra:
these spectra consist almost wholly of atomic (neutral
and ionized) lines of the elements comprising the meteor.
Some evidence of N_2 (1^+) bands has been reported. The
forbidden O line at 5577 Å has been found in the wake
behind fast meteors but the accompanying forbidden lines
at 6300 and 6360 Å have not been found. The glowing meteor
body itself is not generally observed. Particular multiplets
of the elements seem to be favored in meteor spectra. For
instance, the Fe multiplets 2, 4, 41, 42, and 43 are
especially intense of the nearly 100 multiplets of Fe found
in meteor spectra. Many of the most intense lines of meteor
spectra   seem to fit our explosion spectra; and we have
used such identifications in our table. These identifications
include: Na, Mg, Al, Ca, Ca^+, Cr, Fe, Co, and Ni. We shall
find that the N_2 (1^+) bands reported for meteors do not
appear in our explosion spectra.

That explosion spectra and meteor spectra have some spectral
lines in common is not terribly surprising. An explosion
particle will contain many impurities that can be excited
by collisions with air molecules -- especially the excitations
requiring only a few electron volts. Our explosion particles
move out from the charge at speeds like 1 cm/μsec; meteors
move at speeds like 1.5 cm/μsec (slow) to 5 cm/μsec (fast)
when their luminosity first appears (altitude ~100 km for
fast and 75-100 km for slow).

On the other hand, that there should be any agreement between
spectra of comets and of explosions is, indeed, surprising.

A-12

A comet is thought to be a cold, icy body unable to supply the excitation energy itself for luminosity. The observed luminosity is believed to be fluorescence radiation excited by the sun and is supported by observations of the luminosity dependence on distance from the sun.

SWINGS has given an excellent summary of cometary spectra which we will now use. In comet heads identification is pretty certain of OH, NH, CH, CN, C_2, C_3, NH_2, CH^+, and Na; less certain are OH^+, Fe, and Ni. In the tails, which can extend to thousands of kilometers, are found CO^+, N_2^+, CO_2^+, CH^+, and probably CH^+. Metallic compounds such as the hydrides (possibly NaH, KH, MgH, CaH, AlH, and SiH) may be present but wavelength uncertainties have made identification uncertain. Oxides (FeO, MgO, and CaO) have been looked for; but, again, identification is not certain. A number of prominent wavelengths have not been identified.

The radiation from certain species in comets can differ a little to very much from that from those same species in the laboratory. For example, the CN (violet) bands appear strongly in comets but the CN (red) bands hardly appear, if at all. Both usually appear strongly in the laboratory.

We have found that wavelength coincidences of explosion spectra with cometary values are remarkable and have used the cometary identifications in Table A-1. We have not always agreed with the cometary identifications; and we give identifications in Table A-1 which we think are more appropriate for explosions.

There are other natural phenomena, the spectra of which are pertinent to us: these are lightning, auroras and airglow (including nightglow and dayglow). The first, lightning, we can dismiss rather quickly, since the energies involved are too high to produce many species of interest to us. The others, auroras and airglow, cannot and should not be dismissed so readily. But these are too complex to review in so hasty a manner as we have the spectra of flames or comets,

and we refer the reader to the basic book by CHAMBERLAIN
and the more recent one by McCORMAC. We do note, however,
that a number of airglow species do seem to appear on
explosion spectra. The forbidden bands of O_2 seem unmistakable
on our spectra. Less certain are forbidden lines of O and
N -- the auroral, nebular, and transauroral transitions.
The N_2^+ (1^-) sequence at 3914 Å is bright in many atmospheric
phenomena but is not especially so in explosion spectra.

Laboratory Sources: In addition to the familiar arc and
spark spectra of spectral tables, there are many other
sources for spectra in the laboratory -- electric-wire
explosions, shocktubes, electromagnetic (shock) tubes,
microwave excitation, laser excitations, etc. We have not
found that these sources produce spectra that would be of
particular help in identifying explosion spectra. A large
amount of work on air has been carried out in shocktubes.
Most of this, however, has been done with "equilibrium air",
after reflection of the shock at the downstream wall of the
tube. Few measurements have been made of the incident
(before reflection) shock. Species found for shocktube
equilibrium air do not appear to agree with our explosion
species.

A-1.2.3: Assignment of Species: In Table A-1 we have usually
listed several species for each unknown wavelength when these species
all seemed equally plausible. In some instances, we have not been
able to assign any species. Upon occasion we could only find one,
or perhaps two, possible species. Our listing of several species
for a wavelength does not mean that all these species were present,
although that may have been true. It simply means that all the
possibilities seemed reasonable and we had no basis for further
selection.

A number of assumptions have gone into our choices for the
radiating species listed. These include:

a. We have assumed that cometary and meteor species are
favored in explosion spectra and have given particular
emphasis on fitting the wavelengths from these species to
our known wavelengths.

b. We have chosen the species of lowest energy (if known) for listing. Even so, we have given preference to a species that fitted the largest number of unknown wavelengths, without regard to the energy.

c. We have given particular emphasis to those species identified from 13-gm explosions in air (REED), when these seemed to fit. There may well be big differences in the excitation conditions for the 13-gm explosions and for these larger explosions -- for the·latter a shockwave was present at the earliest times. Many of the 13-gm species. however, appear to be present. Since O_2 species were particularly prominent on the 13-gm spectra, they will also be prominent on our present listings.

d. We did not list any compounds of impurities. Several could have made a reasonably good fit -- FeO, CaO, or SrO, for example. We omitted these primarily on our experience in which we added impurity compounds and obtained unclear results for lighting them up in an explosion. We have also omitted CO_2 as a possible species, since our 13-gm experiments suggested that CO_2 was not detectable on those shots in air.

e. Some atomic radiators, Fe for example, could supply a large number of lines which could have reasonably been fitted. In general, we have only permitted atomic species: (1) with an intensity 500 (or greater) and an attainable excitation energy, or (2) that appear on the lists of bright meteor lines.

f. In listing species we allowed species whose wavelengths deviated from the unknown wavelength by an amount no larger, roughly, than the reproducibility in wavelength appropriate for that part of the spectrum. For example, in the deep blue the unknown wavelengths lie within about ± 2 or 3 Å of the wavelengths of the assigned species.

With these assumptions, we have proceeded to assign the identifications listed in Table A-1; a summary table of the molecular and

atomic radiators present is given in Table A-2. We make the following observations:

a. A wide range of exciting energies is necessary for the molecular species listed -- from about 1.5 ev (for the forbidden O_2 bands) to nearly 20 ev (for the N_2^+ (1^-) bands). We are surprised that such high-energy species can be created by an explosion. Clearly, thermal excitation alone cannot provide the energy to create N_2^+ or O_2^+ species. Obviously, other processes are at work and we suspect that charge-exchange collisions must play a big role in exciting the molecular species.

b. A much narrower excitation energy range exists for the atomic species -- from about 2 to 9 ev. The forbidden nebular O lines at 6300 and 6360 Å require only 1.96 ev. The other forbidden N or O lines listed need no more than about 4 ev. Among the most intense lines on explosion spectra are Ca 4227 Å (2.93 ev), K 7699 + 7665 Å (1.61 ev) and, Na 5890 + 5896 Å (2.11 ev). Of comparable intensity are the Ca^+ H and K lines at 3934 and 3968 Å, requiring the highest energy of all the atomic lines listed in Table A-1: 9.2 ev.

c. The presence of certain species, such as CH, CO, NH, CH, C_3, in explosion spectra is not too surprising. They are, after all, rather good radiators appearing in many different luminous phenomena. There are, however, two peculiarities: (1) C_2 does not appear to be present and (2) the CN (Red) system does not appear to be present. The first, absence of C_2, appears more peculiar than the second. The CN(Red) bands occasionally do not appear in various circumstances: for example, they are absent (or almost so) in comet spectra. But C_2 is nearly always present, especially if CN(Violet) appears. CN (Violet) and C_2 (Swan) bands often are the major sources of light excited by shockwaves. We cannot dismiss them from our spectral identifications out of hand. Clearly, a number of unknown wavelengths could be assigned to C_2 (Swan). But we do not think the assignments are convincing, especially since (1) many of these "Swan wavelengths" do not appear consistently from one shot to another of the same explosive and (2) shots in which graphite was purposely added to the explosive failed to produce any expected increase in luminosity at the Swan wavelengths.

d. The O_2-bands seem to predominate over the N_2-bands in producing light;[*] that is, we get a rather complete list of O_2 radiators, whereas our N_2 list is very limited. The presence of O_2-(Shumann-Runge) bands is not too surprising. Although not especially common in the laboratory, the S-R bands readily occur in certain low-energy flames. But the presence of the forbidden airglow, or the afterglow, systems of O_2 is, indeed, surprising. Although they require only a few ev for excitation, their forbiddenness makes them very difficult to excite in the laboratory -- hours to days being required to obtain good laboratory exposures. If we have really produced any forbidden O_2 band in μ-seconds with an explosion, then we must be surprised. Yet the identifications appear to be rather good. We can tie some of the unknown wavelengths, also, to less exotic species besides forbidden O_2; but a large number can only be tied to these bands and we believe that they are real. Possibly these bands are excited by the large number of free electrons that we know occur on an explosion (c.f., Appendix C).

e. The N_2 bands that appear are not only limited in number but are surprising in identity. We do not believe that the $N_2(1^+)$ bands are present -- (1) because the expected wavelengths do not line up convincingly with our unknowns; (2) because we do not detect any increased radiation at these wavelengths when we fired in nitrogen rather than air, and (3) because the far-red radiation on explosion spectra is unusually intense and long-lived. We do not believe that it is likely that the (1^+) bands could be so much more intense than the (2^+) bands nor last about one thousand times longer. Some other bands must be present.[**]

---

[*] To the contrary, VANYUKOV has found in a spark discharge in air and in nitrogen both at 1 atm that the spectral outputs, at least over the range 5,000 to 10,000 Å, were identical. Undoubtedly, the excitation energy in the Russian experiments was higher than that available in our explosions; but the situation is by no means clear.

[**] WRAY has recently conducted experiments in hot air to determine what species produce 10 times more light in the deep red than has theoretically been predicted (largely $N_2(1^+)$ bands) for equilibrium shocktube air. He finds that both N and O are necessary and attributes the radiation to some new states of NO -- the Rydberg states. His calculated wavelengths agree rather well with a number of our unknown wavelengths. Further verification of these new radiators would make them logical additions to Table A-1.

In various situations the $N_2(1^+)$ system disappears completely or becomes very faint, especially at pressures near 1 atm. For example, we cite the results of HEATH, HUDDLESTON, GRÜN, and NOXON. Working with mild excitation in a discharge tube of air, HEATH found the $N_2(1^+)$ system disappeared when the gas pressure approached 1 atm and was replaced by a weak continuum. This result was similar to that earlier obtained at 1 atm by HUDDLESTON, who varied the gas pressure to much higher pressures and obtained a number of unusual changes with pressures above 1 atm. GRÜN found, under circumstances in which he suppressed the (1^+) bands, that the N_2 (Gaydon) bands appeared, the intensity of which increased with gas pressure. DIXON found in a nitrogen afterglow set-up at 1 atm that the (1^+) bands were weak compared to the Vegard-Kaplan system. Because of these experiences, we believe that the identifications we have listed in Table A-1 of the N_2 (Gaydon) γ, β, γ bands and the N_2 (Vegard-Kaplan) bands may be unusual but not unbelievable.

The $N_2(2^+)$ bands seem to fit well -- occasionally being the only species that can be assigned. Presence of the $N_2^+(1^-)$ system is not so certain. The (0,0) 3914 Å and (0,1) 4278 Å of $N_2^+(1^-)$ should both be rather prominent. But 4278 Å appears much more intensely than 3914 Å. In fact, clear recognition of 3914 Å appears only on the grating spectrographs; whereas 4278 Å appears on all spectrographs.

　　　f. Light can be seen from an explosion until extremely late time. When barely a wisp or two remains of the explosion gases, that wisp radiates rather brightly. We have been unable to make any wavelength measurements at such late times with our spectral instrumentation (c.f., Appendix B). We deduce, however, that the wisp radiation is longer than about 6300-6500 Å or so. Now, these wavelengths appear essentially at zero time and remain almost unchanged in character until the last bit of light goes out on our spectral records and probably remains unchanged for tens of milliseconds (for an 8-lb charge). What radiators could put out such intense light for so long a time?

We have listed several possibilities in Table A-1. These include several bands of N_2 -- such as the Gaydon and the Meinel bands that are well known -- and an obscure afterglow group, the LeBlanc-Tanaka-

Jursa bands. These, and the others we have listed (such as NH_2 and H_2O), fit the unknown wavelengths credibly. But we have little reason to believe that these species can radiate with high intensity for tens of milliseconds.

A number of wavelengths in the 6300 Å-on part of our table die out in μ-seconds; K at 7682 Å, for example, certainly doesn't radiate for many milliseconds, nor should we expect it to radiate much differently from Na 5893 Å which dies out, clearly, in 1-2 milliseconds on our records. But we lack late-time spectra and we cannot isolate from our early-time spectra which wavelengths last for tens of milliseconds and which don't. The intense, long-lived explosion species are, therefore, probably not correctly identified.

A-1.2.4: <u>Summary of Spectral Features</u>: Over 400 wavelengths can be found for Table A-1 by combining the records from different spectrographs of various explosive materials (TNT, pentolite, RDX, PETN, (NM + TNM) and RDX + NM). The range is from about 2500 to 9000 Å. Undoubtedly, even more lines and bands are present on the records which cannot be recognized and measured as individual features.

A wide range of possible species -- both molecular and atomic -- over an energy range from about 2 to 20 ev can be assigned. A number of these can be considered as "impurities" -- such as CN, Ca, and Na. Others can be directly attributed to the presence of explosion products, such as C_3, CO, and NH_2. Many of these impurity and explosion-products species can be found in the spectra of meteors and comets. But the preponderant number of wavelengths must be assigned to air species (i.e., N_2, O_2, O or N) alone, somehow excited by the explosions. Many of these species are unusual -- such as the forbidden O_2 Broida-Gaydon bands or Vegard-Kaplan bands of N_2. Certain species that might well be expected to appear on explosions -- C_2, CN (Red), and $N_2(1^+)$ bands -- do not seem to occur on these spectra.

Although species can be assigned to wavelengths from about 6300-9000 Å, there seems little reason to believe that these species can create the intense radiation for tens of milliseconds that has been observed on explosions.

A-1.3:   Comparison of Explosion Species: In Table A-1 we have
lumped all spectral films together, ignoring any differences among
explosive materials.   In this section, we ask, what are the differ-
ences?   (r largest collection of data is from the AVCO and we
confine our comparisons to these μ-second records.

In Table A-3 we list wavelengths for several explosive materials.
Each column is a summary of all AVCO data available for that explosive.
A much larger number of entries can be made for pentolite and RDX
than for TNT and (NM + TNM).   For TNT, the light is there (for the
charges larger than 8 lb) but spectral features cannot be distinguished.
For (NM + TNM) the light just is not there -- on these μ-second
records.   The later-developing light from this explosive does register
on the Cine Spectrograph but is so intense that wavelength values are
impossible to read on records for (NM + TNM).

In Table A-3 there are some similarities but we really can conclude
little from looking only at the wavelength values.   A better proce-
dure is to compare the entire spectrum of one explosive with another.

In Figure A-7 we have compared several densitometer tracings.
These were made with a Jarrell-Ash Microphotometer scanned across
the AVCO films, just past zero time.   The tracings were then matched
as closely as possible, in wavelength, to make up the figure.   Only
#50, #56, and #94 were even roughly aligned in amplitude (and this
was done only by using the amplitudes of the Hg reference lines on
each film).   The other tracings have no amplitude relation whatsoever
from one to another.   All records were made on Shellburst film.   No
corrections for film response have been made.

We note the following from Figure A-7:

(1) There are 3 maxima in the red for most shots: at about
5600-5700 $\mathring{A}$, 6000-6200 $\mathring{A}$, and ~5600 $\mathring{A}$.   The relative heights
of these, however, shift around for the different materials.
If we label the above peaks 1, 2, and 3, then we note that
the order for pentolite #50 is 1, 2, and 3 but for (NM + TNM)
#94 is 3, 2, and 1 for decreasing intensity.

(2) Moving from the red into the blue, the amplitude decays
quickly (only partly due to decrease in film sensitivity).
The rise on some of the films occurs roughly 4400-4700 $\mathring{A}$,

especially noticeable on pentolite #50 and (NM + TNM) #56.
The next rise occurs in the neighborhood of the CN 4216 Å
sequence and is particularly noticeable on the pentolite
#50 film. CN seems to be missing on any shot with TNM,
clearly missing on the (NM + TNM) shots. The CN group
is missing on the RDX shots of Figure A-7 but has been
found on other RDX shots, where, possibly, film sensitivity
is more suitable to reveal it.

The presence of lucite or glass in the charge (which was
used in these charges to hold either the liquid or loose
powder materials) does seem to affect the spectrum but not
in measurable terms. CN seems to be missing if either
material is present in the shots of Figure A-7 and in other
shots.

(3) Although we think that there is no doubt about the
identity of CN at 4216 Å and 3883 Å, in these spectra, we
do note that the intensity distribution, say in #50, is
not the expected distribution with wavelength (c.f., dis-
cussion in Appendix B of REED). The identification of C_3
in these spectra suggests that C_3 bands may be overlying
the CN structure and changing the intensity distribution.

The strongest line, usually found in this 4216 Å sequence
if 414X. Such a wavelength is not a part of C_3 and we
cannot find an appropriate species, atomic or molecular,
for this unusually strong line. We have listed this line
in Table A-1 as 4142, 4145, 4140 for the different spectro-
graphs and give N_2 and Fe as possible identifications. This
is probably incorrect.

(4) Finally, we note that the Ca 4227 Å and Ca^+ 3934, 3968 Å
lines that are strong radiators for pentolite and TNT
explosions are not detectable on these shots, except for #50.
Indeed, the strong Na 5890, 5896 Å doublet (that we find
as a broad line at 5893 Å with our resolution) is missing on
both #67 and #68 in Figure A-7. Seldom is the Na line
missing.

Thus, there are variations from one explosive to another in a
broader sense than a wavelength or so missing. These variations
occur over broad wavelength ranges and are usually reproducible --
although there are details that are not reproducible from shot to
shot of the same explosive.

A-1.4: Comparison of Explosion Spectra with Predictions for
Shocked Air: In Section A-1.2.2 we used the results of comparisons
of our spectra with predictions for shocked air to guide us in the
assignment of species to the unknown wavelengths. We now look at
two such possible comparisons in Figure A-8 and A-9.

We have used the predictions of BREENE et al which are conveniently
given as a function of wavelength at thermodynamic conditions near
to those that should hold in our explosions. In Figure A-8, we
have presented the densitometer trace of the AVCO film #73 -- a 32-lb
TNT sphere. The tracing was made just after zero time on the time-
resolved record. Superimposed are data symbols to represent our
estimates of how the computed airshock radiation would have appeared
on the Tri-X film used for #73. These estimates were made from
BREENE's calculated overall radiation results, representing a summation
of the output of several radiating species. The dashed line between
data symbols only connects the symbols; no effort was made to simulate
the BREENE curve in between symbols.

We have arbitrarily superimposed the theoretical data at convenient
viewing positions by adjusting the amplitude of the theoretical value
at 3883 Å. Thus, although the amplitude of one curve has no meaning
with respect to the amplitude of the other, the variation of
amplitude with wavelength that we have given for the theoretical
data does follow BREENE's results.

We see that the predictions have an opposite dependence on wave-
length to what we have observed. This particular theoretical curve
was computed for equilibrium air at $6000^{\circ}K$ and $\rho/\rho_0 = 0.1$, conditions
reasonably close to what we expect (c.f., Section A-1.2.2). Slightly
closer to the experimental situation would be $\rho/\rho_0 = 1$, but the
overall curve for this density ratio should differ only slightly
from the value for which predictions are available.

In Figure A-9, another set of predictions, taken from NARDONE
et al, for shocked air at temperatures of 3000, 10,000, and 25,000°K
are given as solid lines. To make the comparison conveniently with
explosions spectra, we took values from #74, corrected for film
response, and superimposed these data in Figure A-9. Again, ampli-
tudes have to be adjusted arbitrarily; we have set the experimental
value at 4000 Å equal to unity on the log intensity scale.

Our explosion spectra do not look like the predictions for
shocked air in Figure A-8 or A-9.

A-2: Electronic Spectra

A-2.1: Py-I Measurements: Typical records from the Py-I
are given in Figure A-10. Data on spherical explosions are given in
Table A-4. Difficulties in compiling the table arise because each
explosion was slightly to very different from shot to shot. For
example, some of the charges lumped together under "Pentolite Explosions"
were cooled to -50°F; others were not. Again, the experiment #79
(RDX charge) contained an argon-flash bomb behind the charge which,
probably, accounts for the increased Py-I readings. Some of the
scatter in these data results from the variations in the experiments,
but some also results from the basic irreproducibility of the light
from explosions.

With these difficulties in mind, we make the following observations
from Table A-4:

  a. Amplitudes of Band 0 < Band 1 always. In general,
  Band 1 < Band 2 but there are one or two exceptions.
  Band 2 ≤ Band 3 usually; but occasionally Band 2 > Band 3,
  especially for RDX shots. Bands 0 through 3 cover a spectral
  range from about 5200 to 8200 Å. Thus, we conclude that
  explosion luminosity, generally but not always, monotonically
  increases to the red.
  b. The least intense explosions are those from TNT and
  (NM + TNM), according to the Py-I data. But the liquid
  explosive is delayed in developing its light until times
  past the recording capability of the Py-I instrumentation.
  Undoubtedly, the liquid explosive produces much more light
  than TNT, but we have no measure of that late light. Pentolite,

RDX, and (RDX + TNM) rank in increasing intensity over 5500-9200 Å. But in Band 0 (6200-5800 Å) RDX produces less intensity than pentolite.

c. In side-on views of the explosions (entries in Table A-4 do not distinguish the different viewing points at 1", 2", and 3" from the surface of the charge) pentolite is generally brighter than RDX, because of the greater opacity of the pentolite explosion products. The addition of graphite, at least in the RDX shots, cuts down (or leaves unchanged) the light intensity over various bands. The spectral coverage on shots from #84 on ran from 4350 to 9500 Å so that the C_2-Swan bands that we had expected to increase radiation were entirely observable by the Py-I. Since the radiation was not increased, we suspect (along with other reasons cited in Section A-1.2.3) that the C_2-Swan bands were not present. Addition of Al, on the other hand, in #75 produced a tremendous increase in the light in Band 0 and slight increases in Bands 1-3 over normal pentolite. Dramatic increases were also obtained from addition of Al in the times for light to decay.

d. The times in Table A-4 jump around rather badly. Generalizations are difficult. There may be a trend: Band 3 > Band 2 > Band 1 > Band 0; but it is difficult to be sure. On the whole RDX times are smaller than those for pentolite.

A-2.2: Other Photoelectric Measurements: The Py-I records can give false impressions of the overall light produced by an explosion. The Py-I is constructed to look at a fixed area. After being initiated, the charge was lit up asymmetrically, as the detonation wave reached the edge of the charge non-uniformly. (This asymmetry accounts for much, but not all of the rise time to peak radiation in Figure A-10 and in Table A-4.) When, however, the luminous front had expanded beyond the distance where the Py-I was focused, the light reaching the photodiodes of the Py-I necessarily decreased -- without regard for what the intensity of the luminous front really was doing.

We can look at this in Figure A-11. Trace (a) sees the same
view as does the Py-I. (To obtain this signature, a Solar Cell
was placed at the mirror position of the Py-I and the prism was
removed.) We see that the signal rises and falls, pretty much as
do the signals in Figure A-10 for the various Py-I bands. For
trace (b) an identical Solar Cell was used, but without the fore-
optics of the Py-I, so that the entire surface area of the expanding
luminous front was seen by the Solar Cell.

The traces from two much faster responding detectors are given
in traces (c) and (d), which also have different spectral-response
characteristics from those of the Solar Cell. We note that the
faster 931A now saw a double peak, the first part of which was
probably caused by the asymmetrical breakout of the detonation wave
at the edge of the charge. We also note that both the 931A and the
1P28 decreased with time after the peak.

We can, therefore, conclude from use of all four detectors that
the luminous front on an explosion continues to grow, at least
for tens of μ-seconds, past the first peak of intensity but only at
wavelengths greater than, say, 6000 Å. Such a conclusion could
not have been obtained from the Py-I records alone.

A-4: CONCLUSIONS

A number of spectra have been obtained of explosion lumin-
osity with photographic and electronic instruments of varying time
resolution.

The spectral coverage, varying from instrument to instrument,
is from, roughly, 2500 to 9000 Å. Characteristically, explosion
spectra are weak in the blue, increasing to intense maxima in the
red. There are variations in the spectral details from one explosive
to another. The peak radiation of RDX charges occurs near 6500 Å
(Band 2 peak). Pentolite peaks near 7300 Å (Band 3 peak). The
observed dependence of explosion light on wavelength is opposite
to that expected from equilibrium shocked air, which has been
theoretically predicted to decrease in intensity going from the blue
to the red.

The observed radiating lifetimes vary with wavelength. Radiators
in the blue die out rapidly; our spectrographs record blue radiators

only for a few μ-seconds. Radiators in the deep red last, on the other hand, for many milliseconds.

Disregarding the differences in spectra from different explosives, we have compiled a list of over 400 wavelengths distinguishable on the photographic records. Identification of the species producing these wavelengths is, by no means, clear. We have made reasonable, even if incorrect, assignments of species to most, but not all these wavelengths. The intense lines of Ca, Ca$^+$, Na and K are readily identified in nearly all the spectra. The intense violet bands of CN and, probably, C$_3$ are also readily identified on most, but not all, spectra. Inexplicably, certain systems do not appear to be present -- the red CN, the C$_2$-Swan, and the N$_2$(1$^+$) bands. Other identifications that we have made vary over a wide energy range -- from about 2 ev (for forbidden O$_2$ bands) to over 20 ev for ionized N$_2^+$ bands. The existence of low-energy forbidden O$_2$-bands in an explosion is as startling to us as the existence of such high-energy systems as N$_2^+$ and O$_2^+$, since the mechanisms of producing either energy extreme in an explosion is obscure to us. Much more remains to be done to clarify the identifications and to understand the reactions that occur.

Identification is particularly uncertain in the red, above, say, 6000 Å. We have not found likely species to account for the intense, long-lived radiators that occur on explosions in this part of the spectrum.

Finally, there appear to be remarkable wavelength coincidences between explosion spectra and the spectra produced by comets and meteors.

TABLE A-1 SUMMARY OF WAVELENGTHS SEEN IN EXPLOSIONS

EXPLOSIONS				COMET	POSSIBLE IDENTIFICATION		
HILGER	GRATING	CINE	AVCO				
2478						O_2^+ 2478 (2⁻)	
2490					NO 2488 (β)	O_2^+ 2488 (2⁻)	
2500						O_2^+ 2501 (2⁻)	
2528					NH 2530	O_2 2528 (SR)	
2542						O_2 2540 (HI)	
2550					NO 2552 (β)	O_2^+ 2546 (2⁻)	
2555					NO 2558 (β)	O_2 2554 (HI)	
2595							Cu 2593
2610					NO 2608 (β)	NH⁺ 2614	Cu 2618
2703						O_2^+ 2705 (2⁻)	
2715				BEGIN		O_2^+ 2730 (2⁻)	
2730				2725 NH⁺	NH⁺ 2730	O_2 2732 (HI)	
2740						O_2 2737 (HI)	
2755					NO 2755 (β)	O_2 2756 (HII)	
2770						O_2 2773 (HI)	Cu 2766
2777						O_2^+ 2777 (2⁻)	
2785					CO 2786	O_2 2788 (HII)	
2792					CO 2793	O_2 2794 (HI)	
2802						N_2 2804 (2⁺)	
2812				2811 OH	OH 2811	O_2 2814 (SR)	N_2 2814 (2⁺)
2835					OH 2829	O_2^+ 2840 (2⁻)	Cu 2824
2868						O_2 2870 (SR)	
2890				2885 NH⁺	NH⁺ 2886	O_2^+ 2890 (2⁻)	NO 2885 (β)
2895						O_2 2894 (HI)	NO 2893 (β)
2908						O_2^+ 2907 (2⁻)	
2940						O_2^+ 2937 (2⁻)	N_2 2936 (VK)
2950					CN⁺ 2953	O_2 2952 (HII)	
2965					CO 2969	O_2^+ 2963 (2⁻)	
2973					CO 2971	O_2^+ 2970 (2⁻)	O 2972
2995					N_2 2997 (VK)	O_2 2997 (HII)	
3010						O_2^+ 3005 (2⁻)	
3034					NH 3035	NO 3035 (β)	Ni 3037
3040					NO 3043 (β)	O_2 3039 (SR)	
3045					NH 3043	O_2 3044 (2⁻)	
3050					NH 3051	O_2 3047 (HII)	Ni 3051
3058					NH 3055	O_2^+ 3053 (2⁻)	Ni 3057
3062					OH 3064	O_2 3063 (HI)	CN⁺ 3063
3067		BEGIN			OH 3068	O_2^+ 3070 (2⁻)	
3075		3075			NH 3076	CO 3074	
3080				3079 OH	OH 3078	O_2 3080 (HI)	
3087		3085		3086 OH	OH 3090	O_2^+ 3089 (2⁻)	N_2 3088 (2⁺)

TABLE A-1 (CONTINUED)

EXPLOSIONS				COMET	POSSIBLE IDENTIFICATION		
HILGER	GRATING	CINE	AVCO				
3095		3095		3094 OH	CO+ 3093	CN+ 3092	Al 3093
					N2 3104 (2+)	O2 3104 (SR)	Ni 3102
3100		3105				O2 3111 (HI)	
3111		3110		3107 OH	NH 3119	O2+ 3114 (2-)	
3115				3122 OH	OH 3126	O2+ 3130 (2-)	CO+ 3123
3127		3130		3135 OH	OH 3135	N2 3131 (VK)	Ni 3134
3135				3143 OH	OH 3147	O2+ 3141 (2-)	CH 3144
3146				3148 OH		O2+ 3149 (2-)	
3150				3154 OH		CH 3157	
3155		3155		3159 OH		O2 3163 (SR)	
3162		3158			CO+ 3169	O2 3165 (HI)	
3169		3170					
3175					CO+ 3181	CN+ 3185	
3180		3185				NO 3198 (β)	
3195						N2 3197 (VK)	
3199							
3204		3200			CO+ 3210	O2+ 3211 (2-)	NO 3207 (β)
3210							
3215		3215			CO+ 3222	O2 3223 (SR)	
3220		3217			CO 3235	O2 3233 (SR)	Li 3233
3234					CO 3241	NH 3240	Ni 3243
3240					NH 3252	O2 3252 (HII)	Cu 3248
3250					CO+ 3260	O2 3257 (HI)	CN+ 3263
3260	BEGIN					N2 3268 (VK)	
3270	3270				CO+ 3274	NH 3273	Cu 3274
3275	3275				NH 3281	O2 3284 (HI)	
3285						N2+ 3294 (1-)	
3290						O2 3294 (SR)	
	3294				CO+ 3301	O2+ 3300 (2-)	N2+ 3299 (1-)
	3299					O2+ 3304 (2-)	Na 3303
3302	3302				CO 3306	NH 3308	
	3307	3308			CO+ 3314	O2+ 3313 (2-)	
3310					CO+ 3316	O2 3316 (HI)	Ni 3316
3318	3319					O2+ 3323 (2-)	Ni 3322
3325		3325				OH+ 3332	
	3329					O2+ 3334 (2-)	
3335	3338						
3341				3351 NH	CO+ 3352	N2 3352 (VK)	
3350	3347			3354 NH	CO+ 3353	O2 3357 (SR)	
	3355			3358 NH	NH 3360		Ni 3362
3360		3360		3365 NH	CO+ 3366	O2 3368 (HI)	Ni 3366
	3365			3369 NH	NH 3370	O2 3370 (SR)	Ni 3370
3370				3372 NH			Ni 3374
	3374	3372		3378 CO2+	NO 3376 (β)	O2 3382 (HI)	Ni 3381
3380	3380	3380		3398 CO2+	NO 3386 (β)		Ni 3391
3390	3391			3388 CO2+		O2+ 3393 (2-)	Ni 3393
3395	3397	3395					

TABLE A-1 (CONTINUED)

EXPLOSIONS				COMET	POSSIBLE IDENTIFICATION		
HILGER	GRATING	CINE	AVCO				
3402	3404						Co 3405
3407							Co 3409
3410	3411	3412			CO^+ 3413	CO 3412	Co 3412
3417	3415			3416 CO^+	CO^+ 3415	O_2 3215 (HI)	Ni 3415
3420	3423				N_2 3425 (VK)	O_2^+ 3421 (2$^-$)	Ni 3423
3430				3431 CO^+	CO^+ 3428	OH 3428	Co 3432
3435					OH 3432	O_2 3433 (SR)	Co 3433
3440		3442					Ni 3437
	3446						Ni 3446
3450	3452					O_2 3450 (HI)	Co 3454
3460	3462	3462			OH 3459	O_2 3457 (HI)	Co 3463
	3465				N_2 3466 (VK)	O_2^+ 3466 (2$^-$)	N 3466
	3470					OH 3472	Co 3474
3475	3477	3475					
3480	3479			3478	CO 3482	O_2 3479 (HI)	
3486					CO 3485		Ni 3484
	3490	3490					
3495						O_2^+ 3494 (2$^-$)	Co 3496
3500	3497				N_2 3502 (VK)	O_2 3499 (SR)	Co 3502
	3505	3508				CH 3505	
3510	3512	3515		3509 CO_2^+		CO^+ 3510	Ni 3515
	3516				CO^+ 3512	O_2 3517 (SR)	
3520	3520					O_2^+ 3518 (2$^-$)	Ni 3520
3525				3525			Ni 3525
3530	3531				CO^+ 3527	N_2^+ 3533 (1$^-$)	Co 3530
	3535					N_2^+ 3538 (1$^-$)	
3540	3543	3540				O_2 3540 (HI)	
	3546	3545		3545 CO_2^+		O_2^+ 3542 (2$^-$)	
3550	3550					N_2^+ 3548 (1$^-$)	Ni 3548
3555	3556					O_2 3553 (HI)	
3560	3561	3560					
	3563			3565 OH^+	OH^+ 3562	N_2^+ 3564 (1$^-$)	
3570	3568			3572 CN		O_2^+ 3568 (2$^-$)	Ni 3566
3575	3574	3574		3577 CN	NO 3572 (β)		Ni 3572
	3581			3580 CN	N_2 3581 (VK)	O_2 3582 (SR)	N_2^+ 3582 (1$^-$)
3585				3584 CN	NO 3584 (β)	CO^+ 3586	CN 3584
3590	3590	3590				CN 3590	
	3596	3596		3594 CO^+		O_2 3596 (BG)	Ni 3598
3600	3603				N_2 3602 (VK)	O_2^+ 3604 (2$^-$)	CN 3603
3610	3612	3610				NH 3610	Ni 3610
	3619			3616 OH^+		O_2^+ 3619 (2$^-$)	Ni 3619
3625		3622		3626	NH 3627	O_2 3628 (HII)	
	3631					O_2^+ 3630 (2$^-$)	
3635					CH 3636	O_2 3635 (HI)	
3643	3642	3640				N_2 3642 (2$^+$)	
3650						O_2 3651 (SR)	
3655	3657					O_2^+ 3653 (2$^-$)	
	3659						
3665	3667	3665					

TABLE A-1 (CONTINUED)

EXPLOSIONS				COMET	POSSIBLE IDENTIFICATION		
HILGER	GRATING	CINE	AVCO				
3675	3674			$3674\ CO_2^+$	$N_2\ 3672\ (2^+)$	$O_2\ 3673\ (SR)$	
3680	3683			$CO\ 3680$	$N_2\ 3682\ (VK)$		
3685	3687	3685			$O_2\ 3685\ (HII)$		
3690	3689			3693	$CO^+\ 3688$		
3695				$3695\ CO^+$	$OH^+\ 3695$	$O_2\ 3696\ (BG)$	
3700	3699			3700	$CO\ 3699$	$O_2^+\ 3701\ (2^-)$	
3710	3710	3705		$3709\ CO^+$	$CO^+\ 3705$	$N_2\ 3711\ (2^+)$	
3720	3719	3715		3718			
	3727			$3726\ CO^+$	$CO^+\ 3725$	$O_2^+\ 3728\ (2^-)$	
	3731	3730			$CO^+\ 3730$	$O_2^+\ 3734\ (2^-)$	
3735	3737			$3739\ C_3$		$O_2\ 3738\ (HI)$	
	3745	3745		3741	$CH^+\ 3744$	$O_2\ 3742\ (SR)$	$NH\ 3743$
3755	3753					$O_2\ 3750\ (HII)$	$NH\ 3752$
	3756				$N_2\ 3755\ (2^+)$		
3760	3763	3765		$3762\ C_3$		$O_2\ 3764\ (BG)$	$N_2\ 3767\ (VK)$
	3773	3773				$O_2\ 3771\ (Ch)$	$Ni\ 3776$
3780	3782			3780		$CO^+\ 3780$	
3785				3785			$Ni\ 3784$
3790					$NO\ 3789\ (\beta)$	$O_2\ 3791\ (Ch)$	
	3797	3796			$CO^+\ 3796$		
3800	3803			$3803\ CO^+$	$NO\ 3801\ (\beta)$	$Na\ 3804\ (2^+)$	$NH\ 3804$
	3806			$3804\ C_3$		$CH^+\ 3806$	$Ni\ 3807$
	3811			$3809\ C_3$		$O_2\ 3812\ (Ch)$	$CH^+\ 3811$
3815	3818	3815				$O_2\ 3818\ (HII)$	
3820						$O_2\ 3822\ (HII)$	$4\ Fe\ 3824$
	3826	3827				$O_2\ 3828\ (HI)$	
	3831	3834		$3829\ C_3$	$OH^+\ 3830$	$O_2 + 3831\ (2^-)$	$Mg\ 3835$
3840	3837	3840		$3829\ CO_2^+$		$O_2\ 3841\ (SR)$	
3845	3847					$O_2\ 3844\ (Ch)$	
3850	3853	3850		$3851\ CN$		$CN\ 3851$	
3855	3855	3855		$3854\ CN$		$CN\ 3855$	
3865	3862	3862		$3862\ CN$		$CN\ 3862$	
3870	3872	3870	BEGIN	$3869\ CN$		$CN\ 3871$	
3883	3883	3883	3883	$3883\ CN$		$CN\ 3883$	
3895	3895			$3893\ CN$	$CO\ 3891$	$N_2\ 3895\ (2^+)$	$Co\ 3894$
3904	3902	3905		$3903\ CH$	$CH\ 3903$	$O_2\ 3904\ (HII)$	$4\ Fe\ 3900$
3908	3908	3912	3910	$3908\ CH$	$CH\ 3909$	$CO^+\ 3908$	$4\ Fe\ 3906$
	3915			$3914\ N_2^+$	$CH\ 3915$	$N_2^+\ 3914\ (1^-)$	$O_2\ 3913\ (SR)$
3920	3920			$3922\ CH$	$CH\ 3922$		$4\ Fe\ 3920$
	3926				$CO\ 3924$	$O_2^+\ 3929\ (2^-)$	$4\ Fe\ 3928$
3934	3934	3934	3934	$3935\ NaH$		$Ca + 3934$	
3940						$O_2\ 3940\ (HI)$	
3944	3945					$N_2\ 3943\ (2^+)$	$Al\ 3944$
	3949	3950		$3950\ C_3$	$N_2\ 3948\ (VK)$	$O_2\ 3953\ (HII)$	$C_3\ 3950$
3958	3959	3960		$3960\ C_3$	$OH + 3958$	$O_2^+\ 3959\ (2^-)$	$C_3\ 3960$

TABLE A-1 (CONTINUED)

EXPLOSIONS				COMET	POSSIBLE IDENTIFICATION		
HILG	GRATING	CINE	AVCO				
3965	3964				CH + 3962	C₃ 3964	Al 3962
3968	3968	3968	3968			Ca + 3968	
3980	3980			3980 C₃	N₂ 3976 (VK)	O₂ 3982 (Ch)	C₃ 3980
3990	3989			3987 C₃		O₂ 3987 (SR)	C₃ 3987
3995	3998	3994		3993 C₃	N₂ 3998 (2+)	O₂ 3994 (HII)	Co 3995
4000	4001	4000		4000 C₃	C₃ 4002	O₂ 4005 (Ch)	4 Fe 4005
4015	4015			4018 CO⁺	CO⁺ 4017		C₃ 4013
	4019	4020		4020 C₃	C₃ 4019	O₂ 4021 (SR)	Cu 4022
4025	4027			4022 C₃	C₃ 4028	O₂ 4028 (Ch)	CH 4028
4030		4030		4028 C₃		O₂ 4033 (BG)	
4035	4036	4040		4033 C₃	NO 4047 (β)	O₂ 4041 (Hi)	K 4044
4050				4051 C₃	43 Fe 4046	O₂ 4050 (BG)	K 4047
	4058					N₂ 4059 (2+)	C₃ 4054
4060	4062		4065	4064 C₃	N₂ 4059 (2+)	O₂ 4062 (BG)	43 Fe 4064
4068	4068	4070		4068 C₃	N₂ 4072 (VK)	O₂ 4068 (Ch)	C₃ 4068
4075	4076	4080	4078	4074 C₃	C₃ 4074	O₂⁺ 4082 (2⁻)	
4085	4088			4084 C₃	C₃ 4085	O₂ 4085 (Ch)	CH 4083
4090	4090		4093	4093 C₃	C₃ 4090	O₂ 4092 (Ch)	Co 4092
4095	4096			4096	C₃ 4099	O₂ 4096 (SR)	
4103	4105			4099 C₃		O₂ 4106 (Ch)	C₃ 4109
4108				4109 C₃	C₃ 4109	O₂ 4109 (Ch)	Co 4111
4115		4115			NO 4114 (β)	O₂⁺ 4116 (2-)	Co 4118
	4119				NH 4120	O₂ 4120 (BG)	Co 4121
4125				4124 CO⁺	C₃ 4124	CO 4124	
4130	4132				CO⁺ 4130	O₂ 4129 (Ch)	K 4132
	4135			4138 C₃	C₃ 4138	O₂ 4133 (Ch)	CO⁺ 4139
4142	4145	4140		4140 CO⁺	N₂ 4144 (VK)	N₂ 4142 (2⁺)	43 Fe 4144
4150	4149		4151			O₂ 4146 (BG)	42 Fe 4148
	4155				CO⁺ 4152	CO 4157	NH₂ 4153
4160		4160				CN 4158	
4165	4165		4167	4170 NₐH		CN 4168	
	4176		4178		CH⁺ 4178	O₂ 4173 (SR)	CO 4173
4180	4183	4185	4181	4180 CN		CN 4181	
4190				4193 CN		CO 4188	
4195	4194		4196	4197 CN		CN 4197	
	4201	4200			NO 4201 (β)	N₂ 4200 (2⁺)	42 Fe 4202
4205				4206 CN		O₂ 4204 (BG)	
4210	4213			4210 CN	NO 4215 (β)	O₂ 4213 (Ch)	CO⁺ 4210
4215	4218	4216	4216	4215 CN		CN 4216	
4227	4227	4227	4227	4231 CO⁺		Ca 4227	
4240	4238			4239 CH⁺	CH⁺ 4237	O₂ 4240 (Ch)	N₂⁺ 4237 (1⁻)
	4242				CO⁺ 4244	O₂ 4242 (Ch)	
	4247			4245 AlH		CO⁺ 4246	
4250	4250			4249 CO⁺		CO⁺ 4248	42 Fe 4250
	4251			4252 CO⁺		CO⁺ 4251	

TABLE A-1 (CONTINUED)

EXPLOSIONS				COMET	POSSIBLE IDENTIFICATION		
HILGER	GRATING	CINE	AVCO				
	4253			4254 CH$^+$		O$_2$ 4252 (HII)	Cr 4254
4260		4257		4264 AlH			
4270	4267			4272 CO$^+$	CO$^+$ 4271	O$_2$ 4266 (HII)	N$_2$ 4270 (2$^+$)
4275	4277	4275	4277	4274 CO$^+$	N$_2^+$ 4278 (1$^-$)	O$_2$ 4275 (RG)	Cr 4275
4280	4281			4281 CH		O$_2$ 4281 (BG)	
	4282					O$_2$ 4285 (BG)	
4290	4288		4287	4286 CH		NO 4288 (β)	
	4293	4292	4295	4292 CH	NO 4294 (β)	O$_2$ 4292 (SR)	Cr 4290
4300	4300			4303 CH		CO 4297	
	4302		4302		CO 4302	O$_2$ 4302 (BG)	NO 4303 (β)
4305	4305			4304 CH			
	4308		4308		NO 4310 (β)	O$_2$ 4306 (HI)	42 Fe 4308
	4311				CO 4312	CH 4312	
	4314			4314 CH	CO 4314	O$_2$ 4314 (Ch)	
4320	4318		4320				
	4324				CH 4323	O$_2$ 4325 (Ch)	
	4326				CO 4326	CH 4327	2 Fe 4326
	4328					CO 4329	
4330	4330		4330			O$_2$ 4331 (HII)	
	4334	4333		4334 CH		CO 4332	
	4335					OH 4336	
	4338			4339 CH	CO 4339	O$_2$ 4339 (HII)	41 Fe 4337
	4343			4344 CH	CO 4343	N$_2$ 4344 (2$^+$)	
4350				4348 CH		N$_2$ 4355 (2$^+$)	2 Fe 4347
	4360	4358				O$_2$ 4363 (BG)	
4365				4364 C$_2$		O$_2$ 4368 (HII)	
4370	4371			4371 C$_2$	CO 4370	O$_2$ 4373 (SR)	
4375	4275					CO 4374	2 Fe 4376
4380	4379		4379	4381 C$_2$	CO$^+$ 4378	O$_2$ 4379 (Ch)	CO 4380
	4384	4385	4383		NO 4386 (β)	CO$^+$ 4381	41 Fe 4384
	4390			4392 CH		CO 4390	2 Fe 4389
4395		4395	4398		NO 4401 (β)	O$_2^+$ 4399 (2$^-$)	Ni 4402
4407	4406		4405		CO$^+$ 4406	O$_2$ 4402 (BG)	2 Fe 4405
	4411	4410				O$_2$ 4412 (BG)	
	4418				N$_2$ 4417 (2$^+$)	O$_2$ 4415 (BG)	41 Fe 4415
	4421	4420				O$_2$ 4421 (HII)	
4425	4425	4425	4425			O$_2$ 4423 (SR)	
	4426			4429 KH			2 Fe 4227
	4435	4435				CH$^+$ 4434	2 Fe 4435
4440	4439						
	4442					CH$^+$ 4444	
	4447		4445			CO 4445	
4450	4451		4449				
	4454	4455	4453				
	4459		4460		CO 4460	O$_2$ 4457 (BG)	Ni 4459
4465	4467			4463 C$_2$	N$_2^+$ 4467 (1$^-$)	CO 4466	2 Fe 4467
	4475	4473					2 Fe 4472
4480			4483		Mg$^+$ 4481	CO 4478	2 Fe 4482

TABLE A-1 (CONTINUED)

EXPLOSIONS				COMET	POSSIBLE IDENTIFICATION		
HILGER	GRATING	CINE	AVCO				
	4486		4488	4485 C_2	N_2 4490 (2$^+$)	CO 4488	
4490	4494	4490	4494		N_2 4495 (VK)	CO 4494	2 Fe 4490
	4504	4509		4504 C_2	NH 4502	O_2 4504 (SR)	CO 4505
4515		4515		4511 NH_2	N_2^+ 4516 (1$^-$)	CO$^+$ 4518	NH_2 4511
4520			4519		CO$^+$ 4521	O_2 4522 (HII)	CO 4521
	4527				NH 4523	CO 4524	Co 4531
	4535		4536		N_2 4534 (VK)	CO$^+$ 4539	
4543			4540	4541 C_2	CO$^+$ 4543	O_2 4544 (BG)	CO 4541
	4546	4545		4544 CO$^+$			
	4554		4551	4554 M_gH	N_2^+ 4553 (1$^-$)	Ba$^+$ 4554	Cs 4450
		4560					
4565	4569		4565	4569 CO$^+$	CO$^+$ 4568	O_2 4568 (BG)	Co 4566
4580						C_2 4579 (HI)	Co 4582
4597		4593	4593	4598	NO 4595 (β)	O_2 4591 (HII)	Cs 4593
4609		4613		4613	Sr 4607	O_2 4609 (HII)	Li 4603
			4617	4619			
	4623			4622			
4630		4630		4629			Co 4629
4635	4640			4632,34		O_2 4637 (HII)	
4650					N_2 4650 (VK)	Ni 4649	
4655		4655		4655	N_2^+ 4652 (1$^-$)		
	4661			4662	CO 4661		Co 4663
4670		4670	4672	4670	CO 4668	N_2 4667 (2$^+$)	
			4677	4676 C_2	CO 4680	O_2^+ 4679 (2$^-$)	
4683				4683 C_2	CO 4685	O_2 4686 (BG)	CO$^+$ 4683
4705		4706		4705 C_2	CO 4702	O_2 4704 (BG)	N_2^+ 4709 (1$^-$)
			4714	4713 C_2	CO 4717		Ni 4714
		4725		4728	NH_2 4720	O_2^+ 4721 (2$^-$)	N_2 4724 (2$^+$)
4733			4733	4735 C_2	OH 4730		
4742				4743 C_2			
			4748	4746		CO 4749	Co 4750
	4754						
4760		4760			CO 4764	O_2^+ 4760 (2$^-$)	O_2 4761 (SR)
		4770	4767				
4775						CH$^+$ 4776	Co 4780
		4792		4791	CO 4787	CH$^+$ 4794	Co 4793
4804		4808	4810	4801 KH		O_2 4806 (HII)	
4815		4820			N_2 4815 (2$^+$)	O_2 4816 (SR)	Co 4813
4833					CO 4835	CO$^+$ 4837	
4840				4839 HCO	N_2 4837 (VK)	O_2 4840 (BG)	N 4842
4850	4852					O_2 4848 (BG)	
	END	4857			CO 4855	CH 4857	Co 4859
4862							
		4869		4872	CO 4869	CO$^+$ 4869	Co 4868
4883		4880		4877 SiC_2	CO 4881	O_2 4881 (HI)	

TABLE A-1 (CONTINUED)

| EXPLOSIONS | | | | | POSSIBLE IDENTIFICATION | | |
HILGER	GRATING	CINE	AVCO	COMET			
4887				4890	CO^+ 4884	CH 4888	
			4910		CO^+ 4911	O_2 4905 (SR)	
4920		4915		4924	CH 4914	N_2 4917 (2^+)	NH_2 4925
			4932	4925 NH_2	CO 4936	O_2 4935 (HII)	Ba + 4934
		4948		4946			NH_2 4946
		4980	4975		N_2 4976 (2^+)	CO 4980	Ni 4980
			4990		CO 4988	O_2 4997 (SR)	Co 4988
		5019					Co 5023
5035				5029	CO^+ 5040	O_2^+ 5035 (2^-)	
			5051	5054		N_2 5047 ($G\alpha$)	Co 5053
5105		5100		5097 C_2	N_2 5090 ($G\beta$)	O_2^+ 5102 (2^-)	Cu 5106
			5136			O_2^+ 5143 (2^-)	
5153				5153	Na 5149,54	O_2 5156 (SR)	Cu 5153
		5160	5169	5165 C_2		NH_2 5166	
		5187	5179	5182		Mg 5176	Co 5176
5210				5201	CO^+ 5204	Cr 5208	N 5201
		5225	5215	5220	NO 5224	CO 5216	Cu 5218
		5260	5263		CO 5256	O_2^+ 5259 (1^-)	Co 5266
		5272		5271		N_2 5272 ($G\alpha$)	
			5290	5284	CO^+ 5286	N_2 5290 ($G\beta$)	Co 5281
5317			5317	5316	CO^+ 5318	N_2 5309 ($G\alpha$)	CO 5318
5358		5356	5355	5352		CO 5351	Co 5353
			5381	5381		CO 5378	NH_2 5385
		5397			CO^+ 5394	O_2 5395 (BG)	CO 5397
		5420		5417 NH_2	NH_2 5417	O_2 5425 (SR)	Cr 5410
5433				5428	N_2 5435 ($G\alpha$)	O_2 5435 (HII)	NH_2 5428
5450		5448		5444		O_2^+ 5443 (2^-)	CO 5449
		5465		5466 C_2	NH_2 5465	O_2 5466 (SR)	CO + 5461
			5482	5483 C_2	OH 5481	N_2 5480 ($G\alpha$)	Co 5483
		5535	5534	5539 C_2	OH 5534	N_2 5527 ($G\alpha$)	Ba 5536
5565		5560			NO 5559	O_2^+ 5567 (1^-)	
			5574	5577 O	NH_2 5575	N_2 5574 ($G\alpha$)	O 5577
			5585	5583 C_2			Co 5590
			5595		N_2 5594 ($G\beta$)	O_2^+ 5598 (1^-)	
		5605		5612	CO 5610	N_2 5602 ($G\alpha$)	
		5640	5643	5634	CO 5648	N_2 5640 ($G\alpha$)	Co 5647
5655					$CO + 5653$	N_2 5661 ($G\beta$)	Co 5661
		5680	5680	5679	H_2O 5683	O_2^+ 5678 (2^-)	
5690			5695		NH_2 5703	O_2 5702 (HII)	CO^+ 5694
		5736	5730	5733		NH_2 5730	
5745		5762			CO^+ 5764	N_2 5776 ($G\beta$)	
5790				5798		CO 5781	Cu 5782

TABLE A-1 (CONTINUED)

HILGER	GRATING	CINE	AVCO	COMET	POSSIBLE IDENTIFICATION
5893		5893	5893	5893 Na	Na 5890, 96
5902					NO 5900 CO+ 5900 H2O 5900
5912				5910	NO 5907 N2 5294 (G α) CO+ 5906
		5946			H2O 5949
		5969			CO+ 5970 O2+ 5973 (1⁻)
		5982	5984	5982	NH2 5977 H2O 5989 CO+ 5976
		5996			NO 5999 N2 5995 (Gα) Co 5992
6033		6024	6030	6031	N2 6026 (Gα) O2+ 6026 (1⁻)
		6038		6034	NH2 6042 CO 6037
			6044		O2 6052 (HII)
6090			6099	6095	N2 6091 (Gα) NH2 6087
		6109	6110	6107	N2 6101 (Gα) Li 6104
6150		6158	6165	6157	H2O 6166 N2 6161 (G α)
6180		6173		6178	H2O 6182 N2 6183 (G β) Ni 6177
		6192	6200	6187 C2	N2 6202 (LTJ) N2 6192 (G α) H2O 6203
		6214	6213		H2O 6220 NO 6213
6223					NH2 6233
		6250	6257		NO 6259 N2 6246 (G α) Ni 6256
		6295	6294	6297 NH2	NH2 6295 O 6300
6310					NH2 6302 NO 6308
6355			6359	6361 NH2	N2 6360 (G β) O2+ 6351 (1⁻) NO 6355
6397		6380	6392	6381	H2O 6377 NO 6378
6435					NO 6429 CO 6433
			6449	6455	H2O 6458 NH2 6455 Co 6450
6478		6474	6477		H2O 6468 NH2 6470 Co 6465
6500			6500		H2O 6490 Ba+ 6496
6505				6510	
6515			6522		H2O 6517 NH2 6525 Co 6514
			6535	6539	O2 6541 (HII)
		6560		6557	H2O 6575
			6599	6597	N2 6585 (LTJ) Ba 6595
6617				6616	NH2 6618 H2O 6629 Co 6620
6662			6666	6670	NH2 6652 NO 6673
		6698	6707		NO 6700 Li 6708
		6715	6720	6722	NO 6729
6750			6750	6749	N2 6750 (LTJ) NO 6746
6797		6805	6800		CO 6804 NO 6797
6817			6816		NO 6812
			6838		
			6880		N2 6904 (LTJ) NO 6872
		6991			CO 6990

TABLE A-1 (CONTINUED)

EXPLOSIONS				COMET	POSSIBLE IDENTIFICATION		
HILGER	GRATING	CINE	AVCO				
			7101				
			7129		NO 7140	Ni 7122	
7158					H_2O 7165		
		7196					
			7215		CO 7210		
			7259		N_2 7241 (LTJ)		
			7401		N_2 7418 (LTJ)		
			7441				
		7508			H_2O 7502		
			7551		N_2 7600 (LTJ)		
7682			7682		K 7664, 99		
		7721					
		END	7772		N_2 7789 (LTJ)	O 7774	
			7832		N_2^+ 7826 (M)	CO 7834	Rb 7800
8035				7906	N_2^+ 8054 (M)	NO 8021	N_2 8055 (LTJ)
			8121	8106	N_2^+ 8105 (M)		Li 8127
			8224		N_2 8260 (LTJ)	CO 8223	
8360			8330		N_2^+ 8348 (M)	O_2^+ 8347 (1⁻)	
8530			8533		N_2^+ 8546 (M)	N_2 8471 (LTJ)	Cs 8521
			8728		N_2 8689 (LTJ)	NO 8731	

NOTES FOR TABLE

1. N_2

    G (α, β, γ): Gaydon green bands
    LTJ: Le Blanc, Tanaka, Jursa bands
    M: Meinel bands
    VK: Vegard – Kaplan bands

2. O_2

    BG: Broida – Gaydon bands
    Ch: Chamberlain bands
    H (I, II):   Herzberg bands
    SR: Schumann – Runge bands

3. 1^+, 2^+ etc.:   first positive, second positive etc.

4. Number before Fe identifies multiplet

REFERENCES FOR TABLE A-1:

A. GENERAL
1. Chamberlain, Joseph W., Physics of the Aurora and Airglow, Academic Press, New York 1961.
2. Gatterer, A., Junkes, J. and Salpeter, E.W., Molecular Spectra of Metallic Oxides, Specola Vaticana 1957.
3. Mavrodineanu, Radu and Boiteux, Henri, Flame Spectroscopy, John Wiley & Sons, Inc., New York 1965.
4. Moore, Charlotte E., A Multiplet Table of Astrophysical Interest, National Bureau of Standards Tech. Note 36, November, 1959.
5. Pearse, R.W.B. and Gaydon, A.G., The Identification of Molecular Spectra, 3rd Edition with Supplement, Chapman and Hall Ltd, London 1965.
6. Wallace, L., "A Collection of the Band - Head Wavelengths of N_2 and N_2^+," Ap. J. Suppl. Ser. 6, 445, 1962 and "Band - Head Wavelengths of C_2, CH, CN, CO, NH, NO, O_2, OH, and Their Ions," Ap. J. Suppl. Ser. 7, 165, 1962.
7. Zaidel, A.N., Prokov'ev, V.R., and Raiskii, S.M., Tables of Spectral Lines, Pergamon Press, New York 1961.

B. COMETARY SPECTRA
1. Arpigny, C., Ann. Rev. Astrom. and Astro. 3, 351, 1965.
2. Rosen, B., Swings, P. and Honzioux, L. Ann. d'Ap. 20, 76, 1957.
3. Stawikowski, A., Bull, Soc. Royale Sci. Liege, 31, 414, 1962.
4. Swings, P. and Haser, L., Atlas of Representative Cometary Spectra, University of Liege Astrophysical Institute, Liege 1956.
5. Swings, P., "Astronautical Investigations of Comets" in Space Science and Technology, edited by F.I. Ordway III. Academic Press, New York 1965.
6. Swings, P., Quart. J. Roy. Astro. Soc. 6, 28, 1965.
7. Woszczyk, A., Bull. Soc. Royale Sci. Liege 31, 396, 1962.
8. Wurm, K., "The Physics of Comets" in The Moon, Meteorites and Comets (Vol IV of The Solar System), edited by B.W. Middlehurst and G.P. Kuiper. University of Chicago Press. Chicago 1963.

C. METEOR SPECTRA
1. Bronshten, V.A. and Liubarsky, K.A., "The Radiation from Meteors and Bolides" in Meteoric Matter in the Earth's Atmosphere, edited by V.V. Fedynskii, Nauka, Moscow 1966. Translated by J.B. Gazley, Rand Corporation, February 1968.
2. Russell, J.A., Ap. J. 131, 34, 1960.
3. Millman, P.W., "A General Survey of Meteor Spectra," in Vol. 7, Smithsonian Contributions to Astrophysics, 1963.
4. Millman, P.W. and McKinley, D.W.R., "Meteors," in The Moon, Meteorites and Comets (Vol. IV of The Solar System), Edited by B.W. Middlehurst and G.P. Kuiper, University of Chicago Press, Chicago 1963.

D. SPECIFIC SPECIES
1. C_3: Kiess, N.H. and Broida, H.P. Can. J. Phys. 34, 1471, 1956.
2. CH: Babrovnikoff, N.T., Ap. J. 99, 173, 1944.
   McKellar, Andrew, Ap. J. 99, 162. 1944.
3. N_2: Grün, A.E., Zeit. für Naturfor, 9a, 1017,1954.
   Heath, D.F., "New Data on the Emission Spectrum of Air," Los Alamos Rpt. LA – 2335. January 1960.
   Kurzweg, U.H., Bass, A.M. and Broida, H.P. J. Molc. Spec. 1,184, 1957.
   Le Blanc, F., Tanaka, Y., and Jursa, A., J. Chem. Phys. 28, 979, 1958.
   Lofthus, A., "The Molecular Spectrum of Nitrogen," University of Oslo Spectroscopic Rpt. #2. Blindern, Norway. December 1960.
   Noxon, J.F., "Active Nitrogen at High Pressure," Thesis, Harvard University, Cambridge, May 1957.
   Tyte, D.C. and Nicholls, R.W., "Identification Atlas of Molecular Spectra, 2. The N_2 C^3 $\pi_u - B^2$ π_g Second Positive System," University of Western Ontario, October 31, 1964.
   Tyte, D.C. and Nicholls, R.W., "Identification Atlas of Molecular Spectra, 3. The N_2^+ B^2 $\Sigma_u^+ - X^2 \Sigma_g^+$ First Negative System of Nitrogen," University, of Western Ontario, April 1965.
4. O_2: Herbert, G.R., Innanen, S.H. and Nicholls, R.W., "Identification Atlas of Molecular Spectra, 4: The O_2 B^3 $\Sigma_u^- - X^3 \Sigma_g^-$ Schumann – Runge System." University of Western Ontario, January 1967.

TABLE A-2: SUMMARY OF RADIATING SPECIES IDENTIFIED IN EXPLOSIONS
IN AIR

MOLECULAR (NEUTRALS AND IONS)

C_3
CH
CH^+
CN violet
CN^+
CO Angstrom, Asundi, Herzberg, Third Positive, Triplet
CO^+ Baldet – Johnson, Comet – tail
N_z Gaydon (α, β, γ,) Le Blanc – Tanaka – Jursa, Second Positive, Vegard – Kaplan
N_2^+ First Negative, Meinel
NH
NH_2
NO β, Ogawa
O_2 Broida – Gaydon, Chamberlain, Herzberg, Schumann – Runge
O_2^+ First Negative, Second Negative
OH
OH^+

ATOMIC (NEUTRALS AND IONS)

Al	Li
Ba	Mg
Ba^+	N (forbidden)
Ca	Na
Ca^+	Ni
Co	O (forbidden)
Cr	Rb
Cs	Sr
Fe	
K	

TABLE A-3 SUMMARY OF WAVELENGTHS SEEN ON AVCO SPECTRA
OF VARIOUS EXPLOSIVE MATERIALS

PENTOLITE	RDX	TNT	NM + TNM	PENTOLITE	RDX	TNT	NM + TNM
				4549		4551	
3883	3883	3883			4565		
				4593	4593		
3910		3909					
3937	3934	3934		4617			
3968	3968	3968		4672		4677	
4065		4075		4714			
4093				4733			
				4748			
4151	4150	4155		4767			
4163	4166	4169		4810			
4181	4178	4184	4178				
4198	4197	4200		4910		4910	
						4932	
4213	4220	4216		4975			
4226	4227	4227	4227	4990			
4285	4277	4287					
					5051		
4301	4295	4304			5136		
	4308			5169		5167	
4320		4325			5179		
	4330						
4398	4405	4384			5215		
				5260	5265	5255	
4426	4425	4425		5290			
4449	4445	4453					
	4460				5317		
4488	4483	4494				5354	
				5380	5382		
4519							
4536	4540				5482		

TABLE A-3 (CONTINUED)

PENTOLITE	RDX	TNT	NM + TNM	PENTOLITE	RDX	TNT	NM + TNM
5531	5537	5527			6666		
5574							
5594	5585	5590	5590	6708	6705		6720
					6750		
	5643						
5695	5680	5697	5690	6800	6816		
	5730				6838		
					6880		
5893	5893	5893	5893				
	5984			7129	7101		
6027	6030			7215	7259		
	6044						
6110	6099			7401	7441		
	6115			7682	7677		
6162	6165				7772		
6213		6200					
6257				7832	7836		
	6294			8121			
6359					8224		
	6392				8330		
6447	6449				8533		
6477							
	6500				8728		
	6522		6535				
6617	6599						

TABLE A-4 PY-I MEASUREMENTS OF SPHERICAL EXPLOSIONS

SHOT NO.	VIEW	AMPLITUDE (VOLTS)				AVER. TIME TO PEAK (μ SEC)	TIME TO DECAY TO 1/2 PEAK (μ SEC)			
		BAND 0	BAND 1	BAND 2	BAND 3		BAND 0	BAND 1	BAND 2	BAND 3
				PENTOLITE EXPLOSIONS						
49	HEAD-ON		0.54	0.53		5.0		28.5	34.1	
50	HEAD-ON		0.48		0.57	6.0		22.4		38.9
52	HEAD-ON		0.34	0.37	0.48	7.2		23.2	25.4	29.2
65	HEAD-ON	0.34	0.48	0.60	0.61	6.2		24.2	34.1	45.9
77	HEAD-ON	0.29	0.42	0.47		11.4	14.6	16.8	13.8	14.6
78	HEAD-ON	0.18	0.32	0.49	0.42	10.1	13.0	14.4	16.4	23.4
75*	HEAD-ON	0.53	0.58	0.50	0.52	10.0	39.7	62.5	78.1	85.0
82	SIDE-ON	0.08	0.16	0.23	0.28	12.7	19.0	20.1	21.0	23.4
83	SIDE-ON	0.07	0.13	0.19	0.27	10.0	22.3	22.9	22.4	24.8
89	SIDE-ON	0.02	0.05	0.10	0.17	4.7	8.0	8.6	8.8	9.3
90	SIDE-ON	0.01	0.02	0.04	0.08	3.9		6.9	6.4	7.6
				TNT EXPLOSIONS						
66	HEAD-ON		0.20	0.34	0.44	8.0	30.0	34.0	36.0	
72	HEAD-ON				0.30	13.0			120.0	
				(NM + TNM) EXPLOSIONS						
56	HEAD-ON		0.22	0.28	0.42	11.3		15.3	13.6	16.1
58	HEAD-ON		0.20	0.29	0.41	14.3		15.4	14.3	17.2
67**	HEAD-ON		0.65	0.75	0.69			15.8	22.0	23.2
				RDX EXPLOSIONS						
53***	HEAD-ON			0.36	0.46	3.4			6.0	6.2
54***	HEAD-ON	0.16	0.22	0.31	0.39	2.6	4.7	5.2	5.6	5.5
55	HEAD-ON			0.17	0.23	2.0			8.1	8.3
57	HEAD-ON		0.47	0.53	0.54	4.4		14.3	17.7	18.9
60	HEAD-ON	****	0.52	0.61	0.59	4.1		13.4	16.8	20.2
61	HEAD-ON	****	0.39	0.51	0.52	4.1		7.2	11.2	15.8
63	HEAD-ON	0.05	0.51	0.60	0.57	4.7		15.6	19.2	23.6
64	HEAD-ON	0.12	0.54	0.63	0.63	4.7	4.8	17.0	22.6	25.2
68	HEAD-ON	****	0.47	0.55	0.52	3.6		17.3	20.8	26.6
79	HEAD-ON	0.31	0.55	0.72	0.89	3.2	10.7	12.7	13.0	13.7
91	SIDE-ON	0.02	0.05	0.08	0.14	3.8	6.1	7.3	7.3	7.0
96	SIDE-ON	0.03	0.08	0.12	0.13	3.5	5.8	6.7	5.9	7.7
94 †	SIDE-ON	0.02	0.06	0.04	0.08	2.6	5.4	3.2	6.1	6.7
95 †	SIDE-ON	0.01	0.02	0.04	0.07	2.9		7.6	8.3	7.6

* - 20% AlO$_3$ added
** - (RDX - TNM) charge
*** - Full lucite cover

**** - Signal just detectable
† - 20% graphite added

Hg 4047
Co 4227
Hg 4358
Hg 5460
Hg 5780
Na 5893
LASER 6943

Ca+ 3934
Ca+ 3968
Hg 4047
CN 4216
Hg 4358
Hg 5460
Hg 5780

(NOMINAL) TIME (μ SEC)
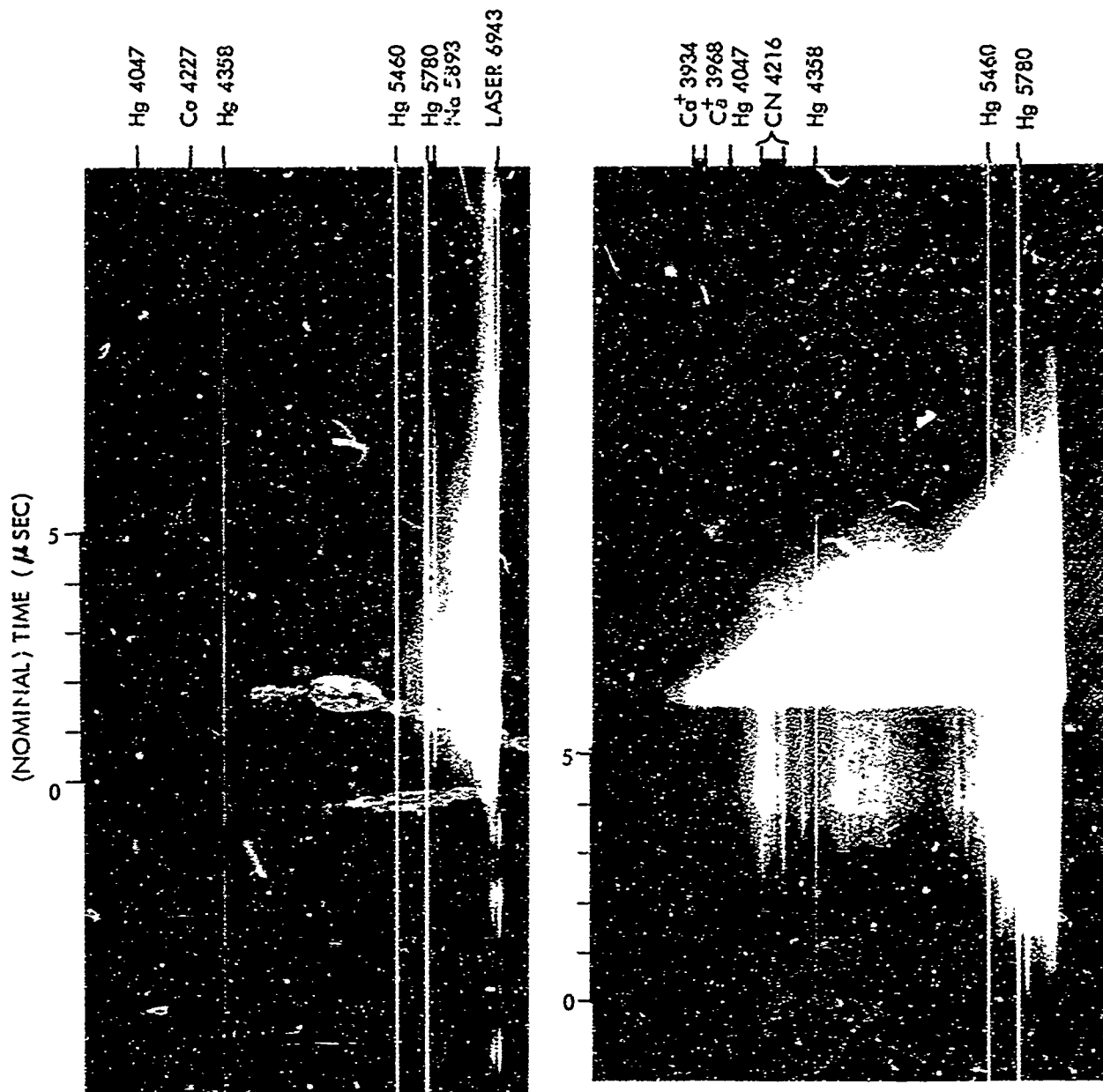
CHARGE: 8-LB SPHERE, SHOT 89
VIEW: 1" FROM SURFACE
CONDITIONS: LASER ILLUMINATION
FILM: 2475

CHARGE: 8-LB SPHERE, SHOT 78
VIEW: HEAD-ON
CONDITIONS: GLASS PLATE (1/4X6X6")
               AT 1.5" FROM SURFACE
FILM: TRI-X
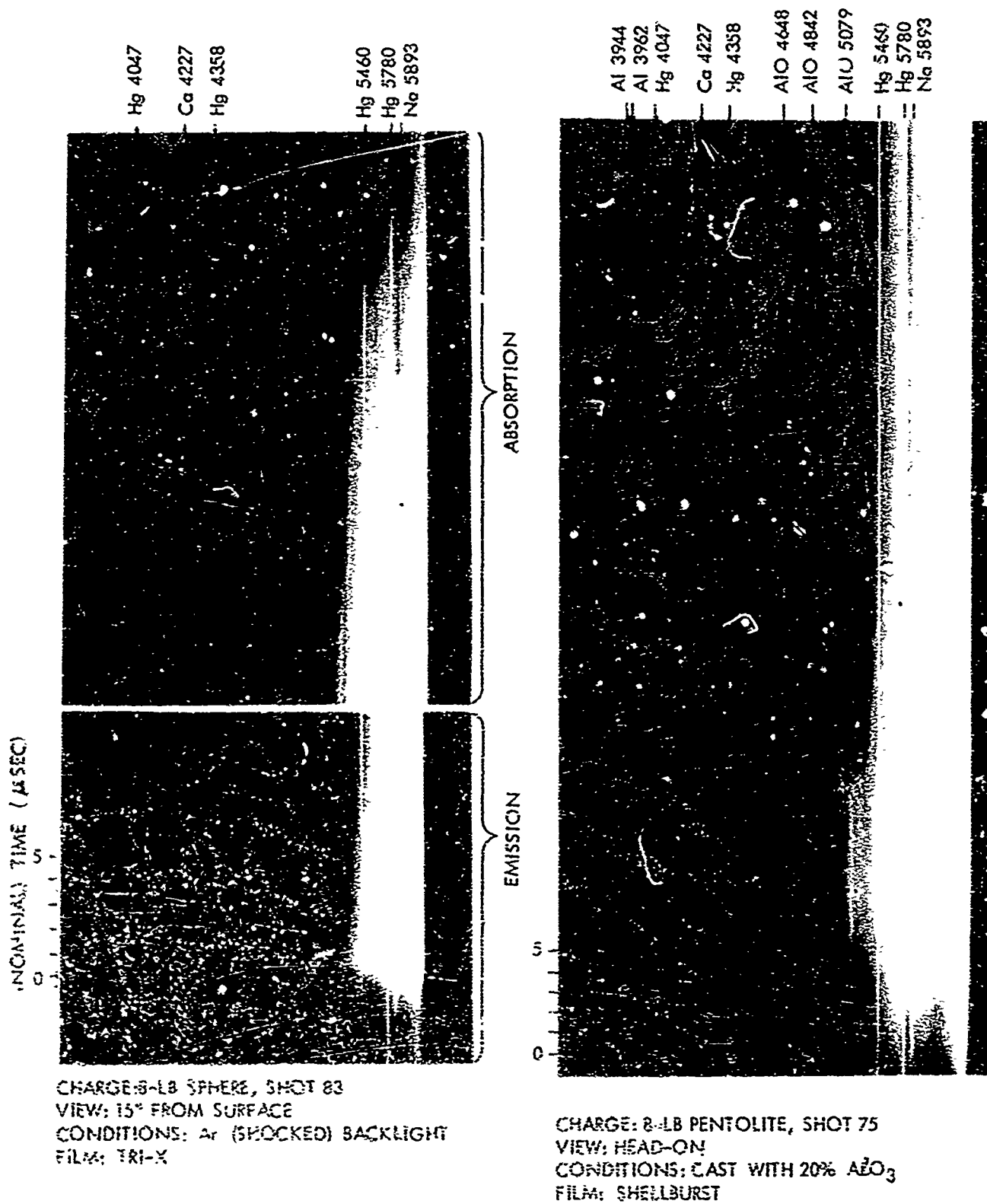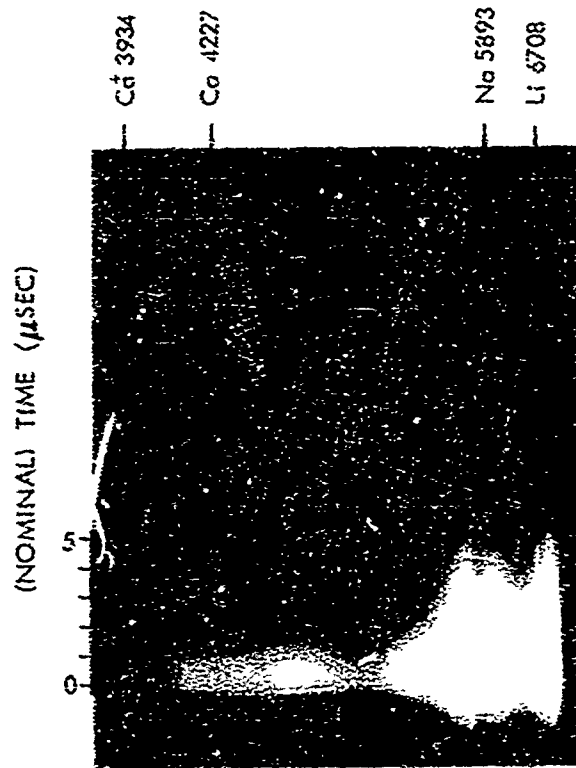
FIG. A-1 AVCO SPECTRA OF PENTOLITE EXPLOSIONS

Hg 4047
Ca 4227
Hg 4358
Hg 5460
Hg 5780
Na 5893

Al 3944
Al 3962
Hg 4047
Ca 4227
Hg 4358
AlO 4648
AlO 4842
AlO 5079
Hg 5460
Hg 5780
Na 5893

ABSORPTION

EMISSION

(NOMINAL) TIME (μSEC)

CHARGE: 8-LB SPHERE, SHOT 83
VIEW: 15° FROM SURFACE
CONDITIONS: Ar (SHOCKED) BACKLIGHT
FILM: TRI-X

CHARGE: 8-LB PENTOLITE, SHOT 75
VIEW: HEAD-ON
CONDITIONS: CAST WITH 20% AlO_3
FILM: SHELLBURST

FIG. A-2 AVCO SPECTRA OF PENTOLITE EXPLOSIONS

CHARGE: 2.6-LB RDX + 1.5-LB TNM
SPHERE, SHOT 67
VIEW: HEAD-ON FILM: SHELLBURST
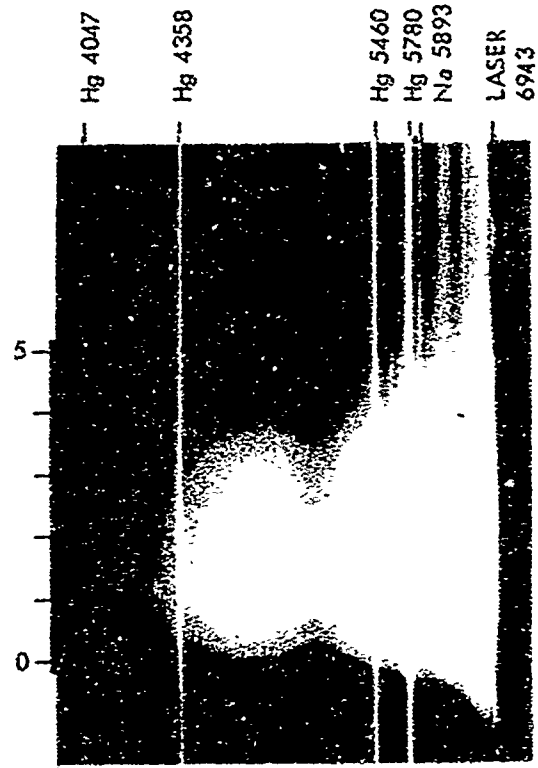
CHARGE: 3-LB RDX, SHOT 96
VIEW: 1" FROM SURFACE, FILM: 2475
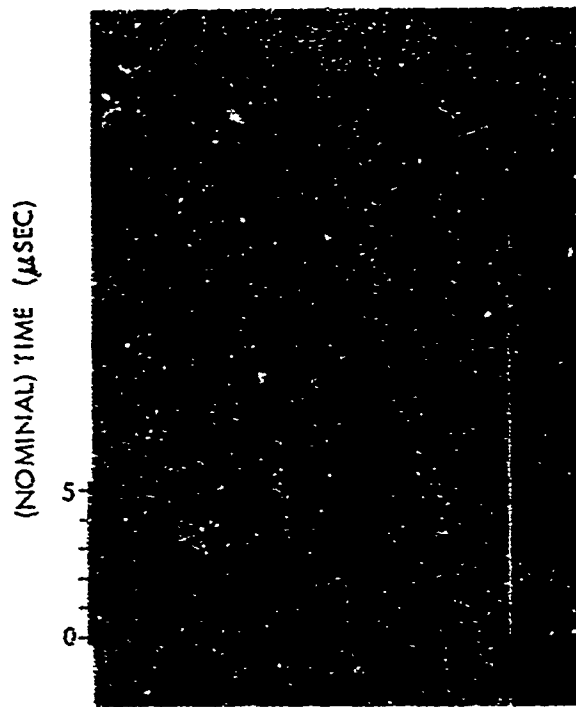
CHARGE: 8-LB TNT SPHERE, SHOT 66
VIEW: HEAD-ON   FILM: SHELLBURST
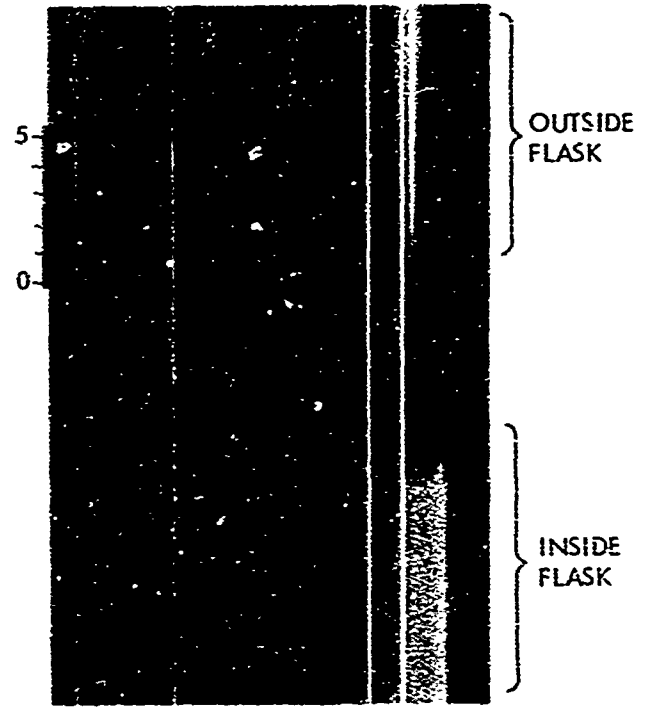
CHARGE: 10.7-LB NM + 4.5-LB TNM
IN GLASS FLASK, SHOT 84
VIEW: HEAD-ON FILM: TRI-X

FIG. A-3 AVCO SPECTRA OF SEVERAL EXPLOSIVE MATERIALS

NOLTR 69-74
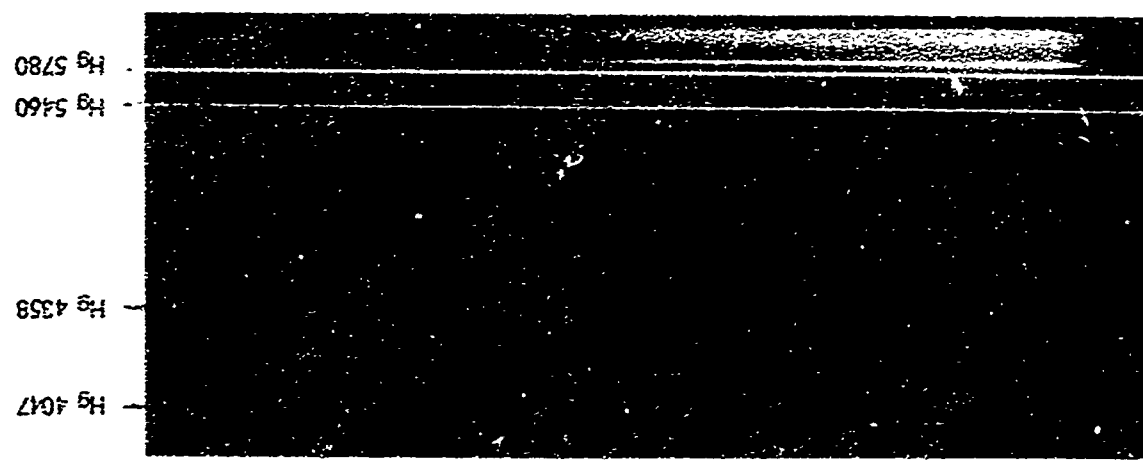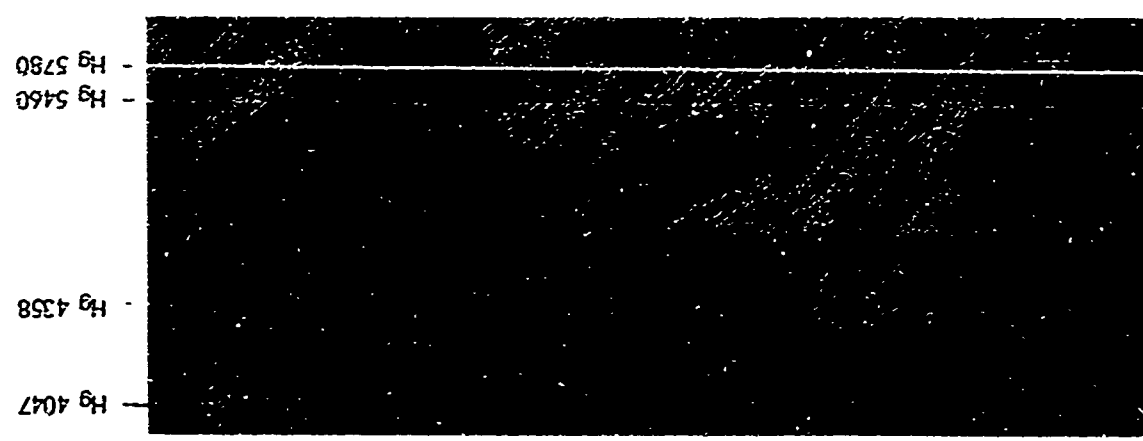
FIG. A-4 AVCO SPECTRA OF TNT SPHERES

VIEW: HEAD-ON   FILM: TRI-X
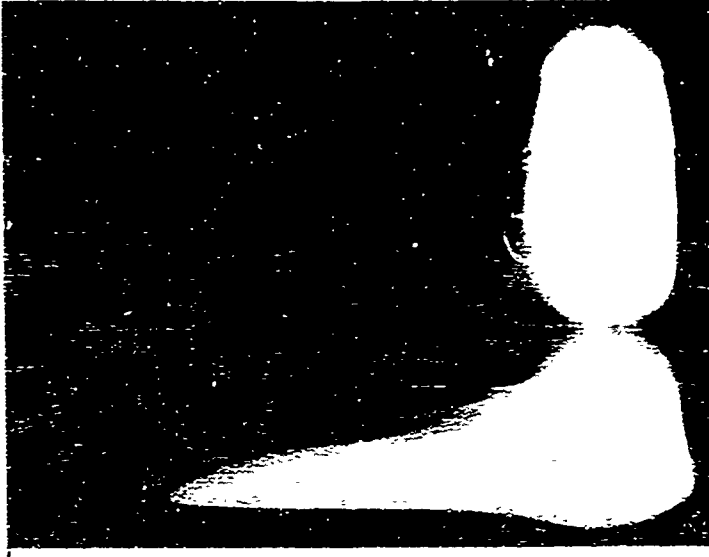
TWO 8-LB PENTOLITE SPHERES,
SHOT 88 INFPA-RED FILM

10.7-LB NM + 4.5-LB TNM IN
GLASS FLASK, SHOT 84 TRI-X FILM
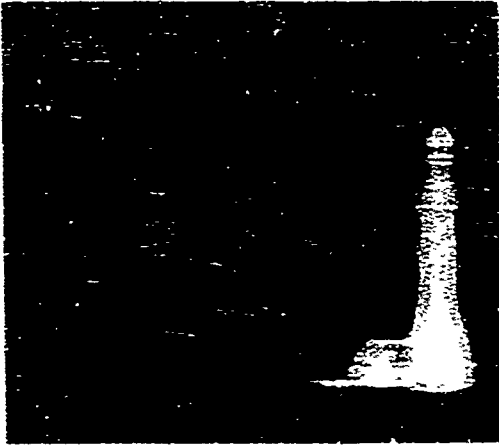
2-LB PETN IN LUCITE
HEMISPHERE, SHOT 76 TRI-X FILM
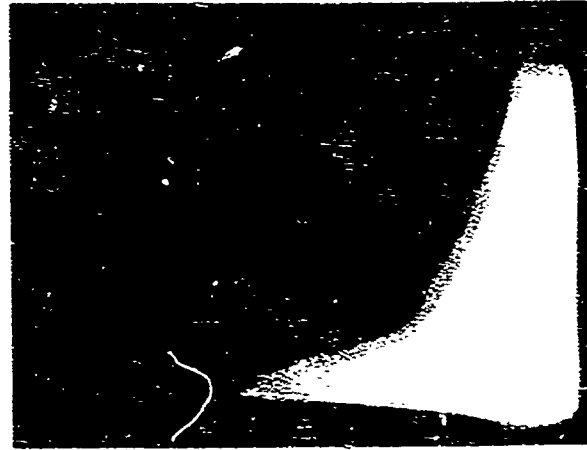
8-LB PENTOLITE (WITH 20% Al_2O_3),
SHOT 75 TRI-X FILM

NH 3370, 3360
NH 3360
CN 3590
CN 3883
Cd 3968
Ca 4227
Na 5893
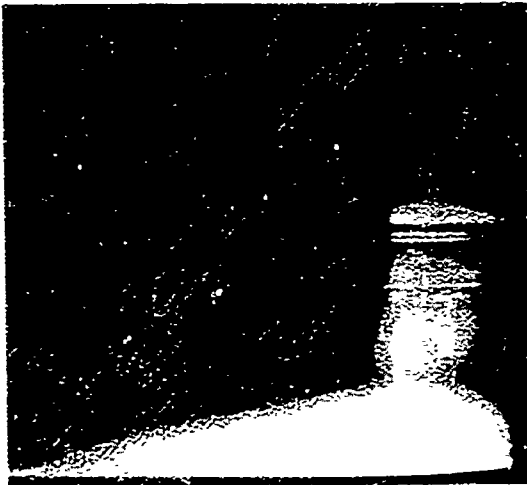
8-LB PENTOLITE SPHERE, SHOT 50 TRI-X FILM

8-LB TNT SPHERE, SHOT 72
TRI-X FILM

(NOMINAL) 1 MILLISEC.

FIG. A-5 CINE-SPECTROGRAPH SPECTRA OF VARIOUS EXPLOSIVE MATERIALS (HEAD-ON VIEW)

NOLTR 69-74
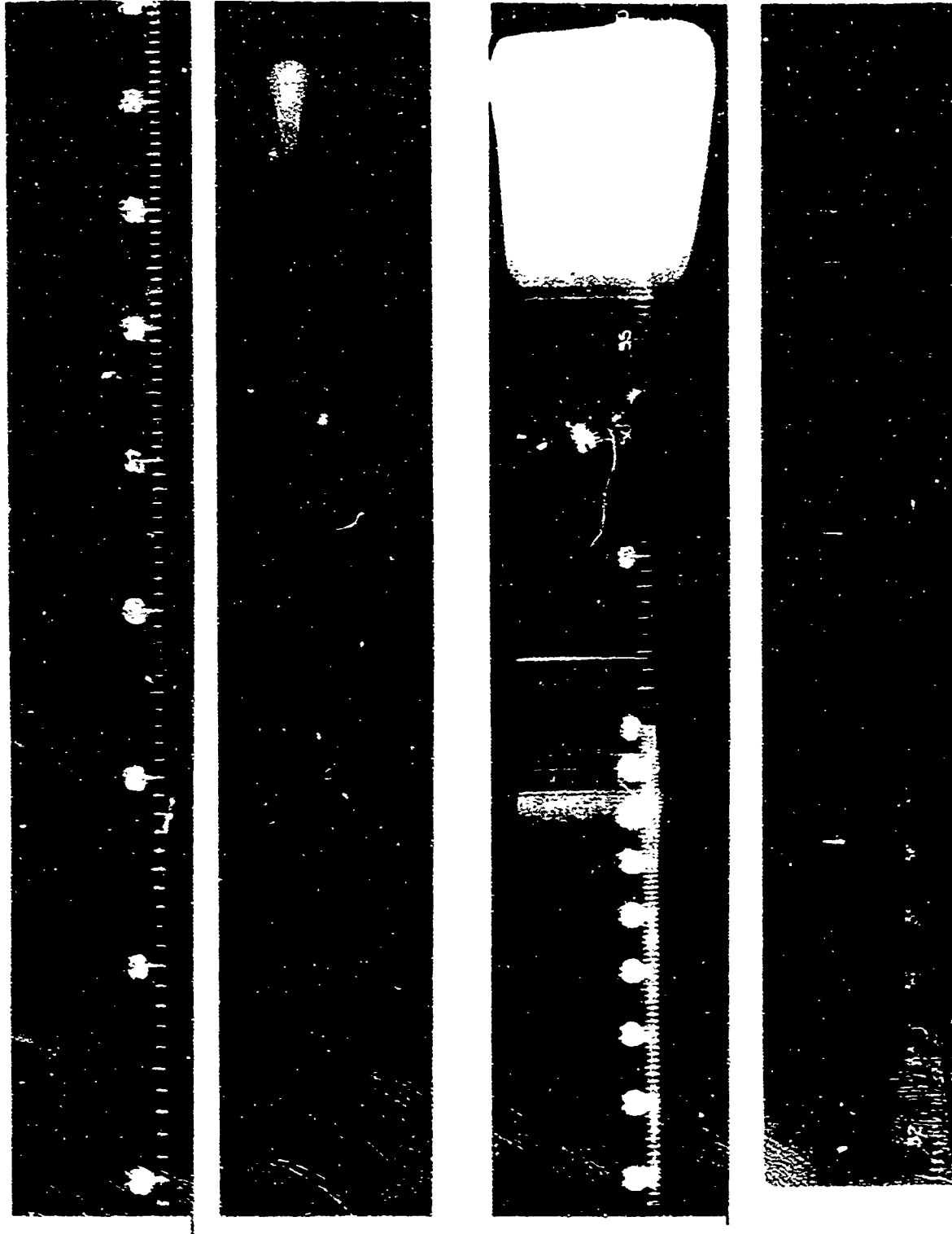
SHOT 106
2475 FILM

SHOT 102
HIGH-SPEED
INFRARED FILM

SHOT 109
SHELLBURST
FILM

NOTE: SCALE MARKINGS ARE NOT LINED UP WITH SPECTRA

FIG. A-6 HILGER SPECTRA OF 8-LB PENTOLITE SPHERE EXPLOSIONS (HEAD-ON VIEW)
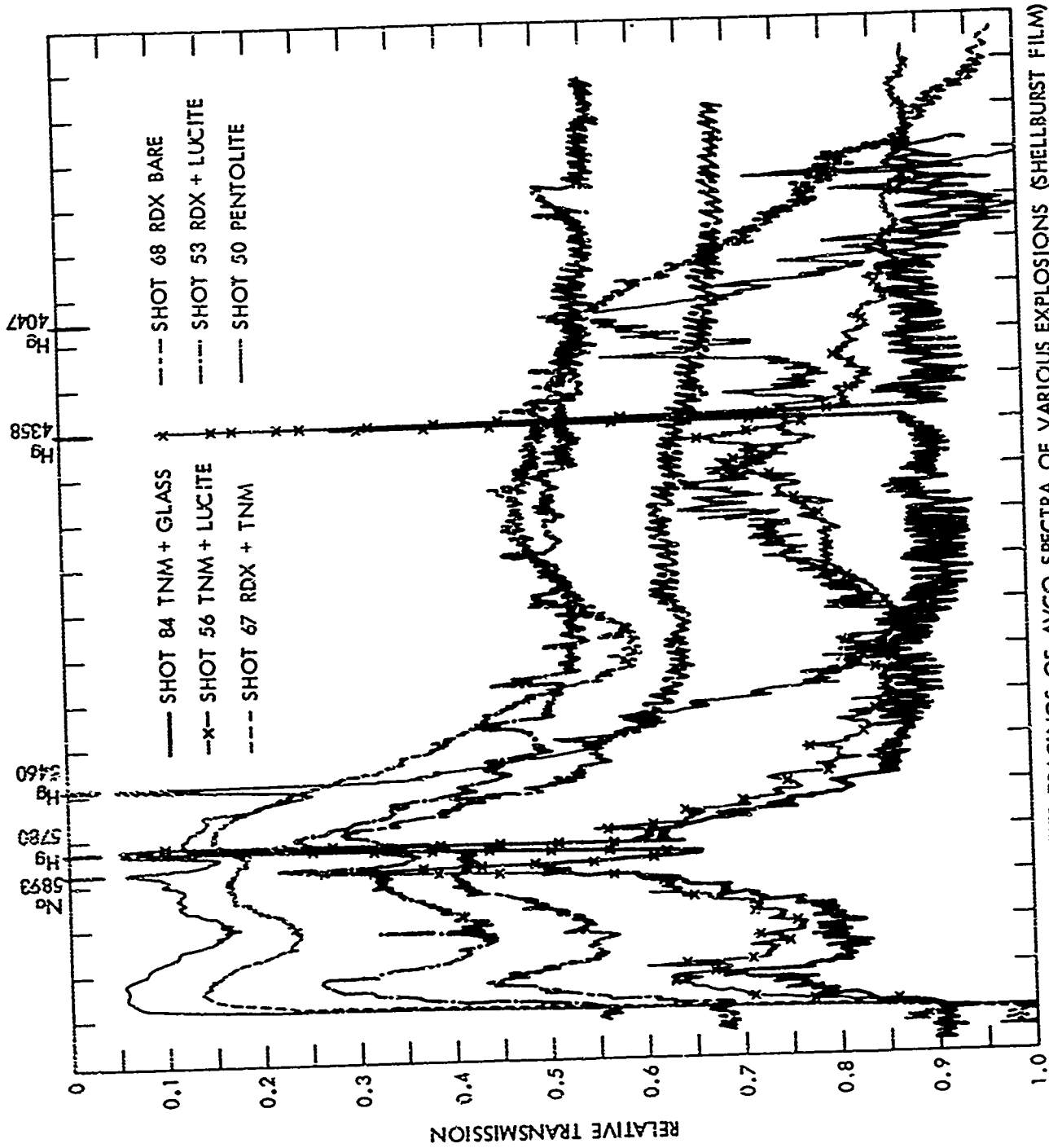
FIG. A-7 DENSITOMETER TRACINGS OF AVCO SPECTRA OF VARIOUS EXPLOSIONS (SHELLBURST FILM)
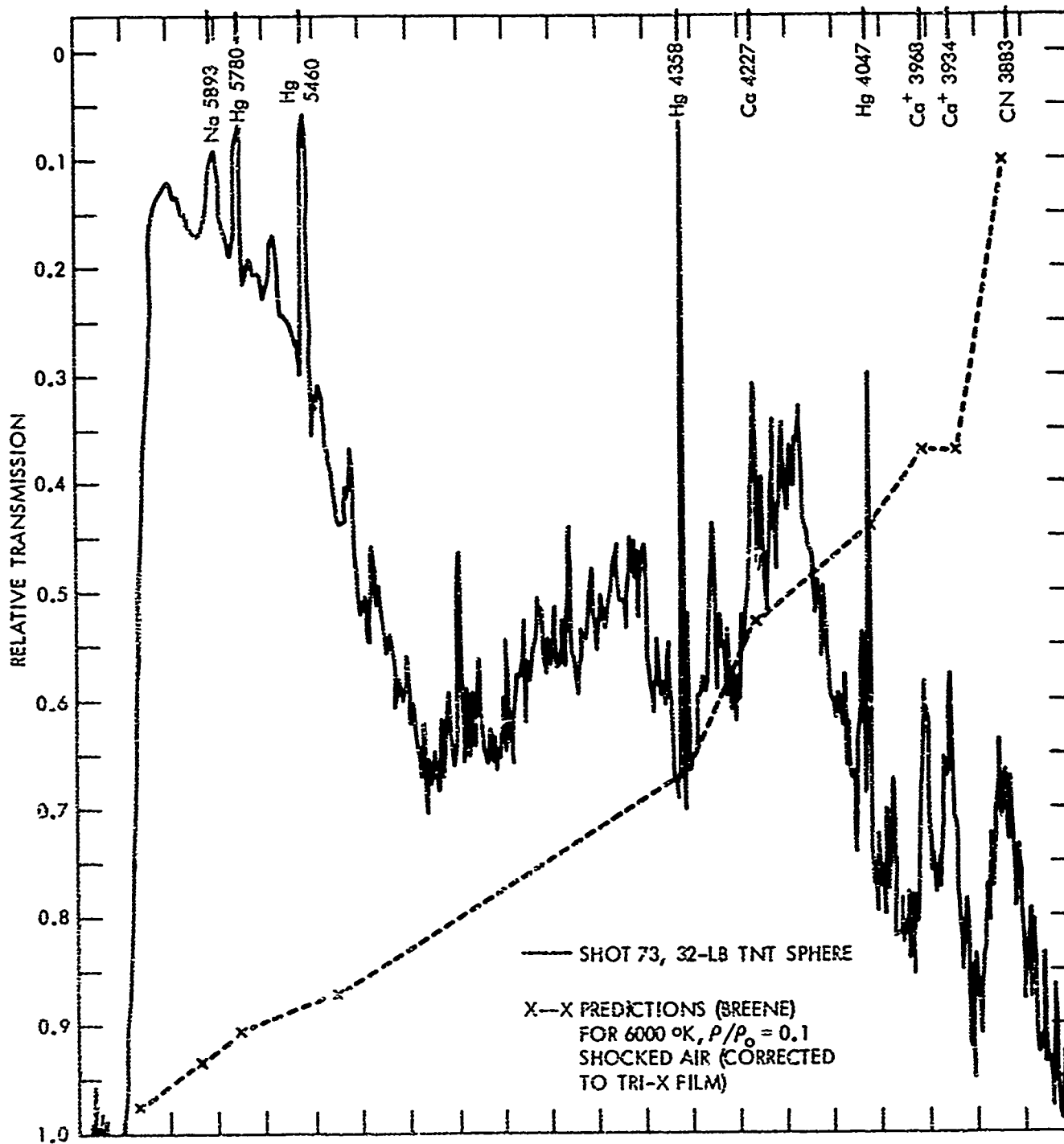
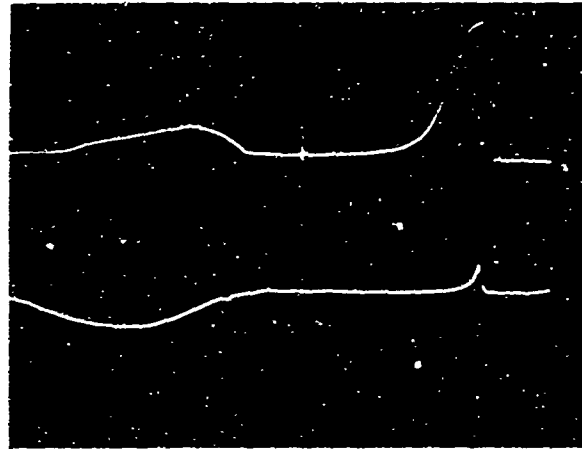FIG. A-8 COMPARISON OF EXPLOSION SPECTRUM WITH PREDICTIONS FOR SHOCKED AIR
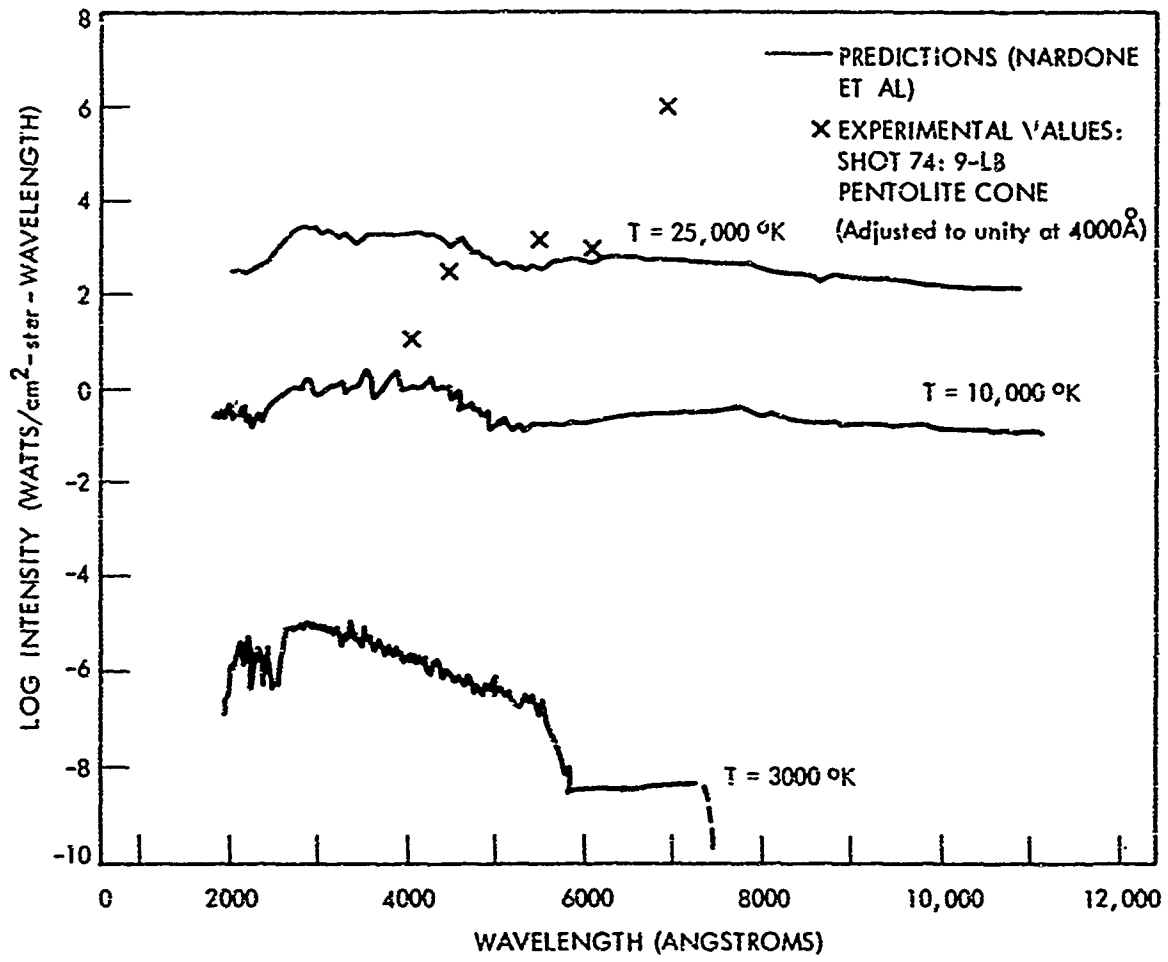
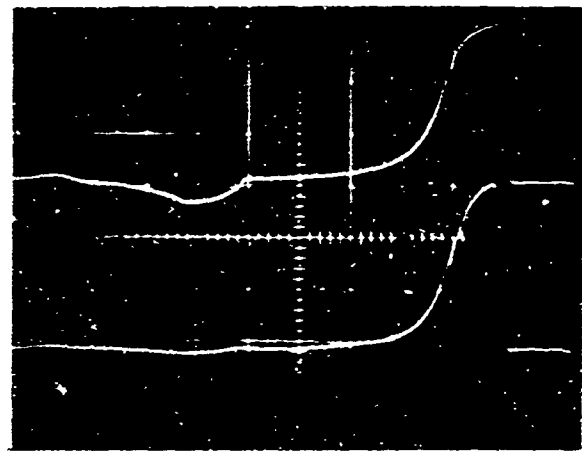FIG. A-9 COMPARISON OF THEORETICAL PREDICTIONS FOR SHOCKED-AIR
RADIANCE WITH ESTIMATED VALUES FROM SHOT 74.

SCOPE A

BAND 1 (5500 – 6350 Å)

BAND 0 (5160 – 5840 Å)

SCOPE B

BAND 3 (6650 – 8200 Å)

BAND 2 (6000 – 7150 Å)

1 BLOCK = 20 μ SEC
TIME ◄───────

FIG. A-10 Py-I RECORDS OBTAINED ON SHOT 64 (RDX)
(WANDERING OF TRACE AT LEFT IS CAUSED BY
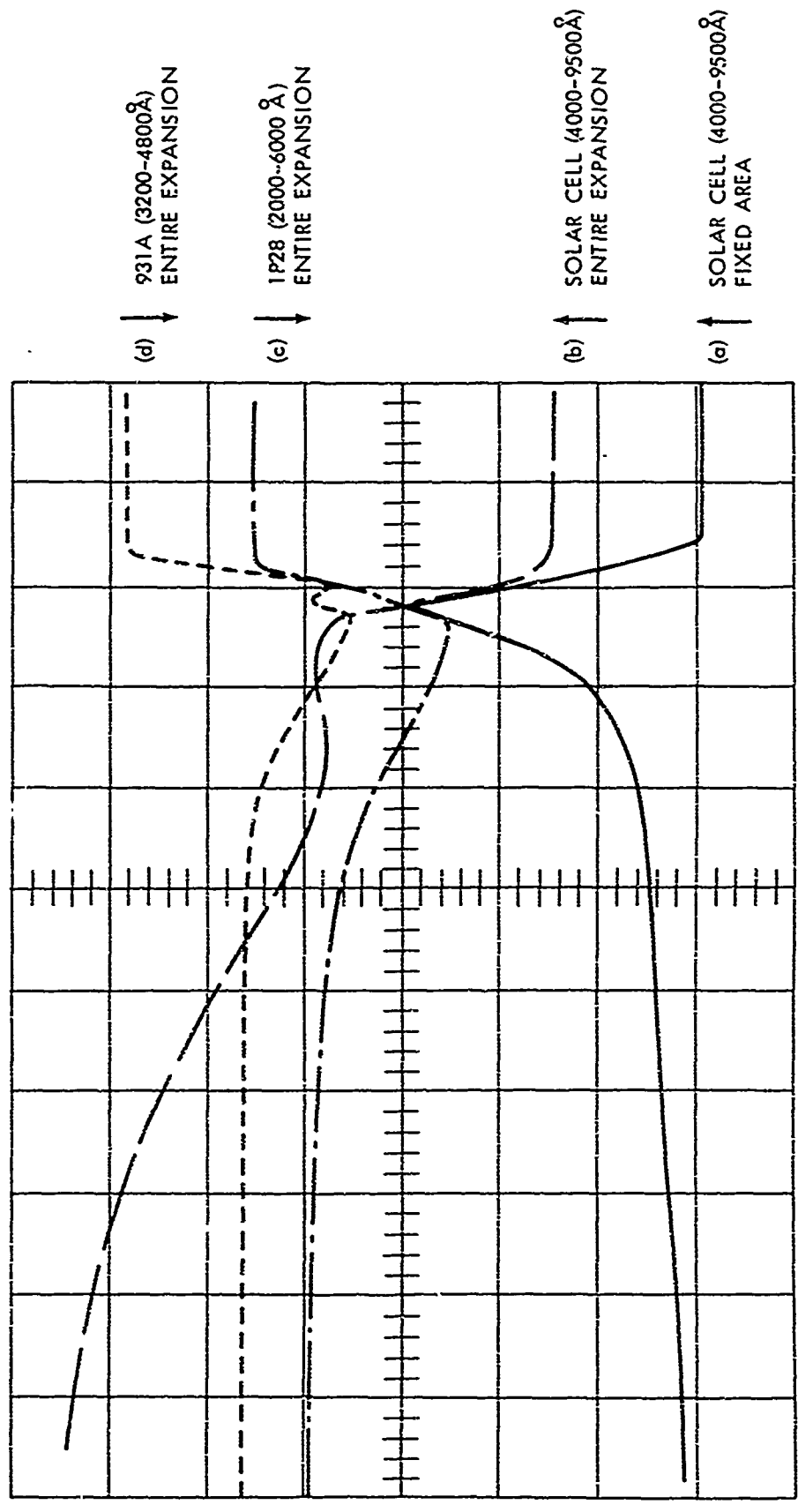SHUTTER CUTTING OFF LIGHT TO DETECTORS)

(d) → 931A (3200-4800Å) ENTIRE EXPANSION

(c) → 1P28 (2000-6000 Å) ENTIRE EXPANSION

(b) ← SOLAR CELL (4000-9500Å) ENTIRE EXPANSION

(a) ← SOLAR CELL (4000-9500Å) FIXED AREA

1 BLOCK = 10 μSEC

FIG. A-11 SIGNATURES OF SEVERAL PHOTODETECTORS ON 1-LB PENTOLITE SPHERE EXPLOSION

APPENDIX B: SECOND-SHOCK LUMINOSITY

The existence of a rebrightening of the explosion fireball, upon passage of the second shock, was first described by RUDLIN (1967). The intense light from an explosion was found to decay to a minimum (~1.2 millisecond for 1-lb sphere), then to rise to a second maximum (weak compared to the first output of light) at ~1.8 millisecond. Several possible reasons for the second brightening were listed, such as a triggering of metastable species in the fireball or an increased density of already radiating species at the second-shock-front. But a concrete explanation was not given.

Various efforts have been made during these experiments to obtain a spectrum of the second-shock light to find what species radiated during the second-shock passage thr ogh the fireball. Both photographic and electronic spectrographs have been used. No useful spectra have been obtained -- largely because of the low intensity of the second-shock light.

One of the best, but still unuseable for identification, spectra obtained is shown in Figure B-1. This was made on the Cine Spectrograph with Tri-X film. The charge was a 32-lb rectangular block, made by gluing together two half-blocks of TNT which had been cast at two different establishments.

The spectral film was deliberately overexposed so that the first few spectra obtained at earliest times are unreadable. The first spectrum, at the bottom of column (a), consists of four stepped views of the earliest light (roughly first 100 μsec). These stepped views were made by use of varying transmission filters. The light was intense enough to record through 100, 30, 10, and 3 percent filters. As time increased, the light decreased so that, at about 4-5 millisecond, only the 100%-transmission record was recorded. The next spectrum (at ~6 millisecond) was barely recorded. Then the film is clear for 6-7 millisecond, during the minimum in the explosion light. At about 11-12 millisecond the rebrightening was strong enough to record and we can see that this light rose to a flat maximum, then decayed to extinction about 70 milliseconds later. It is remarkable that second-shock light, sufficiently intense to record through the slow Cine Spectrograph, lasted for such a long time. The only species that we can identify in the second-shock spectrum is sodium, the D-lines at 5890 and 5896 Å.
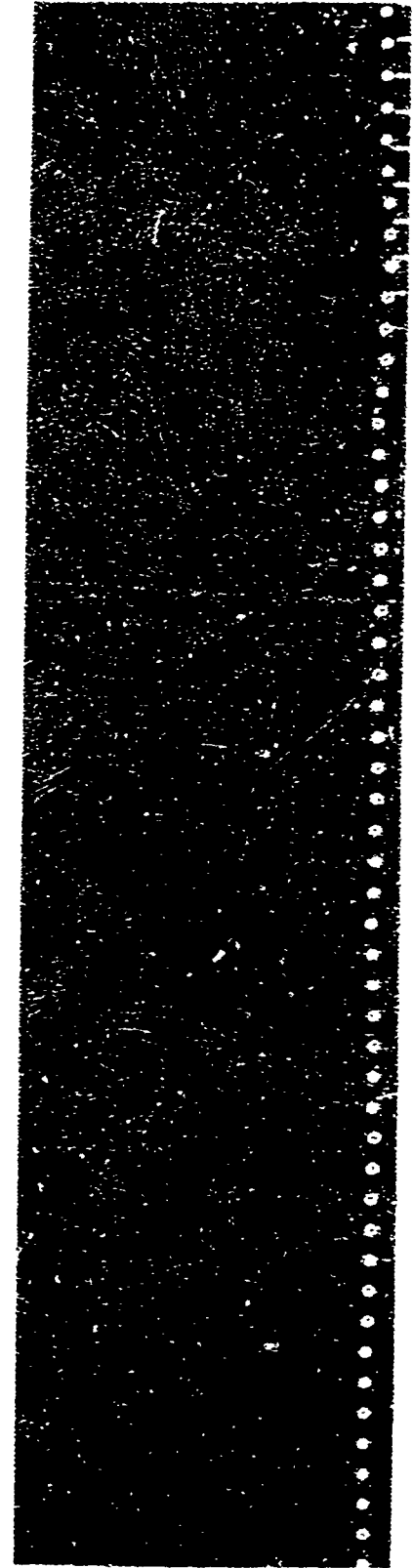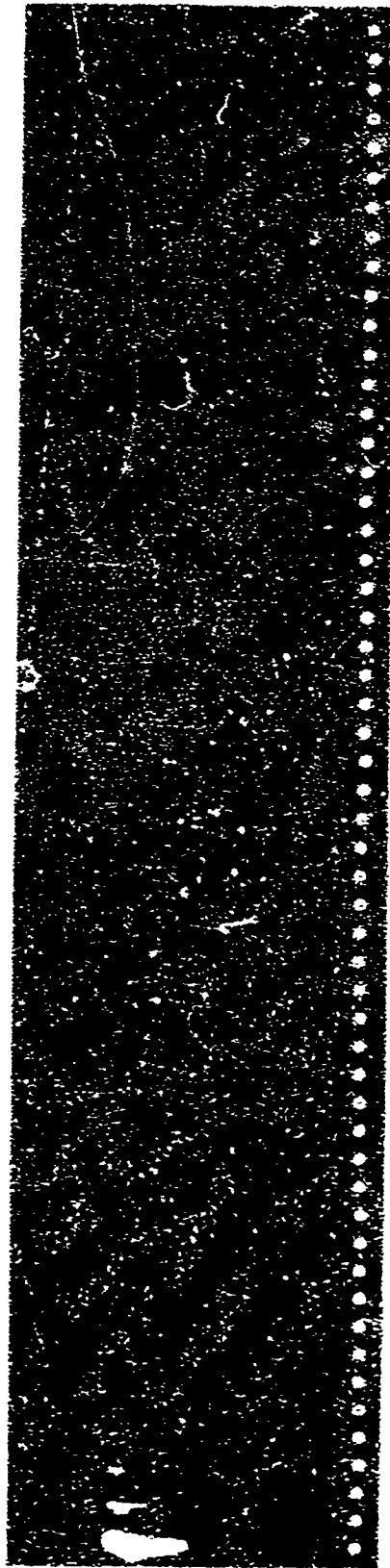
TIME :

a. EARLY

b. LATE

TRI-X FILM (←RED BLUE→)

FIG. B-1 SPECTRUM SHOWING SECOND-SHOCK LIGHT (SHOT 85)
(TIMING MARKERS: 1 MILLISEC APART)

APPENDIX C: PRESSURE AND IONIZATION MEASUREMENTS

C-1: Pressure Signatures: Initially, we had hoped to make
pressure-time measurements at close-in distances from the charges.
But we soon became disillusioned by the lack of reproducibility
from shot-to-shot and, especially, by the differences in the
signatures on the same shot from different sensors at the same
distance. We then used these "pressure" records only to indicate
the arrival times of pressure signals, which we used to correlate
with the motion of shockwaves in the μ-second photography. Because
we have found no records in the explosions literature of close-in
pressure signatures, we include here a brief discussion of our
unsuccessful experiences.

In Figures C-1 to C-4 we show some samples of the records that
were produced.* In Figure C-1 we have compared the standard far-out
blast gage at DRI -- the tourmaline Tulsa Laboratory gage -- with
throw-away quartz gages of different size. All gages were placed
along an arc at 8 a_0. In Figure C-2 we show the records obtained
on Shot 55, the photographs of which appear in Figure 1 of the text.

In Figure C-3 are shown signatures from throw-away gages using
quartz sensors coated with a silver-chrome layer, on the TNT series
of 8-, 32-, and 100-lb spheres. Finally, in Figure C-4 are shown
samples from RDX explosions taken at 1 a_0 from the charge surface.
In these shots we (1) compared the 1/8-inch quartz sensors with two
different coatings, silver-chrome and gold-chrome and (2) compared
these sensors with no sensor at all. For this latter comparison
we omitted the quartz disc, leaving the micarta holder and the wiring
and other details exactly the same. It is rather startling to see
that the magnitude of the signals from these dummy gages is comparable
to that from the "real" gages. Perhaps more startling, we think, is
that the dummy records look far handsomer than the "real" record.
Most dummies had no hole where the quartz disc would have been
placed in a "real" gage. Upon occasion we used a dummy with a hole
drilled through the micarta holder -- this is such a record labeled
"Dummy (hole)" in Figure C-4.

In two explosions we placed 1/8-inch quartz sensors (Ag-Cr coatings)
inside the explosive. The records on these shots are given in
Figure C-5. The sensors were glued to the ends of the detonators
and the leads brought out of the detonator holes in the charges. We
knew that the Engineer Special detonators blew out the sides and
not out the ends as designed, and thought that there was a fair chance
of their remaining intact throughout a long-enough time period.
Apparently the "gages" did remain intact throughout the time of our
records. These were inserted to look for a second shock leaving
the center of the explosion.

These also seem to be two shocks on some of the records from
sensors outside the explosion. But the appearance is so inconsistent

* All except Figure C-2 are tracings made from ...e original 4-beam
records. These have been traced so that we could line up and orient
signatures which are often difficult to follow on the originals.

from sensor to sensor that we cannot establish the existence of multiple shocks outside the charges from our records.

We believe that there is little to learn from our records close-in to an explosion -- except that much more needs to be done to learn how to make shock pressure measurements in the midst of the strong electromagnetic fields, ionization and other effects created by an explosion.

C-2: <u>Ionization Signatures</u>: Our ionization sensors were used to detect the times when ionization might be present, not to measure magnitude of charge -- a much more difficult problem. In Figure C-6 we have given sample records from sensors on the surface of the charge. Two records are given for Shots 60, 61, and 68; the one labeled "outside charge" was glued onto the outside surface of the lucite hemisphere supporting the loose-powder charge, whereas, the "inside charge" sensor was placed within the explosive with the midpoint of the lead disc just behind the lucite-explosive boundary.

Our records are not particularly reproducible and often are erratic. Nevertheless, there does seem to be a pattern of multiple pulses in them which is good enough to be tabulated in Table C-1. Despite the obvious scatter in the values we see a

Pulse 2 at about 3 to 4 $(t + \tau)/\tau$

Pulse 3 at about 7 to 9 $(t + \tau)/\tau$

and, possibly, a Pulse 4 at about 10 to 15 $(t + \tau)/\tau$, where τ is the time for the detonation wave to cross the explosive from the center to the outer surface.

C-3: <u>Doppler Microwave Signatures</u>: Observations were made of a small number of TNT, pentolite, and PETN explosions, both in cylindrical and spherical configurations. Some sample records are shown in Figure C-7. No measurable Doppler return can be detected on the PETN records.

A second Doppler return can often be seen on the TNT and the pentolite records, appearing at:

Shot 19 - 120 µsec

Shot 22 - 70 µsec

Shot 28 - 120 µsec

Shot 29 - 140 µsec.

Since a Doppler return could only be produced by free electrons having a density greater than 10^{12} electrons/cm^3, these second pulses indicate that a new mechanism for creation of electrons in an explosion, after passage of the first airshock, has been detected. The times above appear close to the time of 10-15 T (where $T = (t + \tau)/\tau$) for

Pulse 4 that we have noted above on the ionization gages. We see no evidence of Pulse 2 or Pulse 3 on the microwave records. Assuming that these pulses are real, we conclude that these waves of ionization are hidden behind a larger ionization front, whereas, no such front masks Pulse 4. Doppler signals usually disappeared when the fireball growth had reached 5 to 7 a_0.

C-4: _Analysis_: The records presented in this Appendix are unsuitable for detailed analysis. Nevertheless patterns in the records from the ionization sensors and the microwave sensor cannot be ignored. In this section we use these patterns to construct a new model for the creation of airshocks from an explosion.

There are two reasons why such a new model is necessary: (1) although theory and experiment agree fairly well for the first airshock, there is substantial disagreement for the second shock and for the contact surface (c.f., LUTZKY); and (2) the multiple pulses from our ionization records cannot be fitted into present models.

We base our discussion on Figure C-3. Here we have drawn the theoretical results in solid lines for a 1-lb TNT explosion at ambient conditions typical of those at Denver, Colorado, where these experiments were performed. We have omitted experimental data for the first airshock.

We have labelled the usual "second shock" in the computational results the Wecken* shock -- this to avoid confusion with our multiple shocks to be discussed shortly. We have put on four data symbols in the range 30 to 100 a_0 for the Wecken shock values, read from the p-t records published in Part 2, each symbol being the average of a number of values. We draw attention to the fact that the computed WUNDY curve for the Wecken shock and the experimental values do not agree.

Next, we have put on data symbols for the fireball -- luminous front -- positions over the range 8 to 30 a_0, taken from the films of TNT explosions reported in Part 2. We draw attention to the fact that these data also do not agree with the computed contact surface.

We now try to patch up this model to fit the experimental results at both early and late times. We begin at A. The transmitted portion of the detonation shock proceeds out into the air, as shock 1. We use the theoretical WUNDY curve here for shock 1 because our data cannot supply a better curve. Also at A, a shocklet begins moving inward toward the origin. RUDLIN (1961) found a discontinuity in the variables at the back end of the reaction zone behind the detonation shockfront in a spherical TNT explosion. This discontinuity could behave like a little shock. When the rarefaction wave created at the explosive-air boundary by the detonation shock sweeps inward, it would sweep the shocklet back toward the origin. During this

* After F. Wecken, French-German Research Institute, St. Louis, who first gave a theoretical explanation for this shock often seen experimentally.

inward passage the strength of the shocklet would increase and it would leave the origin as a full-fledged shock.

We determine the inward path of the shocklet, AB, from use of Figure C-5. The pressure gages of Figure C-5 suggest a rough value of 30 μsec for the second pulses seen at the center of RDX, or a speed of about 0.4 U, where U is the detonation velocity in RDX powder. Using such a speed for TNT, we obtain B and connect A to B along a reasonable path AB.

To find the outward path of shock 2, we recall that the ion gages saw Pulse 2 somewhere between $T = 3$ to 4. Assuming that the ion gages remained sitting at $R/a_o = 1$, we locate C at $R/a_o = 1$ and $T = 3.5$. We connect B to C along a path roughly of slope 2U, since shock 2, now strong, could be moving at speeds not far below U in expanding gases moving at $u \sim U$.

To find D, we recall the convergent-shock experiment illustrated in Figure 1C. Out of the small end of the cone came not one but two pulses of gases. The time of arrival at the end of the cone of the second pulse was such that it would have had to travel, roughly, at twice the speed of the first pulse. We assume, therefore, that shock 2 moves in the flow behind shock 1 with a speed twice that of shock 1. Using the computer values for instantaneous values of the speed of the airshock, we construct a path from C, segment by segment, until we arrive at D. It is intriguing to note that D turns out at $T = 7$, a value close to that we found for Pulse 3 on the ion gages. If shock 2 swept a surface ion gage along until collision with shock 1 at D, then Pulse 3 might be accounted for.

When shock 2 meets shock 1, the main airshock is formed. By "main" airshock, we mean the single shockwave that has been observed and measured in the past primarily in a pressure region, say from 50 to 1 psi (roughly 30 to 200 a_o). In the model we are trying to construct here*, however, this main airshock is not the result of a single event of formation but results from the merging of two distinct

_____

* We must point out that a transmitted airshock is crucial to our model. We think that in certain situations such a transmitted shock may not be formed -- perhaps, for example, in the explosion of small amount of explosives. In those cases our model cannot hold and shock rmation probably occurs from amalgamation of the bow shocks formed about the particles of solid material ejected from the charge or possibly from thermodynamic heating by the explosion gases or possibly from a combination of the two; the airshock in these situations will occur at a relatively late point in the explosion. We are concerned here with a "proper explosion" in which an airshock is created at, or very near, the explosive-air boundary. We contend that such a shock can be formed by transmission of the detonation shock into air and that we have observed such shocks on many of the 117 explosions of this investigation. The causes for failure of this shock 1 to occur is another story for another time (c.f., Appendix D for Soviet results from 0.3-lb and 3.7-lb spheres of Comp B.).

shockwaves. The real release of explosion energy in this model does not come with the first airshock but with shock 2. This results because shock 1 carries only a small amount of energy -- that fraction of the energy available within the reaction zone behind the detonation shockfront which can be transmitted across the interface into air. Shock 2, on the other hand, travels through the gaseous sphere created behind 1: the energy that it can carry will depend upon the detailed characteristics of the plasma within that sphere during its passage.

We now look for a path from D to return inward to the center of the explosion. We expect that an inward-facing shock will be formed when shock 2 overruns shock 1 and sees an interface between shock-heated air and the undisturbed ambient air. We don't know what speed this shock 3 will travel at. To guess at this, we look at the speed that the computer gives for the Wecken shock inward as a rough estimate. Roughly, the Wecken shock moves inward at increasing speeds like $1/5\ a_0/\tau$, $1\ a_0/\tau$, $2\ a_0/\tau$, etc. If we construct segment by segment the inward path at the same speeds, we reach E at about $T = 13$, and continuing the curvature at E inward, we reach F at $T = 14$.

Now $T = 13$, 14 are times familiar from the ionization sensor records and the microwave records. If the model is correct, however, these similar times cannot correspond to the same phenomena. An easy interpretation does exist: the ionization sensors will give a pulse when the path between the lead disc and the detonator shell is sufficiently conducting. If the lead disc was swept out by shock 2 to D or its neighborhood, then shock 3 might carry the disc inwards toward E. Meanwhile the detonator shell has probably begun moving outward. Somewhere along the path DEF, ionization could be sufficient to trigger Pulse 4 which we noted at $T = 10$ to 15. On the other hand, this sort of motion by the lead discs would not be seen by the Doppler microwaves. Until D the microwaves could have seen only shock 1, assuming that its electron density was high enough, or possibly, the late stages of shock 2 before collision of shock 2 with shock 1. Upon moving outward from F shock 3 is at its strongest value. It seems reasonable to assume that this is the shock seen by the microwaves as a second pulse, as it moves outward from F.

Finally, we must construct the path of shock 3 outward into the air where it will be readily detected on p-t gages after the main shock as the Wecken or the "second shock". We start at G. From films of the TNT fireball we note that there seems to be a surge at $T \sim 360$ and 26 to 30 a_0, which we assume to result from passage of shock 3 out of the fireball. We know from the experimental records of Part 2 that the Wecken-shock pressures at high pressures run about 1/10 the main-shock pressures. So we assume that the speed of shock 3 must be about 1/3 the speed of the main airshock at that period of the explosion history. Relying on the computer again for instantaneous airshock speeds, we estimate the path of shock 3 outward along GF, moving from G inward in our construction until we reach 5 or 6 a_0. Thereafter, we simply connect the path of F, completing FG and the model.

We can wonder -- why hasn't the collision of shocks 1 and 2 to form the main airshock been detected before? As far as p-t records go, very few records have been made so close-in to a charge (we estimate that the collision takes place about 5 a_0). And if the records looked like ours do here, interpretation would have been impossible. As far as films go, the overtaking cannot be seen on explosives containing TNT -- the fireball opacity is simply too high. We have looked hard at films from RDX and PETN with less fireball opacity for some sign of shock 2. We have not found a directly observable shock 2, except possibly in one film from PETN. Perhaps the high temperature of the plasma that shock 2 travels through destroys any chance for visualization of shock 2. Or, perhaps, we just haven't had the right combination of elements in our experiments. We have observed shock 2 indirectly: surges in the luminous fronts of certain shots can be detected in the radius-time data of Figures 7a-c.

C-5: Summary: In this new model, three distinct and separate shockwaves take part. Shock 1 results from the transmission of the detonation shockfront across the explosive-air interface into air (c.f., Part 1). At the time of this transmission another wave (in addition to the rarefaction wave) starts to move inward. This wave (a shocklet) may result from the discontinuity that exists at the Chapman-Jouguet boundary behind the detonation wave, separating the region of non-isentropic chemical reaction from the region of subsequently isentropic flow. After converging to the origin this wave becomes strong, shock 2, and moves outward to overtake shock 1, somewhere in the neighborhood of 5 a_0 from the original explosive surface. Thereafter, the two merged shocks move off together as the "main airshock".

Because of the boundary conditions at the time of overtaking, a new wave is created which will move inward toward the origin. After reflection at the origin this wave, shock 3, moves outward, tagging along behind the main airshock as the "second shock", or as we prefer to rename it: the Wecken shock.

TABLE C-1   TIMES TO PULSES ON IONIZATION RECORDS

SHOT	POSITION	TIMES (μSEC)				QUALITY OF SIGNAL	SWEEP TIME μSEC/cm	EXPLOSIVE
		PULSE 1*	PULSE 2**	PULSE 3**	PULSE 4***			
49	SURFACE	+10	50			POOR	10	PENTOLITE
50	SURFACE	+12	50			POOR	20	PENTOLITE
52	SURFACE	+10	140			GOOD	20	PENTOLITE
53	SURFACE	0	70	110	125	GOOD	10	RDX
54	SURFACE	+16	73			GOOD	20	RDX
55	SURFACE	0	46	90	160	GOOD	20	RDX
56	SURFACE	+20	62	150		GOOD	20	NM+TNM
57	SURFACE	0	40	140		GOOD	22	RDX
58	SURFACE	+10	50	100		POOR	20	NM+TNM
60	SURFACE	0	31	70	140	POOR	20	RDX
61	SURFACE	0	32	88	160	POOR	20	RDX
	SURFACE	0	25	94	168	POOR	20	
68	SURFACE	0	20	120	140	POOR	20	RDX
	SURFACE	~	24	70	140	POOR	20	
	SURFACE	~	25	91		POOR	20	
	SURFACE	~	20			POOR	20	
70	SURFACE	+5	27	82	100	GOOD	20	PENTOLITE
72	SURFACE	+10	80		120	FAIR	20	TNT
75	SURFACE	+8	46	66	140	FAIR	20	PENTOLITE
	3 a₀***	~	35		106	GOOD	20	
76	SURFACE	~	40	88	140	GOOD	20	PETN
	3 a₀	~	60	120		GOOD	20	
77	SURFACE	0	31	100	145	GOOD	20	PENTOLITE
	3 a₀	-20	88			FAIR	20	
	6 a₀	-29	100			GOOD	20	
78	SURFACE	+6	20	40	140	GOOD	20	PENTOLITE
	3 a₀	-35	40			GOOD	20	
	6 a₀	-40	40		115	GOOD	20	

TABLE C-1 TIMES TO PULSES ON IONIZATION RECORDS (CONTINUED)

| SHOT | POSITION | TIMES (μ SEC) | | | | QUALITY OF SIGNAL | SWEEP TIME μ SEC/cm | EXPLOSIVE |
		PULSE 1*	PULSE 2**	PULSE 3**	PULSE 4**			
79	INSIDE	+10	48	72		GOOD	20	RDX
	SURFACE	+5	70	120	126	GOOD	20	
	3 a_0	-29	72	100		GOOD	20	
81	INSIDE	+15	94	154		GOOD	20	RDX
	SURFACE	0	80	100		GOOD	20	
82	2 a_0	0	42	68	128	FAIR	20	PENTOLITE
	SURFACE	-25	18	40	80	FAIR	20	
83						UNREADABLE		
	3 a_0	-20	40	68		POOR	20	PENTOLITE
	2 a_0	-10	68	88		POOR	20	
	4 a_0	-36				POOR	20	

* TIME MEASURED WITH RESPECT TO Py-I LIGHT-INTENSITY PEAK

** TIME MEASURED WITH RESPECT TO PULSE 1

*** DISTANCE MEASURED WITH RESPECT TO CENTER OF CHARGE IN UNITS OF CHARGE RADIUS

1/8-INCH SENSOR

1/2-INCH SENSOR

1/4-INCH SENSOR

TULSA GAGE

⟶ TIME

◀——▶ 1 BLOCK

50 μ SEC/BLOCK

TULSA GAGE: 20v/BLOCK
1/4-INCH: 0.5v/BLOCK
1/2-INCH: 1.0v/BLOCK
1/8-INCH: 0.2v/BLOCK
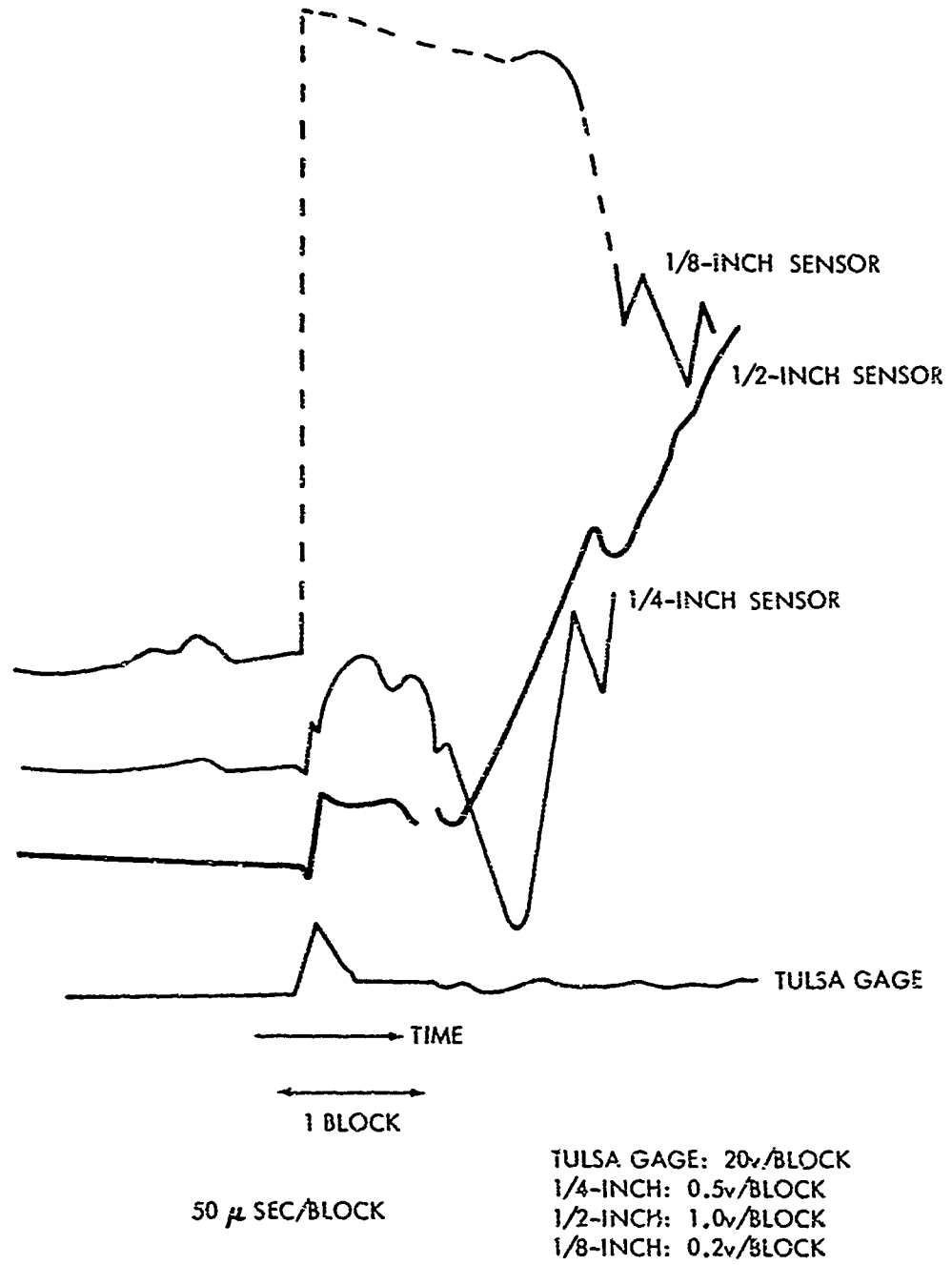
FIG. C-1   PRESSURE-TIME SIGNATURES: SHOT 44 (8-LB PENTOLITE SPHERE)   SENSORS AT $8a_0$
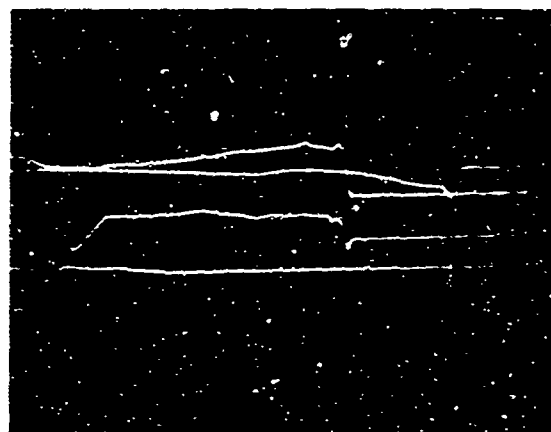(7 CHARGE RADII FROM SURFACE)
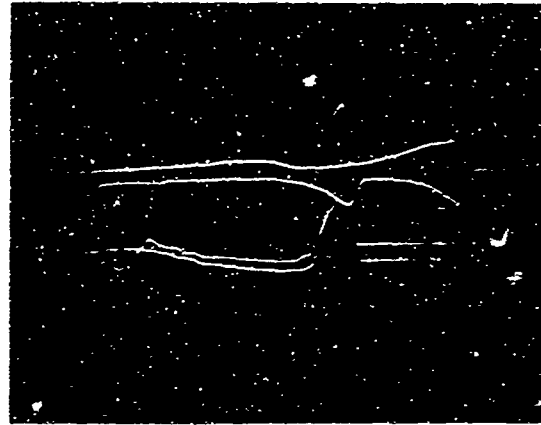
SCOPE A

Py-I
IONIZATION SENSOR
PRESSURE SENSOR
PRESSURE SENSOR

20μ SEC
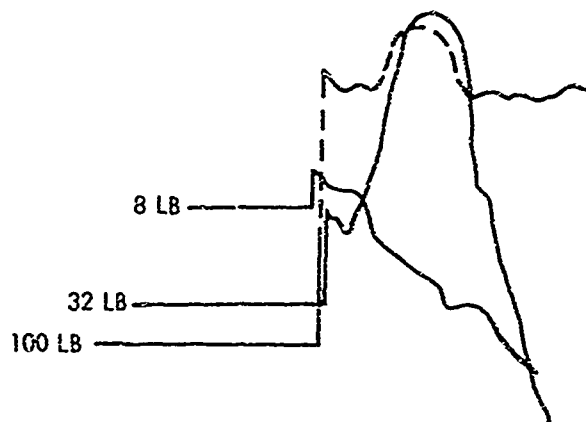
SCOPE B

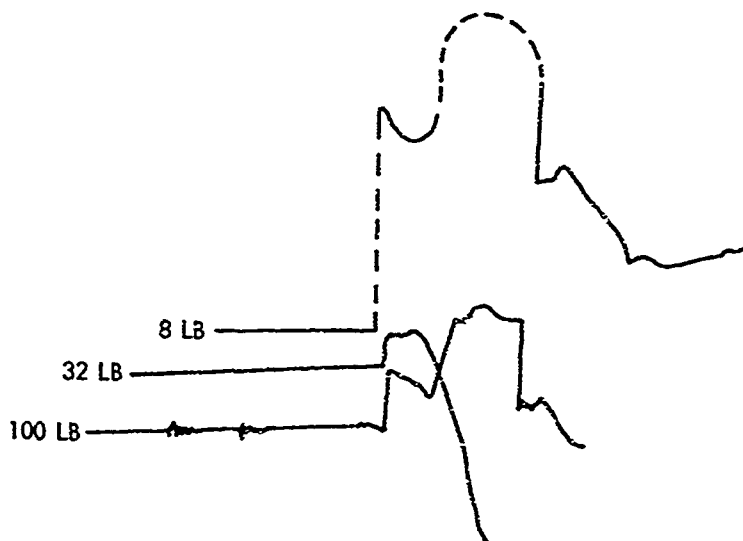Py-I
DUMMY PRESSURE SENSOR
DUMMY PRESSURE SENSOR
RF SIGNAL

FIG. C-2 SAMPLE RECORDS OBTAINED ON SHOT 55 WITH 4-BEAM OSCILLOSCOPES
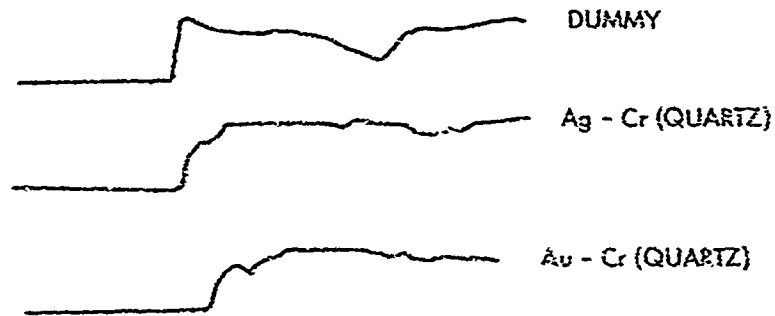
A. SENSORS AT $2a_o$ (1 CHARGE RADIUS FROM SURFACE)

8 LB

32 LB

100 LB

B. SENSORS AT $3a_o$

TIME

20 μ SEC

FIG. C-3 PRESSURE-TIME SIGNATURES: TNT SPHERES (SHOTS 72, 73, 80) 1/8-INCH Ag - Cr QUARTZ SENSORS

Au-Cr (QUARTZ)

Ag - Cr (QUARTZ)

DUMMY (HOLE)
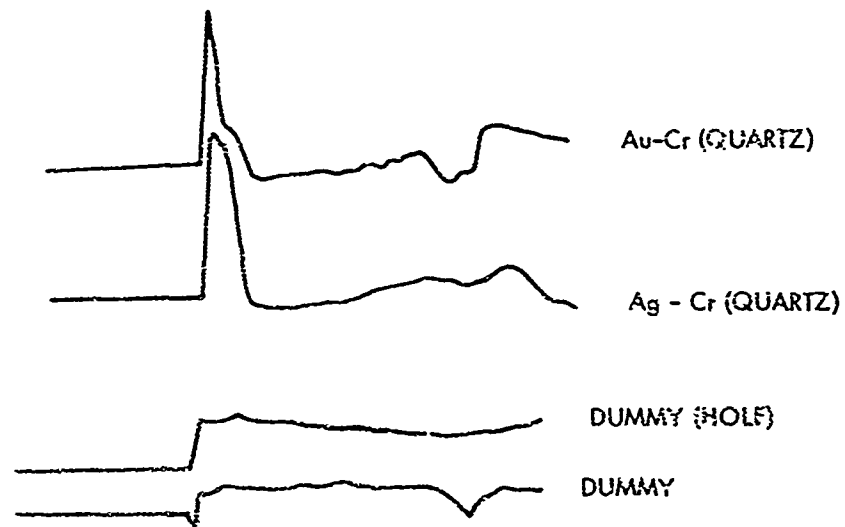
DUMMY

A. SHOT 55 (DUMMY GAGES SET FOR 1/2 THAT OF QUARTZ SENSORS

DUMMY

Ag - Cr (QUARTZ)

Au - Cr (QUARTZ)

B. SHOT 58

←→

20 μSEC

FIG. C-4 PRESSURE-TIME SIGNATURES: RDX EXPLOSIC   ːʰOTS 55, 58) SENSORS AT 2 a_o
(1 CHARGE RADIUS FROM SURFACE)

TIM. OF Py-I PEAK

A. SHOT 60

TIME OF
Py-I PEAK

B. SHOT 68
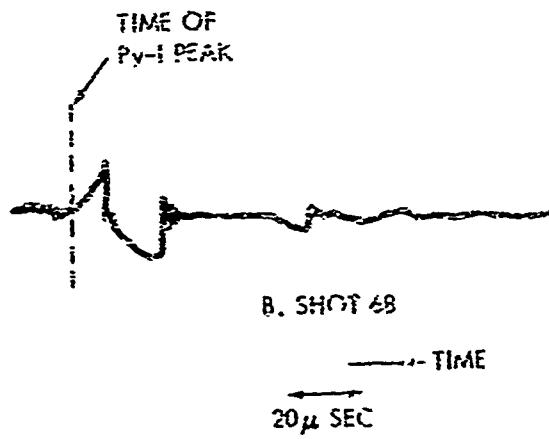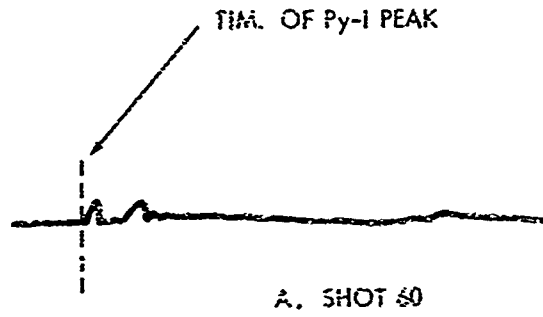
——·- TIME

20 μ SEC

FIG. C-5 PRESSURE-TIME SIGNATURES AT CENTER OF RDX EXPLOSIONS (SHOTS 60, 68) 1/4-INCH
QUARTZ SENSORS

OUTSIDE CHARGE } SHOT 68
INSIDE CHARGE }

OUTSIDE CHARGE } SHOT 61
INSIDE CHARGE }

OUTSIDE CHARGE } SHOT 60
INSIDE CHARGE }

SHOT 57

SHOT 55
SHOT 53

A. RDX EXPLOSIONS

SHOT 83

SHOT 82

SHOT 78

SHOT 77

SHOT 75
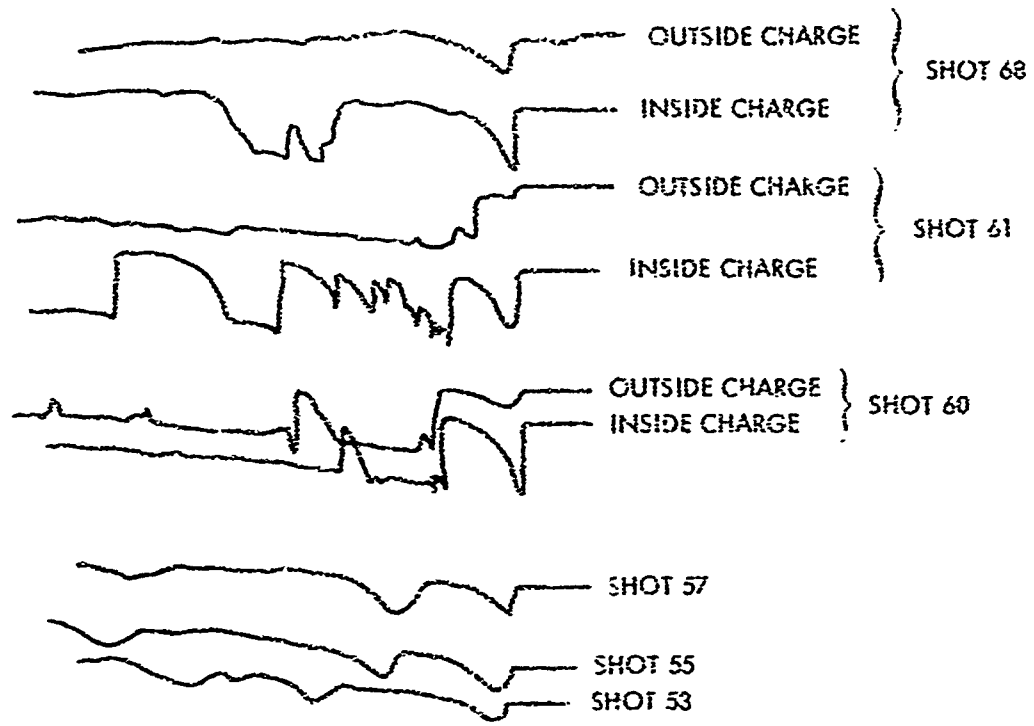
B. PENTOLITE EXPLOSIONS

TIME ⟶   20 μSEC

FIG. C-4   SAMPLE IGNIZATION SIGNATURES FOR RDX AND PENTOLITE EXPLOSIONS

5 μSEC/cm

SHOT 19

SHOT 22

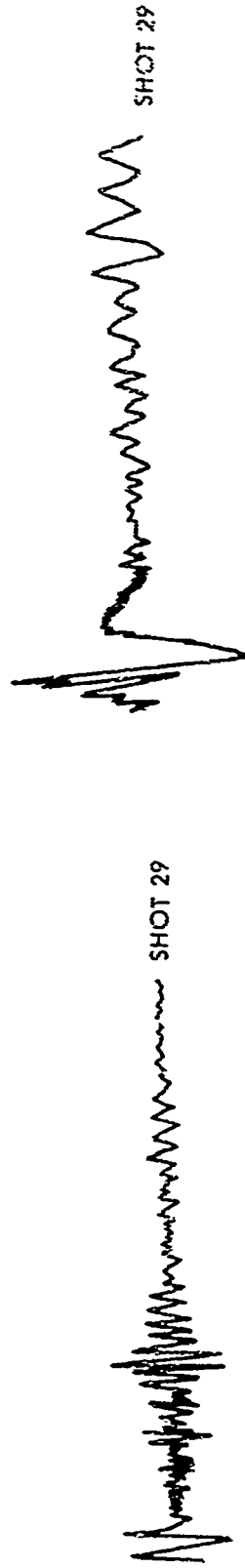PENTOLITE EXPLOSIONS

SHOT 21

SHOT 25

PETN EXPLOSIONS

SHOT 29

TNT EXPLOSION

20 μSEC/cm

SHOT 19

SHOT 22

SHOT 21

SHOT 25

SHOT 29

FIG. C-7 DOPPLER MICROWAVE SIGNALS FROM VARIOUS EXPLOSIONS; NOMINAL 3-cm WAVELENGTH
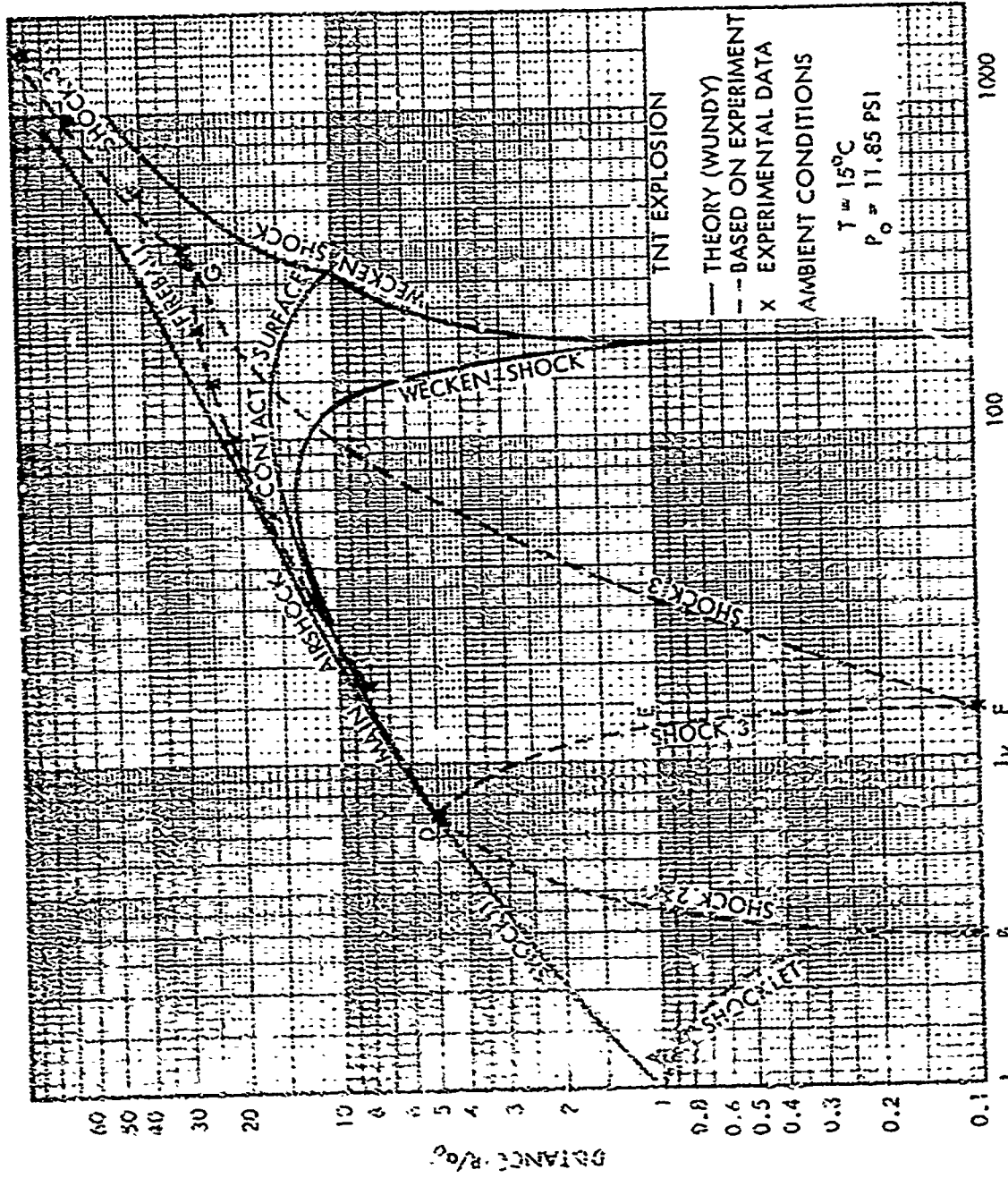
FIG. C-8 COMPARISON OF THEORY AND EXPERIMENT

APPENDIX D: SOME COMPARISONS OF CLOSE-IN AIRSHOCK MEASUREMENTS WITH
SOVIET RESULTS

The most nearly comparable investigations of which we are aware
to those reported here were reported by ADUSHKIN 1961 and ADUSHKIN 1963.
It is of some interest to make comparisons.

In both papers Adushkin aimed at (1) extending the empirical
formulas of Savdovskii for peak pressure, impulses, positive duration,
etc. from the low-pressure region of validity into the region of high
pressures and (2) determining how well the theoretical point-source
solutions for an explosion (which are extremely popular with Soviet
investigators) describe the shock from a chemical explosion.

In 1961, Adushkin's results were obtained from 0.3-lb spheres
of cast 50/50 TNT-hexogen (which we take to be Comp B) with piezo-
electric p-t gages. Since he was worried about the strength of his
gages, he carried out measurements only up to 5-7 a_o from the center
of the charge. In the 1963 investigation, larger charges were used:
3.7-lb cast Comp B spheres, 3.5-lb Comp B powder spheres (possibly
pressed above powder density), and 2-lb spheres of pressed PETN.
Here he used p-t gages up to 4 a_o but used the data only for arrival
times. Closer-in, bare ionization wires were used to detect the
airshock. Camera (instrument SFR-2M) coverage, up to 2×10^5 fps,
was available.

Few records are shown in either paper. In the 1963 report, only
one oscilloscope recording is given -- and that from gages at 11.1 a_o,
despite an obvious interest in shock formation at earlier positions.
We suspect that his records were, also, poor.

ADUSHKIN 1961 gives an excellent description of the formation
of an airshock in the spherical-piston model. Probably this model
was correct for the 0.3-lb spheres, which we think were, probably,
too small to produce a transmitted airshock. Adushkin, however,
appears to have proposed his piston model for all HE explosions,
with which we disagree. We quote verbatim:

"We shall propose a physical mechanism describing
the obtained behavior of the pressure impulse in the
propagating wave. In the first instant after completion
of detonation, the compressed products of the explosion
begin to fly apart, encountering as yet only insignificant
resistance from the surrounding air. Obviously, the specific
energy of these products of the explosion decreases as
they fly apart, owing to the spherical scatter. But before
it is significantly decreased for this reason, a region
of air displaced and compressed by the explosion products
which are flying apart, is gradually formed in front of
them. The products of the explosion are thereby slowed
down more and more. This process of slowing down is
accompanied by the transmission of energy from the

expanding products into the aerial shock wave. Apparently, up to 13 to 15 a_0, the products of the explosion practically give all of their energy to the air (to the shockwave). However, the explosion products continue for a certain time to sustain the air proceeding from the front, until the pressure in them is lowered to atmospheric. This is indicated by the fact that the duration of the compressive phase of the shockwave is more than tripled in the short distance from 11 to 13 a_0."

Information on the nature of the light from an explosion is given in ADUSHKIN 1963. We do not agree with his discussion. Again, we quote verbatim:

"Let us note that in direct proximity to the charge, the source of light is the surface of the front of the shockwave formed by expanding explosion products. Then possibly, glow comes from deeper layers of turbulent air behind the wavefront. In region above 3-4 a_0, which is especially well seen in photographs, obtained on the SFR camera by method of stero survey, surface is bared of the products themselves in the form of a rough cloud. However, it is possible that source of light, nevertheless, is a thin layer of air, adjoining the surface of the explosion products, especially so since temperature of the air behind wavefront increases (especially sharp near contact surface) while temperature of the products themselves is significantly lower than temperature of air behind wavefront . . . .

"Since temperature of the products, during their expansion, is many times lower than temperature of the compressed air behind front of shockwave, it was expected that the ionization probe would sense difference in electrical conductivities of air, compressed in the wave and the products. In Figure 3, results of measurements by the ionization probe of arrival times of the products in region up to 13 a_0, are designated by crosses. On recordings of the ionization probe (Figure 1b), the arrival time of the products was taken as the moment of sharp drop after the second peak of the recording. These measurements of arrival times of the explosion products coincided with optical observations. Thus, under the conditions of the experiment, during photographing of the intrinsic glow of the process of explosion of HE are recorded the hottest layers of air at the very contact surface which is the external layer of the explosion products."

In 1961, Adushkin found "good correspondence" between his Comp B data and the predictions of Brode* for peak shock overpressures and

---

*H. L. Brode. "Blast Wave from a Spherical Charge," Phys, Fluids 2, 217, 1959, is for a TNT explosion.

positive-phase impulse. In 1963 he noted a discrepancy between Brode's contact surface which "ceases at a distance of 13-14 a_o, in contrast to the movement of the explosion products observed in the experiments, which starts at approximately from 5 to 7 a_o." We are mystified why Adushkin claims that the products start at 5-7 a_o, when clearly they start at 1 a_o, but we agree that theory generally does not correspond to the contact-surface motion (or the second shock or any phenomena after the main airshock).

In Figure D-1 and D-2 we can examine the Soviet data more closely. We have taken much of Figure D-1 from our Figure 3, the WUNDY curve for pentolite and data symbols for a single (cast) Comp B and two PETN explosions. To these, we have added two curves from ADUSHKIN 1963: one for (cast) Comp B and one for PETN. We obtained these curves from use of empirical formulas given by Adushkin, corrected to DRI conditions. We have no idea how he obtained his curves -- but we suspect that they were obtained by curve-fitting (to his ionization probe data), a procedure that we think is unacceptable close-in to an explosion. Certainly his published results show none of the scatter that plagued our data. (The high value of ~12,000 psi at $R/a_o = 1$ seems to us a typical end-point problem with polynomial fits and not that Soviet charges are twice more powerful than ours.)

In Figure D-2, we have combined results from both of the Adushkin papers for Comp B, again corrected to DRI conditions. We have superimposed these onto WUNDY curves for TNT and pentolite, simply as bases for comparison. The high-pressure results, are the same as in Figure D-1: we have extended them to 12 a_o in Figure D-2 from his empirical formulas. There is a discrepancy in the over-lapping region from ~5 to 12 a_o of Adushkin's results: the pressures from his 0.3-lb charges lie well below his curve for the 3.7-lb charges. Whether this is a real physical difference or merely a difficulty in the data-processing we do not know. Adushkin obtained his 0.3-lb tabular data from processing r-t data taken from the p-t gage records. These derived pressures were substantially higher than his p-t gage pressures. Adushkin ascribed this difference to lack of frequency response in the instrumentation (channel frequency: 200 kcps; natural frequency of the quartz gages: 300 kcps).

We note, in concluding, that the 0.3-lb Comp B data make a remarkably good fit to our theoretical curve for pentolite -- from about 15 a_o to over 70 a_o.
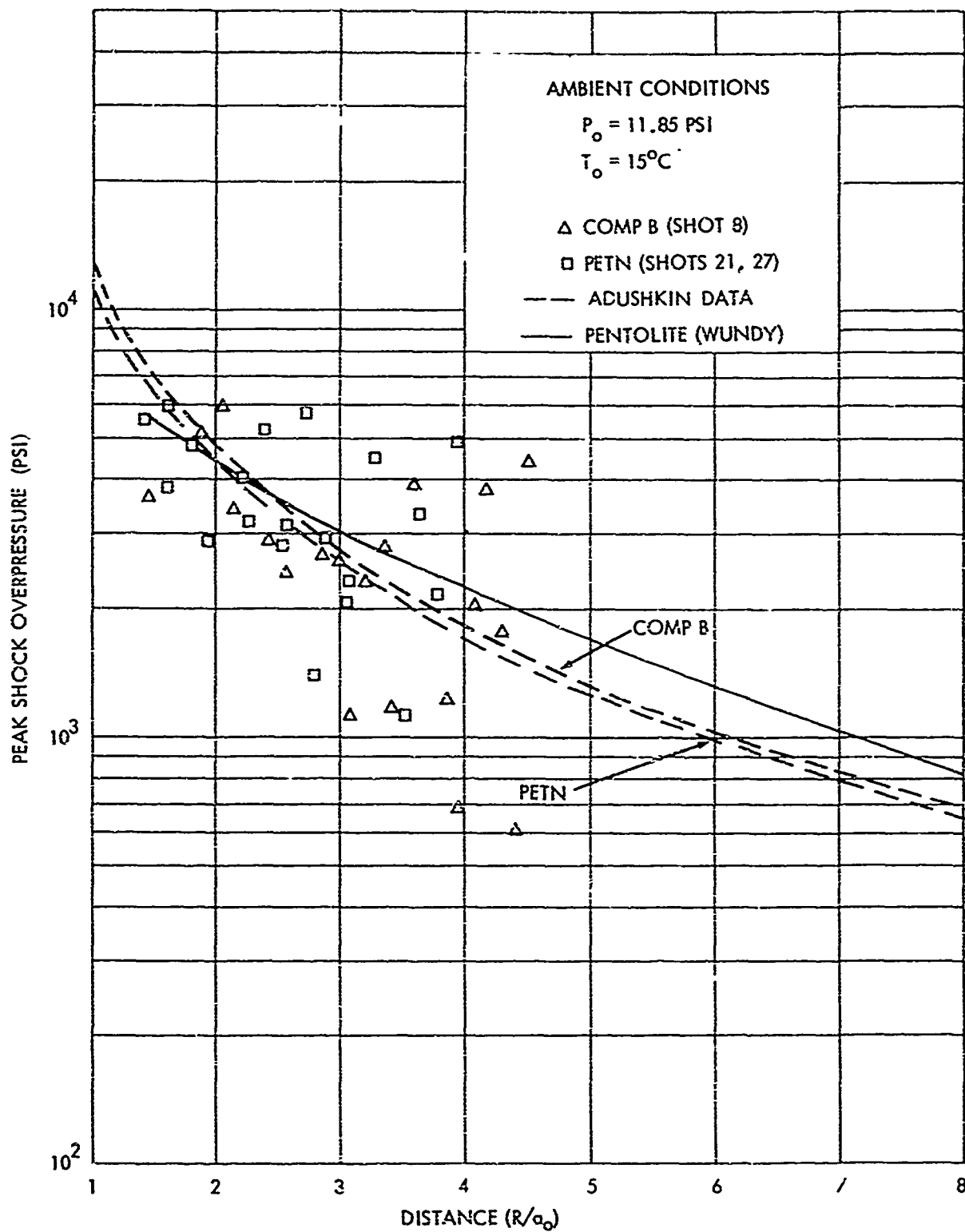
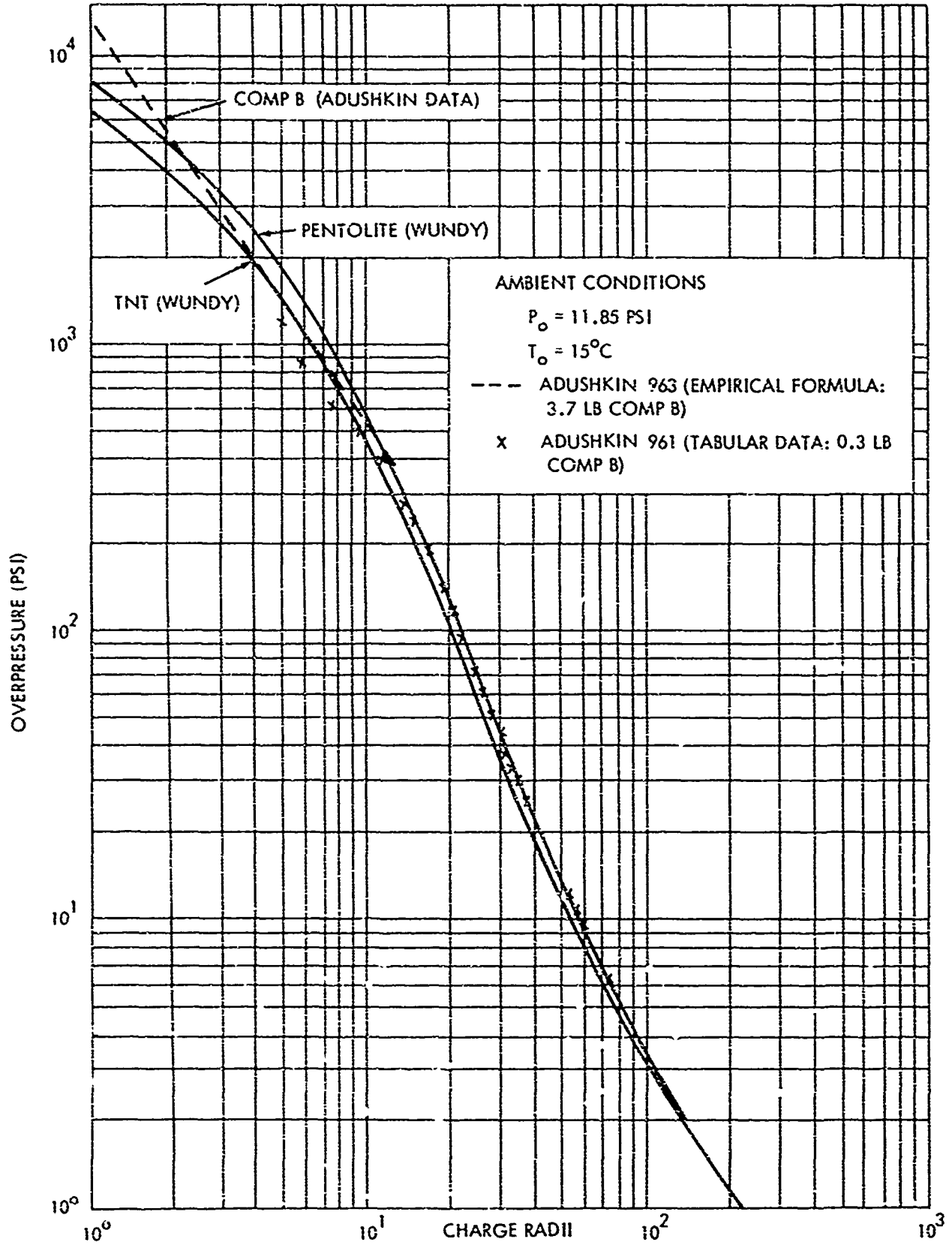FIG. D-1 COMPARISON OF CLOSE-IN SHOCK PRESSURES WITH RESULTS OF ADUSHKIN

FIG. D-2   COMPARISON OF SHOCK PRESSURE WITH RESULTS OF ADUSHKIN

DOCUMENT CONTROL DATA - R&D

(Security classification of title, body of abstract and indexing annotation must be entered when the overall report is classified)

1 ORIGINATING ACTIVITY (Corporate author)	2a REPORT SECURITY CLASSIFICATION
U. S. Naval Ordnance Laboratory White Oak, Silver Spring, Maryland 20910	UNCLASSIFIED
	2b GROUP

3 REPORT TITLE

On the Origin of Shockwaves from Condensed Explosion in Air
Part 3: Airshock Radiation from Small Explosions at Sea-Level
            Conditions

4 DESCRIPTIVE NOTES (Type of report and inclusive dates)

5 AUTHOR(S) (Last name, first name, initial)

Rudlin, Leonard

6 REPORT DATE	7a TOTAL NO OF PAGES	7b NO OF REFS
19 June 1970	94	29

8a CONTRACT OR GRANT NO	9a ORIGINATOR'S REPORT NUMBER(S)
b PROJECT NO NWER Subtask NC002/01	NOLTR 69-74
c	9b OTHER REPORT NO(S) (Any other numbers that may be assigned this report)
d	

10 AVAILABILITY/LIMITATION NOTICES

This document has been approved for public release and sale, its
distribution is unlimited.

11 SUPPLEMENTARY NOTES	12 SPONSORING MILITARY ACTIVITY
	Defense Atomic Support Agency Washington, D. C. 20305

13 ABSTRACT

Photographic and spectral observations have been made of the earliest
stages of HE explosions. Strong (in the neighborhood of Mach
number = 20), non-luminous airshocks have been photographed as close
in as 1/2-charge radius from the explosive surface. The present
results support earlier observations on the existence of a transmitted
airshock created by the detonation shockwave.

The spectra obtained show no evidence of the expected shocked-air
species. Identification of the spectral features suggests that the
intense early light of an explosion is created within the fireball
by a wide range of chemical species requiring from about 2 to 20 ev
for excitation.

DD FORM 1473

DOCUMENT CONTROL DATA - R&D

(Security classification of title, body of abstract and indexing annotation must be entered when the overall report is classified)

1. ORIGINATING ACTIVITY (Corporate author)	2a. REPORT SECURITY CLASSIFICATION
U. S. Naval Ordnance Laboratory White Oak, Silver Spring, Maryland 20910	UNCLASSIFIED
	2b. GROUP

3. REPORT TITLE

On the Origin of Shockwaves from Condensed Explosion in Air
Part 3: Airshock Radiation from Small Explosions at Sea-Level
            Conditions

4. DESCRIPTIVE NOTES *(Type of report and inclusive dates)*

5. AUTHOR(S) *(Last name, first name, initial)*

Rudlin, Leonard

6. REPORT DATE	7a. TOTAL NO. OF PAGES	7b. NO. OF REFS
19 June 1970	94	29

8a. CONTRACT OR GRANT NO.	9a. ORIGINATOR'S REPORT NUMBER(S)
b. PROJECT NO. HWER Subtask NCC02/01	NOLTR 69-74
c.	9b. OTHER REPORT NO(S) *(Any other numbers that may be assigned this report)*
d.	

10. AVAILABILITY/LIMITATION NOTICES

This document has been approved for public release and sale, its
distribution is unlimited.

11. SUPPLEMENTARY NOTES	12. SPONSORING MILITARY ACTIVITY
	Defense Atomic Support Agency Washington, D. C. 20305

13. ABSTRACT

Photographic and spectral observations have been made of the earliest
stages of HE explosions. Strong (in the neighborhood of Mach
number = 20), non-luminous airshocks have been photographed as close
in as 1/2-charge radius from the explosive surface. The present
results support earlier observations on the existence of a transmitted
airshock created by the detonation shockwave.

The spectra obtained show no evidence of the expected shocked-air
species. Identification of the spectral features suggests that the
intense early light of an explosion is created within the fireball
by a wide range of chemical species requiring from about 2 to 20 ev
for excitation.

DD FORM 1473

14	KEY WORDS	LINK A		LINK B		LINK C	
		ROLE	WT	ROLE	WT	ROLE	WT
	Explosions in Gases						
	Shockwaves						
	Explosion Light						
	Explosion Spectra						
	High-Pressures						
	Fast Chemical Reactions						
	Luminosity						
	Optical Radiation						

INSTRUCTIONS

1. ORIGINATING ACTIVITY. Enter the name and address of the contractor, subcontractor, grantee, Department of Defense activity or other organization (corporate author) issuing the report.

2a. REPORT SECURITY CLASSIFICATION. Enter the overall security classification of the report. Indicate whether "Restricted Data" is included. Marking is to be in accordance with appropriate security regulations.

2b. GROUP: Automatic downgrading is specified in DoD Directive 5200.10 and Armed Forces Industrial Manual. Enter the group number. Also, when applicable, show that optional markings have been used for Group 3 and Group 4 as authorized.

3. REPORT TITLE: Enter the complete report title in all capital letters. Titles in all cases should be unclassified. If a meaningful title cannot be selected without classification, show title classification in all capitals in parenthesis immediately following the title.

4. DESCRIPTIVE NOTES. If appropriate, enter the type of report, e.g., interim, progress, summary, annual, or final. Give the inclusive dates when a specific reporting period is covered.

5. AUTHOR(S): Enter the name(s) of author(s) as shown on or in the report. Enter last name, first name, middle initial. If military, show rank and branch of service. The name of the principal author is an absolute minimum requirement.

6. REPORT DATE. Enter the date of the report as day, month, year; or month, year. If more than one date appears on the report, use date of publication.

7a. TOTAL NUMBER OF PAGES: The total page count should follow normal pagination procedures, i.e., enter the number of pages containing information.

7b. NUMBER OF REFERENCES. Enter the total number of references cited in the report.

8a. CONTRACT OR GRANT NUMBER. If appropriate, enter the applicable number of the contract or grant under which the report was written.

8b, 8c, & 8d. PROJECT NUMBER. Enter the appropriate military department identification, such as project number, subproject number, system numbers, task number, etc.

9a. ORIGINATOR'S REPORT NUMBER. Enter the official report number by which the document will be identified and controlled by the originating activity. This number must be unique to this report.

9b. OTHER REPORT NUMBER(S): If the report has been assigned any other report numbers (either by the originator or by the sponsor), also enter this number(s).

10. AVAILABILITY/LIMITATION NOTICES. Enter any limitations on further dissemination of the report, other than those

imposed by security classification, using standard statements such as:

(1) "Qualified requesters may obtain copies of this report from DDC."

(2) "Foreign announcement and dissemination of this report by DDC is not authorized."

(3) "U. S. Government agencies may obtain copies of this report directly from DDC. Other qualified DDC users shall request through
_____."

(4) "U. S. military agencies may obtain copies of this report directly from DDC. Other qualified users shall request through
_____."

(5) "All distribution of this report is controlled. Qualified DDC users shall request through
_____."

If the report has been furnished to the Office of Technical Services, Department of Commerce, for sale to the public, indicate this fact and enter the price, if known.

11. SUPPLEMENTARY NOTES: Use for additional explanatory notes.

12. SPONSORING MILITARY ACTIVITY: Enter the name of the departmental project office or laboratory sponsoring (paying for) the research and development. Include address.

13. ABSTRACT: Enter an abstract giving a brief and factual summary of the document indicative of the report, even though it may also appear elsewhere in the body of the technical report. If additional space is required, a continuation sheet shall be attached.

It is highly desirable that the abstract of classified reports be unclassified. Each paragraph of the abstract shall end with an indication of the military security classification of the information in the paragraph, represented as (TS), (S), (C), or (U).

There is no limitation on the length of the abstract. However, the suggested length is from 150 to 225 words.

14. KEY WORDS: Key words are technically meaningful terms or short phrases that characterize a report and may be used as index entries for cataloging the report. Key words must be selected so that no security classification is required. Identifiers, such as equipment model designation, trade name, military project code name, geographic location, may be used as key words but will be followed by an indication of technical context. The assignment of links, roles, and weights is optional.